NUMERICAL SIMULATION OF SATURATED GROUNDWATER FLOW AND POLLUTANT TRANSPORT IN KARST REGIONS

by

Djoko Luknanto

An Abstract

Of a thesis submitted in partial fulfillment of the
requirements for the Doctor of Philosophy degree
in Civil and Environmental Engineering
in the Graduate College of
The University of Iowa

December 1991

Thesis supervisor: Professor Forrest M. Holly, Jr.

ABSTRACT

In karst regions, groundwater flow and pollutant transport occur in two modes: fast-response flow in cave passages and slow-response flow in the aquifer-matrix. This thesis presents a computationally efficient numerical model that simulates the behavior of the two flow and transport modes.

A finite-difference method is used to discretize all governing equations. First, the fast-response flow in a network of cave passages is mathematically modelled by means of the full unsteady hydrodynamic equations and solved numerically using the Preissmann method. The slow-response flow in the aquifer-matrix is modelled by an unsteady Darcy equation and solved numerically using a fractional-step approach. These two equations are iteratively coupled through an exchange term reflecting the water exchange between cave passages and the aquifer-matrix. Next, the pollutant transport equations in the network of cave passages is solved using a characteristic method and in the aquifer-matrix using a fractional-step approach. These two pollutant transport equations are solved iteratively through an exchange term reflecting the pollutant exchange between cave passages and the aquifer-matrix.

Sensitivity analysis on important parameters affecting groundwater flow and pollutant transport in karst regions shows that the equivalent diameters of the cave passages and their distribution in the aquifer-matrix are the most important parameters of the model, provided the topology of the cave passages is fixed.

The model is capable of simulating dye trace experiments performed in Iowa's Big Spring basin. Time travel of two dye trace experiments from two different sinkholes is simulated. The results show that, for a fixed topology and given boundary conditions, only a

narrow range of equivalent diameters of cave passages, about 1.5 ft, can simulate the correct travel time of the dye.

At the Big Spring basin, for a nondiffusive system, i.e., karst formations with large equivalent diameters of cave passages, it is possible to predict the flow at Big Spring using a reservoir-type formulation, thereby avoiding the complexity of a detailed mathematical formulation that considers all water pathways. The pathways are important for pollutant transport and the reservoir formulation is not adequate to determine the concentration of pollutants in the Big Spring flow.

Abstract approved: Faust M. Holly Jr.
Thesis supervisor
Professor
Civil and Env. Engineering
Title and department

19 Sept 1991
Date

NUMERICAL SIMULATION OF SATURATED GROUNDWATER FLOW AND POLLUTANT TRANSPORT IN KARST REGIONS

by

Djoko Luknanto

A thesis submitted in partial fulfillment of the
requirements for the Doctor of Philosophy degree
in Civil and Environmental Engineering
in the Graduate College of
The University of Iowa

December 1991

Thesis supervisor: Professor Forrest M. Holly, Jr.

Graduate College
The University of Iowa
Iowa City, Iowa

CERTIFICATE OF APPROVAL

PH.D. THESIS

This is to certify that the Ph.D. thesis of

Djoko Luknanto

has been approved by the Examining Committee
for the thesis requirement for the Doctor of
Philosophy degree in Civil and Environmental
Engineering at the December 1991 graduation.

Thesis committee: Jont M. Holly
Thesis supervisor

Member

Member

Member

Member

The Embryo

Read in the name of your Lord who created,
Created man from an embryo;
Read, for your Lord is the Most Bounteous,
Who taught by the pen,
Taught man that which he knew not.

The Glorious Koran, XCVI, 1–5

ACKNOWLEDGMENTS

During the period of work on this thesis, the author received assistance and suggestions from numerous individuals to whom he would like to express appreciation. Special gratitude is due Professor Forrest M. Holly, Jr. for his advice, encouragement and guidance, especially during the last phase of this study. The author wants to express his gratitude to Professor Konstantine P. Georgakakos for his helpful hints in the early stages of this study. The author certainly owes much to Professor George R. Hallberg for his time spent as a member of the exam committee and his studies on the Big Spring Basin, Clayton County, Iowa, from which most of the data for this study is taken. The author also would like to express appreciation to Professor Robert Ettema, Professor Witold F. Krajewski, and Professor Frank H. Weirich for their time spent as members of the exam committee and for their insightful suggestions during the finishing touches of the study.

To Professor Pragnjono Mardjikoen, Dr. Bambang Suhendro, Dr. Sri Harto Br., Ir. Sutojo Tjokrodihardjo, Ir. Soegeng Djojowirono, and Ir. Darmanto, M.S. in the Faculty of Engineering in Gadjah Mada University, the author expresses his gratitude for support. The author also thanks the World Bank Education Project IX staff in the Jakarta office, and Dr. Jean Taylor, Mary Woodward and staff at the MUCIA-INDONESIA project at the University of Wisconsin. For Dr. Andrea S. Dunn, the author wants to thank her for help in transforming the Indonesian-style English in this study into the "correct" one.

To his parents, his wife, Ratna, and his two lovely daughters, Nuri and Nisa, who shared the burden of finishing this study and gave their understanding support, the author expresses his deepest gratitude.

TABLE OF CONTENTS

LIST OF TABLES

LIST OF FIGURES

LIST OF SYMBOLS

a_i, b_i, c_i, d_i	double-sweep coefficients
A	a matrix in megapore computations
A	cross-sectional area
a	megapore radius in Eq. (4.4)
A, B, C	coefficients used in aquifer-matrix computation in Eqs. (3.19), (3.20), and (3.28a)
B	a vector of known quantities in megapore computations
b	width of fracture in Eqs. (2.3)–(2.5)
C_1, C_2, C_t	arbitrary constants in a general equation of boundary conditions in Eqs. (3.22)–(3.27)
CX_i^{n+1}	gradient pollutant concentration at the foot of a characteristic line at a previous time step
CX_ψ^z	gradient pollutant concentration at the foot of a characteristic line at the boundary
C_0	initial pollutant concentration in Eq. (4.3)
C_ξ^n	pollutant concentration at the foot of a characteristic line at a previous time step
C_ψ^z	pollutant concentration at the foot of a characteristic line at the boundary
C_s	pollutant concentration of a source or sink
C_t	Taylor dispersion coefficient in Eq. (4.4)
C	a vector of unknown pollutant concentration in Eq. (3.29)
c, C	pollutant concentration
Cr	the Courant number
CX	gradient of concentration in megapore computations
D_x, D_y, D_z	bulk dispersion coefficients of the aquifer-matrix in x, y, and z directions

D_d	coefficient of molecular diffusion in Eq. (2.6)
D_x^h, D^h	coefficient of hydrodynamic dispersion in Eq. (2.7) and (2.9)
d	differential operator
D	coefficient of diffusion in Eq. (4.1)
e	porosity of an aquifer-matrix
E, F, H	double-sweep coefficients
EE, FF, HH	double-sweep coefficients
E_1, E_2, E_t	arbitrary constants in a general equation of boundary conditions in Eqs. (3.30)–(3.33)
F	a vector of known quantities in aquifer-matrix computations in Eqs. (3.21) and (3.29)
g	gravitational acceleration
$\Delta\mathbf{h_m}$	a vector of unknown correction of piezometric heads in the megapore in Eq. (3.44)
h_s, h_p	piezometric head for aquifer-matrix and megapore, respectively, in Eq. (3.9)
h^x, h^y, h^z	the fractional-step piezometric head of an aquifer-matrix in x, y, and z directions, in Eqs. (3.15)–(3.17)
h_m, h_m^p	the latest estimate and the previous time step value of the megapore piezometric head at the nodal point in Eqs. (3.19) and (3.20)
h_m, h_{ijk}	the megapore piezometric head at the nodal point, and the aquifer-matrix piezometric head at a grid point, in Eqs. (3.12), (3.13), and (3.36)
h	a vector of unknown piezometric heads in Eq. (3.21)
h	piezometric head
x,y,z	(in subscript) indicates x, y, and z directions
K_f	the equivalent hydraulic conductivity of a fracture in Eq. (2.5)
K_g	the permeability in the direction of the gradient
K	hydraulic conductivity of an aquifer-matrix, full-megapore conveyance
L, M, N	double-sweep coefficients of pollutant transport computations in megapores
M	a tri-diagonal matrix in aquifer-matrix computations in Eqs. (3.21) and (3.29)
M	an initial slug of mass in Eq. (4.1)

$^{n,n+1}$	(in superscript) the current and the next time step
n	volumetric fraction of the void space of the fractured rock domain in Eq. (2.9)
p	pressure
Q_{lp}^{n+1}	discharge entering node m from pipe lp in Eq. (3.34)
Q_m^{n+1}	external inflow entering node m in Eq. (3.34)
q_l	the leakage into or out of a fracture in Eq. (2.4)
Q_{lp}	water discharge at a megapore looped node
Q	water discharge
Q, R, S	double-sweep coefficients of pollutant transport computations in megapores
R	the retardation factor in Eq. (4.2)
S_f	megapore energy slope
s	longitudinal megapore coordinate in Eqs. (3.7) and (3.8)
S	specific storage
~	averaging across a fracture in Eqs. (2.7)
t	time
U^*	megapore shear velocity in Eq. (4.4)
U	seepage or average pore water velocity, megapore water velocity
V_{ave}	mean velocity in Eqs. (2.3) and (2.4)
V_x, V_y	velocity in x- and y-directions in Eqs. (2.7) and (2.8)
V	fluid velocity vector in Eq. (2.1)
V	velocity
W_m^{n+1}	inflow entering node m from the aquifer-matrix in Eq. (3.34)
w_s	pollutant volumetric flux per unit volume of a source or sink in Eq. (3.10)
W	volumetric flux of a source or sink
w	volumetric flux per unit volume of a source or sink
x, y, z	the orthogonal Cartesian coordinate axis

α	coefficient of mass exchange between megapore and aquifer-matrix in Eq. (3.9)
δ	second order gradient operator
ε	megapore dispersion coefficient
∇	gradient operator
φ_{ave}	mean piezometric head in Eq. (2.3)
φ	piezometric head in Eq. (2.2)
φ	Preissmann's time weighting parameter in Eq. (3.45)
λ	the radioactive decay constant in Eq. (4.2)
μ	dynamic viscosity
Δ	discretized length operator
π	3.1415926545
∂	partial differential operator
θ	implicitation factor for a finite-difference scheme
ρ	water density
υ	volume of soil in a finite-difference block
ψ	capillary pressure head in Eq. (5.1)

CHAPTER I

INTRODUCTION

1.1. Background

The planning, development, and management of water resources in karst regions and fractured porous media require knowledge about physical, economic, and social factors. In particular, maintaining the quality of groundwater is of great interest. Unfortunately, pollutants are moving into groundwater at an ever-increasing scale. The challenge of maintaining the quality of groundwater has to be met to maintain the quality of life for humans as well as animals.

Karst aquifers, in contrast to aquifers in homogeneous media, are extremely complex because of their inhomogeneous permeability. As shown in Figure 1.1, the relation of structures in rock, such as fracture systems and the orientation of cave passages, establishes secondary permeability. These fractures or cave passages represent less resistance to water flow than does neighboring rock. In contrast to aquifers in homogeneous media, karst aquifers, due to their inhomogeneous distribution of permeability, are extremely complex.

Groundwater flow occurs in two modes: fast-response flow in cave passages and slow-response flow in the aquifer-matrix. These two components of groundwater flow are extremely different in the effectivity of groundwater transmission and groundwater storage. These flow characteristics therefore greatly influence pollutant transport in such a region.

Although unsaturated cases are common in the real world, understanding the behavior of saturated groundwater flow is a very important step toward understanding unsaturated cases.

Insight from saturated cases can be applied to the study of unsaturated cases. Study of the physical behavior of saturated cases is, therefore, the beginning of on-going research in groundwater flow in karst regions.

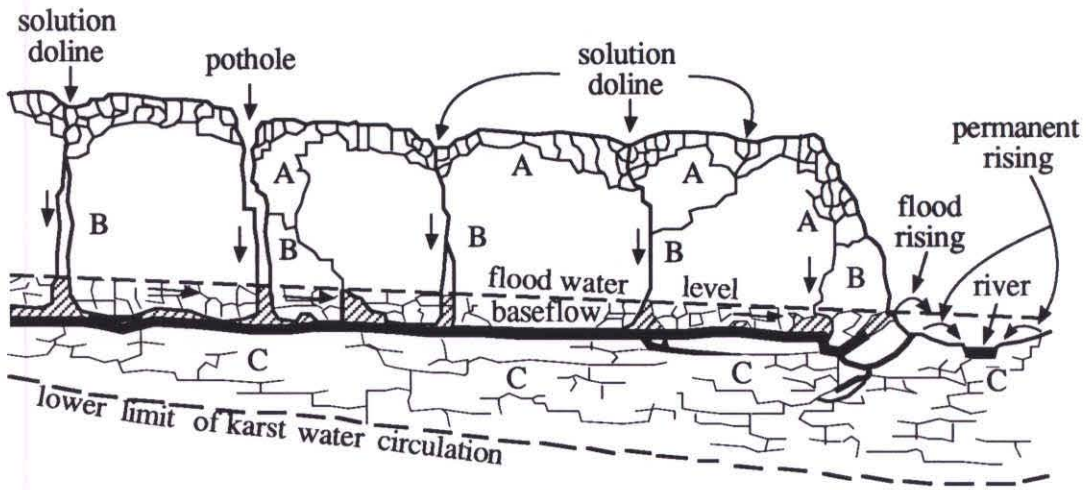

Figure 1.1. A Karst Hydrologic System Based on the Concept of Independent Conduits, after Cavaille (1962)

1.2. Objective

The objective of the present study is to model the behavior of saturated groundwater flow and pollutant transport in karst regions. A new approach is introduced in which the "full" hydrodynamic equation in a cave passage network is solved directly. The pollutant assumed here is a nonreactive, conservative one, meaning that during transport, its quantity does not increase or decrease. As in any study of groundwater flow, little data are available. This is

understandable due to the difficulties in measuring soil parameters, initial and boundary conditions, as well as the high cost involved in obtaining the data. For the purpose of the present study, no new field measurements have been performed. The study uses data obtained from competent published sources.

It is very important to mention that the present study is part of a larger research objective; i.e., the present study serves as the deterministic part of a Monte Carlo simulation of water resources in a karst region. Since available observations are limited, system parameters (aquifer properties, system geometry, initial and boundary conditions) must be generated by statistical techniques. Each realization of the data generated becomes the input data for the "deterministic engine" which processes the data to produce one realization of output. In a Monte Carlo simulation, hundreds or thousands of realizations of input may be generated, each of which produces its corresponding output. These in turn must be interpreted by statistical means. In karst regions, the "deterministic engine" will be a model that simulates numerically the behavior of groundwater water and pollutant transport for unsaturated cases. Since the present study is only capable of handling saturated cases, it must be extended to unsaturated cases in order to become the complete "deterministic engine" for the Monte Carlo simulation. The extension of the present study to unsaturated cases and its inclusion in Monte Carlo simulation are discussed in Chapter V as suggestions for further research.

The topology of cave passages and the boundary of the groundwater flow region are inferred from data obtained for karst formations in the Big Spring Basin, a 103 square mile groundwater basin located in Clayton County, northeastern Iowa (Hallberg et al., 1989), see Figure 1.2. The topography of the region under study is extracted from the USGS (United States Geologic Survey) contour map. Soil parameters, i.e., hydraulic conductivity, specific storage, exchange coefficient, dispersion coefficient, and effective porosity are based on appropriate published literature.

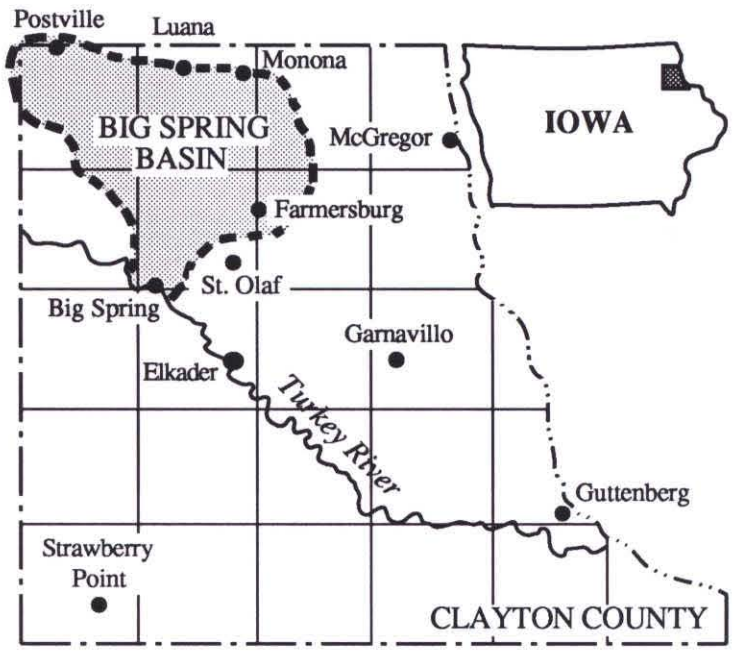

Figure 1.2. The Big Spring Basin in Clayton County, northeast Iowa, after Hallberg et al. (1989)

Chapter II presents a review of related literature. Since groundwater flow and pollutant transport in fractured porous media are closely related to the present study, literature concerning fractured formations is also reviewed.

The development of the model is explained in detail in Chapter III. Firstly, all the equations that govern the physical processes in the aquifer-matrix and cave passages are described. Secondly, the strategy for approximating the governing equations is explained. This strategy is presented in two major sections to reflect the fact that the aquifer-matrix and cave passages have different flow characteristics. One section explains the numerical approximations of the governing equations for the aquifer-matrix. The other section explains the numerical approximations of the governing equations for cave passages. The last section of Chapter III explains the coupling between aquifer-matrix and megapore computations.

In Chapter IV, tests and applications of the model are presented. First, the model results are compared to relevant analytical solutions. Second, sensitivity analysis for various parameters affecting the response of water discharge and pollutant transport at Big Spring is performed. Third, the model is applied to simulate the groundwater flow and transport of pollutants in the Big Spring Basin.

Chapter V discusses the merits of the model. Further research to generalize the model for unsaturated cases is suggested. In addition, the possible inclusion of the present study in a Monte Carlo simulation is explained. Some important aspects of the Monte Carlo simulation are also discussed.

CHAPTER II

LITERATURE REVIEW

2.1. Introduction

The purpose of this chapter is to review the work of other researchers in the field of groundwater flow and pollutant transport. The first part reviews studies on groundwater flow and pollutant transport in fractured porous media. The second part is a review of the literature on groundwater flow and pollutant transport in karst regions. The third part summarizes the review and outlines the new approach to be used in the present study.

Of the many studies on groundwater flow, pollutant transport in karst regions and fractured porous media performed in the past few years, most have dealt with fractured porous media and only a few with karst regions. Relevant studies from the two regions are presented in the following sections.

2.2. Groundwater Flow and Pollutant Transport in Fractured Porous Media

Fractures (cracks and fissures) exist in a broad range of geologic formations. They have been produced under a variety of geological and environmental processes, such as tectonic movements, secondary stresses, weathering, thermal expansion and chemical action of percolating fluids. Given the large extent to which fracturing occurs in aquifers, the modelling of flow and pollutant transport in such formations is of practical importance.

Two basic approaches are used to model groundwater flow and pollutant transport in fractured porous media: the "dual porosity" model and the "equivalent porous medium" approach. In the "dual porosity" approach, a fractured medium is treated as two porous media of known structure. In the "equivalent porous medium" approach, a fractured porous medium

is treated as a macroscopically uniform porous medium. All of the studies reviewed here used the "dual porosity" approach. The second approach is not reviewed since it is not appropriate for a karst region in which cave passages are present. However, the distinguishing characteristics of the two approaches are explained. Bear and Berkowitz (1983) discussed in detail how and when the two approaches should be applied.

To begin with, Bear and Berkowitz explain the concept of a *representative elementary volume* (REV) as a sufficiently large volume of a fractured porous medium within a given domain that contains both a void space and a solid matrix. At the same time, the size of the sample should be small enough so as to represent a sufficiently close neighborhood around the point of sampling. The detailed explanation of the REV concept may be found in Bear (1979).

Using REV, Bear and Berkowitz classified the various problems of flow and pollutant transport in fractured porous media in the following way:

Zone 1, the *very near field*. Interest is focused on transport within a single, well-defined fracture, possibly with transport into the adjacent porous blocks.

Zone 2, the *near field*. Zone 2 treats transport in a relatively small, but well-defined, set of fractures.

Zone 3, the *far field*. Transport in two overlapping continua is considered — one composed of a network of fractures, and the other consisting of the porous blocks — with exchange between them.

Zone 4, the *very far field*. The entire fractured porous medium may be regarded as a single continuum, which reflects the properties of both fractures and porous blocks.

Witherspoon et al. (1988) explained another approach in which the hydraulic gradient, K_g, is used as a parameter to determine the appropriate zone. The permeability of fractured media in the direction of the hydraulic gradient, K_g, can be measured in any direction by rotating the boundaries of the flow region γ degrees and consequently rotating the direction of the gradient. For a homogeneous, anisotropic medium, $(K_g)^{-0.5}$ versus γ is an ellipse when

plotted on polar coordinates (Marcus and Evanson, 1961; Marcus, 1962; Bear, 1972). However, according to Witherspoon et al. (1988), for inhomogeneous fractured media, $(K_g)^{-0.5}$ may not plot as a smooth ellipse. Instead, the shape of a plot using measured values of $K_g(\gamma)$ for a given test volume of rock may be quite erratic. This plot can, therefore, be used as a test of whether or not the given rock can be approximated as a homogeneous porous medium. If $(K_g)^{-0.5}$ does not plot at least approximately as an ellipse, then no single symmetric permeability tensor can be found to describe the medium. If the results cannot be described by a permeability tensor, flow through the medium cannot be analyzed with a continuum technique.

Bear and Berkowitz (1983) explained how to solve problems of groundwater flow and pollution in fractured rock aquifers. In their studies, they assumed that flow occurs in fractures as if it were between parallel plates, and they treated fractures as an equivalent porous medium. For a fracture, they started by using the Navier-Stokes equation for an incompressible fluid of constant density in a fracture:

$$\rho \frac{\partial \mathbf{V}}{\partial t} + \rho \nabla \cdot (\mathbf{V}\mathbf{V}) + \nabla p - \rho \mathbf{g} - \mu \nabla^2 \mathbf{V} = 0 \qquad (2.1)$$

where ρ and μ are fluid density and dynamic viscosity, respectively; p is pressure; $\mathbf{V}$ is the fluid velocity; t is time; and $\mathbf{g}(= -g\nabla z)$ denotes gravitational acceleration, with z the vertical coordinate (positive upward). Definition of the piezometric head as $\varphi = \frac{p}{\rho g} + z$ and substitution into Eq. (2.1) yields

$$\rho \frac{\partial \mathbf{V}}{\partial t} + \rho \nabla \cdot (\mathbf{V}\mathbf{V}) + \rho g \nabla \varphi - \mu \nabla^2 \mathbf{V} = 0 \qquad (2.2)$$

Averaging across the fracture width, with the assumptions that (1) the dispersive momentum flux is much smaller than the advective flux, (2) across any width, the piezometric heads at the fracture wall are almost identical, and (3) the flow is steady, leads to the final form of Eq. (2.2) as follows:

$$V_{ave} = -\frac{\rho g}{\mu}\frac{b^2}{12}\frac{d\varphi_{ave}}{dx} \tag{2.3}$$

where b is the width of the fracture. If the fracture walls are assumed to be permeable, then Eq. (2.2) becomes

$$V_{ave} = -\frac{\rho g b^2}{12\mu + 2b\rho q_1}\frac{d\varphi_{ave}}{dx} \tag{2.4}$$

where q_1 is the leakage into or out of the fracture (q_1 is assumed to be uniform over the fracture length). From the continuum approach point of view, the *equivalent hydraulic conductivity of the fracture* can be deduced from Eqs. (2.3) and (2.4) as

$$K_f = -\frac{\rho g}{\mu}\frac{b^2}{12} \quad \text{and} \quad K_f = \frac{\rho g b^2}{12\mu + 2b\rho q_1} \tag{2.5}$$

for the case of impermeable and permeable fractures, respectively. Bear and Berkowitz extended the analysis into multiple and ordered fracture systems. For randomly oriented fractures, they averaged the aforementioned results over all elements of all fractures within the REV.

Bear and Berkowitz also analyzed pollutant transport in fractured aquifers. They started the analysis for a single fracture by using the mass balance equation as follows:

$$\frac{\partial c}{\partial t} + \nabla\,(c\mathbf{V} - D_d\,\nabla c) = 0 \tag{2.6}$$

where $c = c(x, y, z, t)$ is the pollutant concentration, and D_d denotes the coefficient of molecular diffusion. By averaging across the fracture, they derived the following relationship:

$$\frac{\partial \bar{c}}{\partial t} + \bar{V}_x\frac{\partial \bar{c}}{\partial x} - D_x^h\frac{\partial^2 c}{\partial x^2} + q_c|_{f_2} - q_c|_{f_1} = 0 \tag{2.7}$$

where

$$q_c \equiv \frac{1}{b}\left[(\bar{c} - c)\, V_y + D_d \frac{\partial c}{\partial y}\right] \tag{2.8}$$

and D_x^h is the *coefficient of hydrodynamic dispersion.* For a fractured rock, they did not employ the double continuum approach; that is, they did not treat fractures and porous medium as two different entities. Instead, they treated fractures and porous media as one entity and modeled pollutant transport in a fractured rock domain using a single continuum approach. In the absence of sources, adsorption and decay phenomena, the mass balance equation for an ordinary porous medium is

$$\frac{\partial (nc)}{\partial t} = -\nabla \cdot n\,(c\mathbf{V} - D^h \nabla c) \tag{2.9}$$

where n is the volumetric fraction of the void space, c denotes concentration, **V** is the fluid velocity, and D^h represents the coefficient of hydrodynamic dispersion; both c and **V** are averaged over an REV of the fractured rock domain.

Endo et al. (1984) presented a technique to determine when transport in an anisotropic fracture system can be modeled as equivalent to that of porous media. They stated that to use the continuum approach, one must demonstrate that the fracture system has the same transport behavior as an equivalent porous medium. In their work, hydraulic effective porosity was calculated as the product of specific discharge and mean travel time, divided by linear length of travel. Specific discharge and hydraulic effective porosity were measured in different directions of flow in regions of varying size with constant hydraulic gradients. According to the authors, if the fracture system behaves like an equivalent porous medium, directional flow has the following properties: (1) specific discharge can be predicted from a permeability tensor and (2) hydraulic effective porosity is independent of direction of flow. They developed a numerical model to simulate mechanical transport under steady flow in a discrete fracture network. Endo et al. examined only systems with parallel fracture sets in which all fractures were long compared to the region examined in their study. These systems satisfied

criterion 1 in that flux could be calculated using a porous medium equivalent. However, these systems did not satisfy criterion 2 because hydraulic effective porosity was directionally dependent. They concluded that the flux could be accurately predicted using porous medium assumptions for some fracture systems, but it might not be possible accurately to predict mechanical transport using the same assumptions.

Haldeman et al. (1991) conducted a series of laboratory experiments to determine the flow and transport properties of a fractured porous tuff block (measuring 20 cm x 20 cm x 50 cm). In the experiment, porous ceramic plates controlled the pressure head applied to the upper surface of the fractured rock block. One plate was placed immediately above a fracture and two other plates were placed on either side of the fracture above the rock matrix. Much of the flow from the fracture at the lower surface first passed through the rock matrix despite direct contact with the porous plate. They observed that flow from the fracture plates is diverted to the fracture through the matrix within the first 3 cm and an exchange of fracture and matrix flow occurs at $z = 20$ cm and the fracture opening at $z = 50$ cm. Because of significant channeling of the fracture flow, breakthrough curves deviated from the results of the numerical simulation using the boundary integral method.

Tsang and Tsang (1987) used a channel model to study fluid flow and solute transport in a tight fractured medium. They hypothesized that fluid flow and solute transport through a tight rock medium is by means of a limited number of tortuous and intersecting channels of variable aperture. The parameters that characterized the channel were (1) the aperture density distribution, which gives the relative probability of the occurrence of a given aperture value, (2) the effective channel length and width, and (3) the aperture spatial correlation length, which gives the spatial range within which the aperture values are correlated. The profile of apertures along the channels was generated by statistical methods. In this study, the authors neglected the presence of the aquifer-matrix in which the fractures are embedded. The results of the model agree well with laboratory data obtained by Moreno et al. (1985).

Long and Billaux (1987) described a technique to account for observed spatial variability when processing field data for a fractured network model. In this technique, a network was generated, subregion by subregion, where the properties of each subregion were predicted through geostatistics. The method for two-dimensional analysis is based on data from Fanay-Augères, a uranium mine in France. To generate fractures in a statistically heterogeneous region, they first divided the region into statistically homogeneous subregions. In each subregion and for each fracture set, they specified the areal fracture density and the orientation, length, and aperture distributions. Steady state flux in the fracture elements was calculated using the cubic law under the assumption that the fractures behave like parallel plates. The rock matrix was assumed to be impermeable. The permeability in the direction of the gradient, K_g, could then be described in terms of J, the magnitude of the gradient applied across the flow region, and Q_{in}, the total flux into the flow region in the direction of the gradient, as $K_g = \frac{Q_{in}}{J}$.

Cacas et al. (1990a, 1990b) modeled flow and transport mechanisms in a stochastic discrete fracture network. This fracture network model, assuming negligible matrix permeability, was developed and calibrated using the following field data: (1) geometry of the fracture network and (2) local hydraulic properties measured by injection tests in boreholes. The field data were obtained from a large-scale investigation of fracture flow conducted in a granite uranium mine at Fanay-Augères, France. Using data from the same region, Feuga (1988) used the "regionalized density Poissonian process" to generate fracture fields that are statistically and geostatistically similar to the real fracture field.

From the analysis of trace data and examinations of fracture surfaces, several studies have shown that fractures are likely to be roughly elliptical or circular in shape (Robertson, 1970; Pollard, 1976; Beacher and Lanney, 1978). Witherspoon et al. (1988) generated a three-dimensional fractured network that is compatible with the geometry of fractured rocks in

the field. They adopted a circular shape as a subset of the general elliptical case mainly because this shape simplifies the calculation of flow. Furthermore, the two opposite surfaces of the fractures are assumed to be parallel and the standard parallel plate model for flow is assumed appropriate. The disc-shaped discontinuities are assumed to be embedded in an impermeable matrix. The discs can be arbitrarily located within the rock volume and can have any desired distribution of aperture, radius, orientation, and density. Thus, where the disc model is appropriate, it is possible to generate fracture networks that are statistically similar to those that occur in nature. Billaux extended Witherspoon's three-dimensional model to include channel flow. The channels can be arbitrarily located within the fracture and can have any desired distribution of size, length, orientation and density.

Andersson and Björn (1987) investigated flow through a network of discrete fractures in a three-dimensional domain. They modeled fractures as circular discs of arbitrary size, orientation, transmissivity, and location. A fracture network was characterized by the statistical distribution of these quantities. Their numerical simulation model was capable of generating the fractured network of desired statistical properties and solving for the steady-state flow. On each fracture disc, the flow was discretized with the boundary element method.

2.3. Groundwater Flow and Pollutant Transport in Karst Regions

Avdagic (1976) demonstrated the use of piezometric borehole heads to determine flow through a flooded karst plain. In most flooded karst plains, water inflows and outflows occur through submerged inlets and outlets. The hydrodynamic and continuity equations are used for determining the inflow and outflow of a plain. During flooding, the flow is determined for certain zones by level differences between the water level in the plain and a level or pressure measuring point in a conveyance channel, or by using the velocity head at the

measuring point of the channel. Avdagic used the Fatnicko region in Yugoslavia as an example of the method developed. He visualized the flooded karst plain as a three-reservoir system, in which only one reservoir is periodically flooded. During floods, parts of the system with restricted flow capacities are under pressure while the other parts have free surface flow. The outflow discharges were calculated by the formula $Q = k\ \Delta H^a$ where *k* and *a* are the constants for certain flow conditions. Coefficient *k* depends on the shape and size of the outflow opening, while *a* depends on the flow regime. Q is the outflow discharge and ΔH is the piezometric difference. The coefficients were determined by regression analysis using measurements from the field. Avdagic found that for the region under study the value of k ranges from 0.898 to 16.440 and the value of a is 0.5.

Milanovic (1976) studied the water regime of the Ombla spring drainage area. By comparing the flow hydrograph of the spring and the level hydrographs of numerous piezometric boreholes, he concluded that the Ombla river karst system, especially in periods of high groundwater levels, functions as a hydraulic system under pressure. He presented a detailed geologic mapping to help identify the zone in which a concentration of preferential flow directions could be expected (see Figure 2.1).

Sharp (1986), Iwai (1976), Schrauf and Evans (1986), and Kilbury et al. (1986) have studied fluid flow through individual fractures in the laboratory. They demonstrated that a linear relationship exists between the flow rate and the applied fluid gradient as long as flow is laminar. Within individual fractures, laboratory and field tests, along with simulation models, have documented the effects of fracture roughness (Schrauf and Evans, 1986), and tortuosity and channels (Tsang and Tsang, 1984, 1987) on the measured fluid flow in response to an applied fluid gradient.

Liggett et al. (1988) modeled flow in a three-dimensional network of discrete fractures using the boundary element method. The flow in one fracture is considered to be two-dimensional although the fractures may be connected in a three-dimensional network.

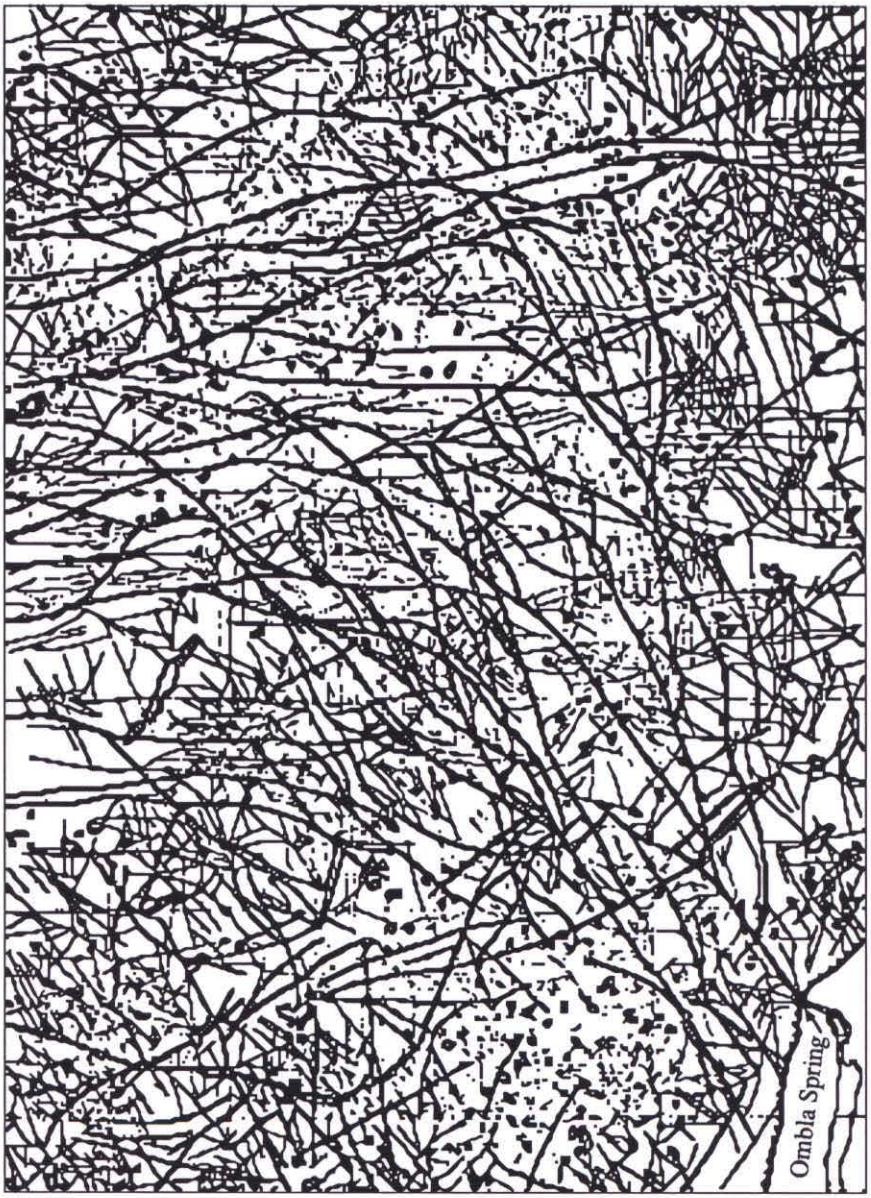

Figure 2.1. Network of Fracture Tectonics in the Catchment Area of the Ombla River, Yugoslavia, with a Surface of about 1500 km^2, after Milanovic (1976)

2.4. Concluding Remarks

Before explaining the approach used in the present study, the following points from other studies should be emphasized:

- Fractures always refer to two parallel plates.

- Flow in fractures is assumed to be steady.
- Flow in fractures may not be analyzed with continuum techniques, if no single symmetric permeability tensor can be found (Witherspoon et al., 1988).
- Endo et al. (1984) pointed out that the equivalent porous medium approach may not accurately predict mechanical transport in a fractured system.
- Haldeman et al. (1991) showed experimentally that indeed there is exchange of water between fractures and the surrounding rock matrix. In addition there is significant channelling of fracture flow.
- Tsang and Tsang (1987) showed that, using the channel approach, their model agrees with laboratory data.
- Laboratory and field tests, along with simulation models, have documented the effects of fracture roughness (Schrauf and Evans, 1986).
- A network of cave passages that resembles the actual one can be generated using statistical methods.
- In a karst region, Avdagic (1976) demonstrated that the outflow discharge of sinks can be modeled as a three-reservoir system and can be calculated by the formula $Q = k\,\Delta H^a$ where k and a are the constants for certain flow conditions.
- Milanovic (1976) showed that in a well-developed karst region, especially in a period of high groundwater levels, the discharge functions as a hydraulic system under pressure.

The present study comprises numerical modeling in a karst region. The author assumed that, in a karst system, independent conduits or passages are developed (see Figure 1.1). This assumption is supported by field observations as depicted in Figure 2.1. Moreover, the studies in fractured rock suggested that, in addition to channel roughness, the channeling effect plays a major role in the fracture flow.

In the karst system of the Big Spring Basin, Clayton County, Iowa, where the present study is based, Hallberg et al. (1983) used the dye tracing technique to show that there are connections between sinkholes and springs. He also pointed out that portions of the karst

system are quite open and very responsive. Small plastic spheres, 0.4 inch diameter, were introduced into several sinkholes along with dye. Some of these spheres have been found at Big Spring. Interestingly enough, during high discharge at Big Spring, cornstalks and an occasional beverage can also emerge from the groundwater. Thus, the independent conduit assumption for the karst system at the Big Spring Basin is strongly supported. Moreover, in saturated cases, these conduits are hydraulic systems under pressure, as suggested by Avdagic and Milanovic.

The present study uses a new approach, based on the aforementioned assumption, to model flow and pollutant transport in a karst region. In this approach, the megapore flow is treated as flow in an equivalent circular pipe. The term megapore is used to represent preferential flow paths/cave passages existing in a karst region. The flow in megapores is governed by Eq. (2.2) and the flow in the aquifer-matrix is governed by the usual equation used in ordinary porous media. Between flow in the megapores and the aquifer-matrix there is water and pollutant exchange. It is interesting to point out that, although megapore flows are governed by the same equation, used by Bear and Berkowitz (1983), Eq. (2.2), the assumption used to reach the final working equations is quite different. Bear and Berkowitz (1983) used further assumptions to simplify Eq. (2.2) into Eq. (2.3), the final working equation. In the present study, after Reynold's and spatial averaging has been applied to Eq. (2.2), the Strickler formula is used to express the energy loss, as usually used in hydraulics, to express the last term in Eq. (2.2). The detailed derivations of the governing equations used in the present model are explained in the next chapter.

CHAPTER III

MODEL DEVELOPMENT

3.1. Introduction

The present study presents a model to simulate a complex, real-life situation. The domain of the model is based on the geometry and topography of the Big Spring Basin, depicted in Figure 3.1. The domain is three-dimensional, and certain topological conventions are required to handle it. To this end, a so-called "soil-topology" convention has been developed which makes it possible to describe any kind of three-dimensional boundary. All numerical approximations of the governing equations are applied within this topology. In the present study, the finite-difference method is used to approximate the governing equations, and the solution grid is generated to conform as closely as possible to the aquifer topography.

This chapter is organized as follows: First, the governing equations for both the aquifer-matrix and the megapore network are presented. From now on the term "megapores" will be used instead of cave passages. Second, to highlight the unique features of groundwater flow in a karst region, a brief description is given of the topological structure of the aquifer. Third, the general computational strategy is briefly described. Fourth, the numerical techniques used to approximate the governing equations are described. Since the numerical techniques for the aquifer-matrix and the megapores are different, they are divided into two sections, one for each topic. Lengthy derivations are omitted in these sections, especially in the numerical approximations, so the basic idea can be delivered clearly. Detailed derivations are found in Appendix A. Fifth, iterative coupling between computation of the aquifer-matrix and of the megapores is explained. All numerical techniques described in this chapter are coded in a FORTRAN program named Labyrinth.

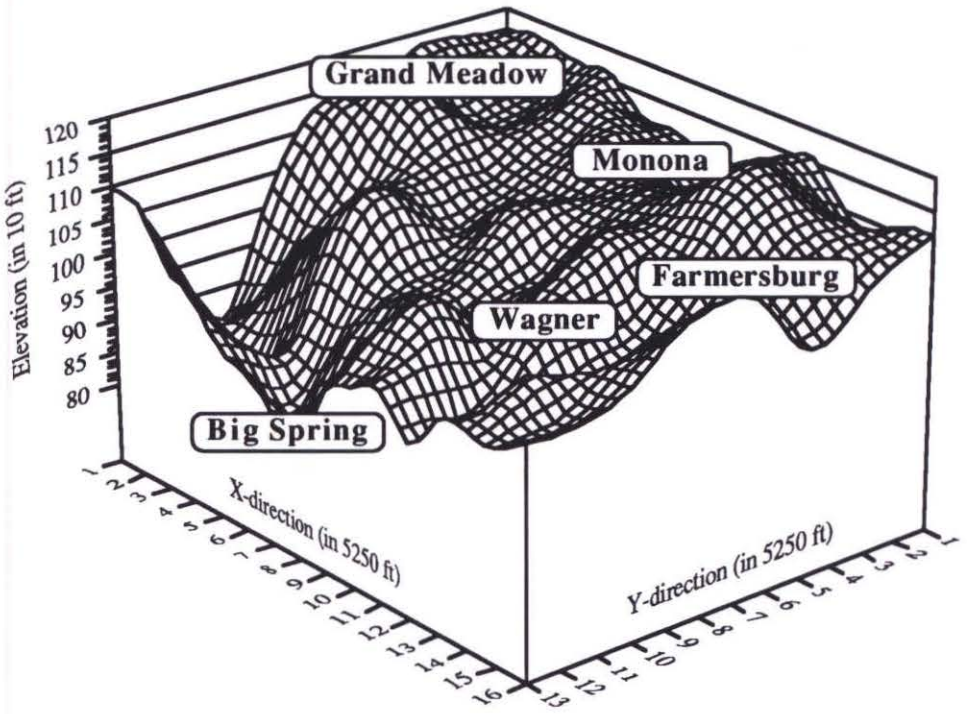

Figure 3.1. Southeast View of the Big Spring Basin

3.2. Governing Equations

This section describes in detail all the governing equations used in the present study: hydrodynamic equations, equations of pollutant transport, and mass exchange equations for both the aquifer-matrix and megapore network.

3.2.1. Hydrodynamic Equation for Aquifer-Matrix

The governing equation of flow in porous media is derived from the mass conservation law applied to a control volume. For practical purposes, the following assumptions are invoked (Bear, 1979, 1972).

(a) the velocity of the solids is small so Darcy's law still holds;

(b) specific storage (S) and hydraulic conductivity (K) are unaffected by the variation of porosity (e);

(c) spatial variations in water density, ρ, are much smaller than the local, temporal ones. Under these assumptions, for a nonhomogeneous, anisotropic saturated porous medium, the governing equation can be written in terms of piezometric head (h) as

$$\Delta x \frac{\partial}{\partial x}\left(A_x K_x \frac{\partial h}{dx} \right) + \Delta y \frac{\partial}{\partial y}\left(A_y K_y \frac{\partial h}{dy} \right) + \Delta z \frac{\partial}{\partial z}\left(A_z K_z \frac{\partial h}{dz} \right) - W = S\, \upsilon \frac{\partial h}{dt} \tag{3.1}$$

where K is hydraulic conductivity (LT^{-1}); h is piezometric head (L); W is volumetric source flux ($L^3 T^{-1}$); S is specific storage (L^{-1}); A is cross sectional area of aquifer in each direction, in a finite-difference block (L^2); Δ is the length of control volume in each direction (L); and

$$W = w\, \upsilon \tag{3.2}$$

In Eq. (3.2) w is the source term, volumetric flux per unit volume (T^{-1}); and υ is the volume of the aquifer in a finite-difference block (L^3). Volumetric flux, W, is the source exchange term between the aquifer-matrix and megapores.

3.2.2. Pollutant Transport Equation for Aquifer-Matrix

The governing equation of pollutant transport in porous media is also derived from the mass conservation law applied to a control volume. For a nonhomogeneous, anisotropic porous medium, the governing equation can be written in terms of concentration (C) as

$$\begin{aligned} &\Delta x \frac{\partial}{\partial x}\left(A_x D_x \frac{\partial C}{\partial x} \right) + \Delta y \frac{\partial}{\partial y}\left(A_y D_y \frac{\partial C}{\partial y} \right) + \Delta z \frac{\partial}{\partial z}\left(A_z D_z \frac{\partial C}{\partial z} \right) - \\ &\Delta x \frac{\partial}{\partial x}(A_x U_x C) - \Delta y \frac{\partial}{\partial y}(A_y U_y C) - \Delta z \frac{\partial}{\partial z}(A_z U_z C) - C_s W = \upsilon \frac{\partial C}{\partial t} \end{aligned} \tag{3.3}$$

$$\text{where } U_x = \frac{-K_x}{e}\frac{\partial h}{\partial x} \quad U_y = \frac{-K_y}{e}\frac{\partial h}{\partial y} \quad U_z = \frac{-K_z}{e}\frac{\partial h}{\partial z} \tag{3.4}$$

In Eq. (3.3) C is solute concentration (ML^{-3}); D is the dispersion coefficient (L^2T^{-1}); U is

seepage or average pore water velocity (LT^{-1}); C_s is solute concentration in the sources or sinks (ML^{-3}); e is effective porosity; and U_x, U_y, U_z and W are known quantities from the hydrodynamic computation.

3.2.3. Hydrodynamic Equation for Megapores

In the present study, the flow is restricted to one-dimensional, incompressible, full-megapore flow, the principal implication of which is that the discharge in a single megapore must at any instant be constant along its length. Of course the discharge may vary from one megapore to another along a series of megapores in a network due to external or aquifer-matrix inflow. From the law of conservation of momentum, the governing equation in any single megapore can be written as

$$\frac{\partial Q}{\partial t} + \frac{\partial}{\partial s}\left(\frac{Q^2}{A}\right) + gA\left(\frac{\partial h}{\partial s} + S_f\right) = 0 \tag{3.5}$$

Since $Q \neq Q(s)$ along a megapore, Eq. (3.5) can be rewritten as

$$\frac{\partial Q}{\partial t} - \left(\frac{Q}{A}\right)^2 \frac{\partial A}{\partial s} + gA\left(\frac{\partial h}{\partial s} + \frac{Q|Q|}{K^2}\right) = 0 \tag{3.6}$$

where t is time; s is the longitudinal megapore coordinate; Q(t) is megapore discharge; A(s) is megapore cross-sectional area; h(s,t) is the megapore piezometric head; $S_f(s,t)$ is megapore energy slope ($= \frac{Q|Q|}{K^2}$); K(s) is full-megapore conveyance; and g is gravitational acceleration. In Eq. (3.6), the four terms are associated with local acceleration, advective acceleration, net normal pressure force, and boundary shear force, respectively.

3.2.4. Pollutant Transport Equation for Megapores

The governing equation for pollutant transport can be derived from the law of mass conservation, with the same assumptions as those used to derive hydrodynamic equation.

Following the derivation given by Fischer et al. (1979), the pollutant transport equation can be generalized as

$$\frac{\partial(AC)}{\partial t} + \frac{\partial(AUC)}{\partial s} = \frac{\partial(A\,\varepsilon \frac{\partial C}{\partial s})}{\partial s} \tag{3.7}$$

Differentiating the left hand side of Eq. (3.7) and recognizing that $\frac{\partial A}{\partial t} + \frac{\partial(AU)}{\partial s} = 0$ from conservation of mass, Eq. (3.7) can be rewritten as

$$A\frac{\partial C}{\partial t} + AU\frac{\partial C}{\partial s} = \frac{\partial(A\,\varepsilon \frac{\partial C}{\partial s})}{\partial s} \tag{3.8}$$

where U(s,t) is velocity of megapore flow, and ε(s) is the megapore dispersion coefficient.

3.2.5. Mass Exchange Between Aquifer-Matrix and Megapores

The mass exchange between aquifer and megapores consists of two constituents, water discharge and pollutant flux. The water discharge exchange uses the same principle used in computing leakage through a semipermeable layer from an overlying (or underlying) aquifer into another aquifer with a different piezometric head (see Bear, 1979, page 36). Therefore, the amount of mass exchange can be computed as a linear function of the difference between the piezometric head inside the megapore and that of the aquifer-matrix surrounding the megapore. The equation of water discharge exchange can be written as

$$w = \alpha\,(h_s - h_p) \tag{3.9}$$

where α is the coefficient of exchange ($L^{-1}T^{-1}$); h_s is the piezometric head of the aquifer-matrix (L); and h_p is the piezometric head of the megapore (L).

For the pollutant flux exchange term the assumption is that the advective exchange term is dominant compared to that of the diffusive one. The equation for the pollutant exchange term thus becomes simply the concentration of pollutant in water multiplied by its water discharge:

$$w_s = C_s\, w \tag{3.10}$$

where w is as defined in Eq. (3.9).

3.3. Topological Structure of the Aquifer

The aquifer is represented by a three-dimensional block of computational grid points, referred to herein as *aquifer-matrix grid points*. The three-dimensional equations for aquifer-matrix water and pollutant movement are solved numerically on this computational grid.

Preferential flow paths, such as root-zone macropores or karst megapores, are represented as an interconnected network of so-called *pipes*, within which water and pollutant transport are represented as equivalent to flow in full pipes.

Exchange of water and pollutant between the aquifer-matrix and megapore passages is taken to occur only at aquifer-matrix grid points through which the pipe network passes; these intersections are called *nodes*. Thus, it is presumed that however the pipe network is generated (e.g., manually, through stochastic simulation, etc.), it is constrained to pass frequently through aquifer-matrix grid points; i.e., that nodes occur as densely as possible.

Figure 3.2 is a schematic depiction of a possible simple topological structure. The aquifer-matrix grid point coordinates of nodes are shown in parentheses. Nodes 1, 6, 12, 20, and 33 (shown as inverted triangles) represent intersections of the megapore structure with the ground surface; i.e., sinkholes. Nodes 5, 8, 16, and 23 are junctions of multiple pipe-network flow paths. Nodes 11, 19, 32, and many others not shown, represent aquifer-matrix grid points through which pass a single pipe-flow path.

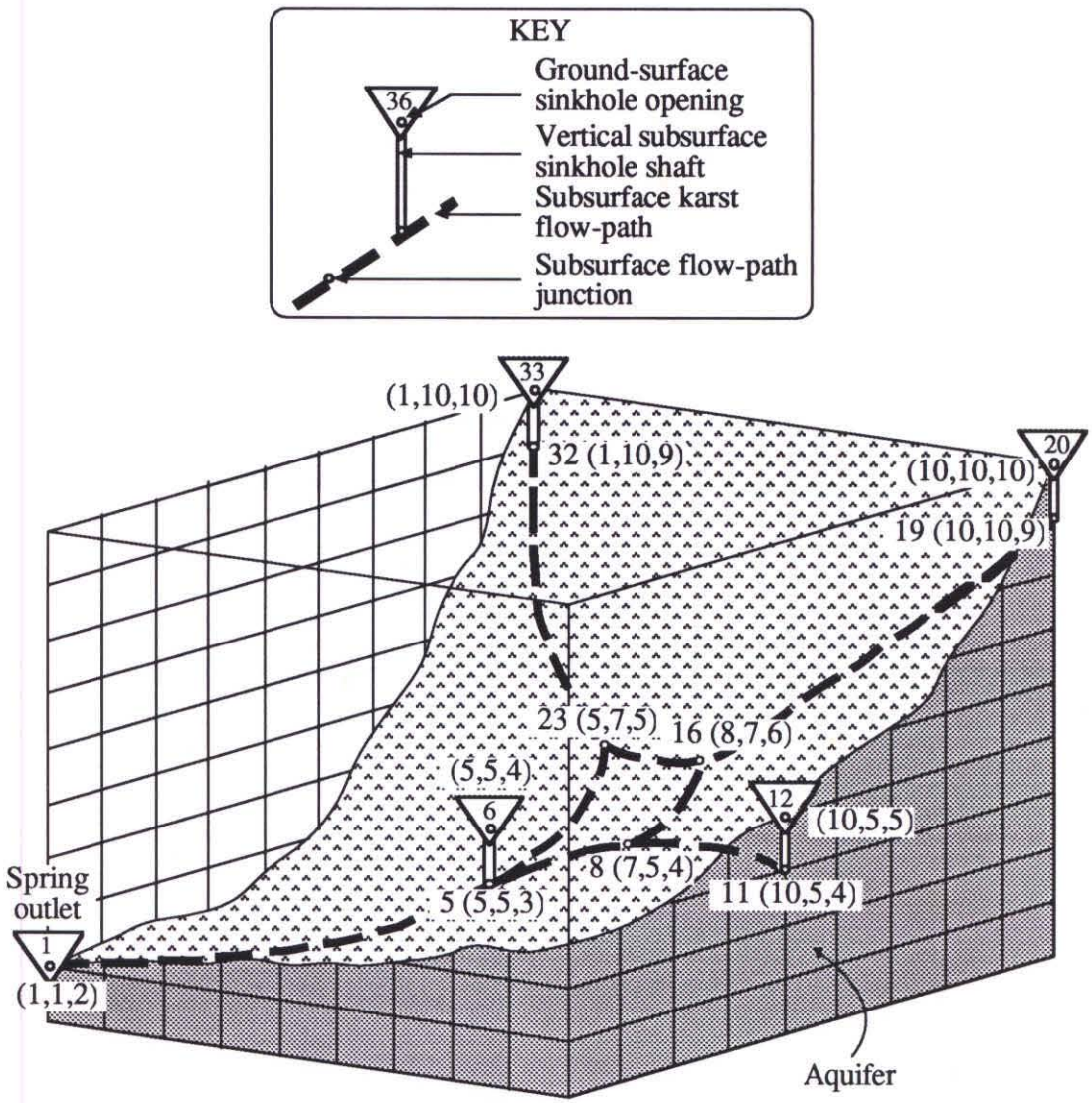

Figure 3.2. Schematic Representation of the Karst Aquifer

3.4. General Computational Strategy

Water and pollutant transport in the aquifer-matrix are essentially diffusive phenomena, governed by diffusion mass conservation equations whose dependent variables are heads and concentrations, respectively. Water and pollutant transport in the pipe network are essentially advective phenomena, governed by energy or momentum and mass conservation equations whose dependent variables are water discharges, heads and concentrations. The water and

pollutant exchange between the aquifer-matrix and pipe network is governed essentially by the differences in head and concentration between the two systems at any node. Recall that a node is defined as an aquifer-matrix grid point through which the pipe network passes. The heads and concentrations of both systems are coupled through the water and pollutant exchange. In principle, the entire system of equations — aquifer-matrix diffusion and pipe-network energy or momentum and mass conservation — must be solved simultaneously.

This simultaneous solution poses no fundamental conceptual problems. However, its practical execution would be extremely demanding of computer resources, especially for large and/or complex systems. Therefore, a fractional-step computational strategy is adopted whereby, for each of several iterations in a computational time interval, the aquifer-matrix and pipe-network equations are solved separately, their exchange-term coupling being represented only approximately in each iteration. The details of this procedure are developed in following three main sections. The first section describes the numerical solution of the governing equation for the aquifer-matrix. The second section explains the numerical solution of the governing equation for the pipe network. The last section elaborates the numerical procedure for approximating the exchange terms between aquifer-matrix and pipe network.

3.5. Numerical Solution for Aquifer-Matrix

3.5.1. Strategy for Approximate Solution

The aquifer-matrix algorithm is built on the principle of water and pollutant mass conservation at aquifer-matrix elemental control volumes. Aquifer-matrix grid points are generated based on the geometry of the Big Spring aquifer (Figure 3.1). Figure 3.3 shows the schematic representation of the aquifer as adjusted to conform with the finite-difference grid. To avoid using excessive computer time and resources, the split-direction approach is used. Thus, the governing equations, at any instant, are solved successively for each direction of the principal axis in Cartesian coordinate directions within the three-dimensional block, as depicted in Figure 3.3.

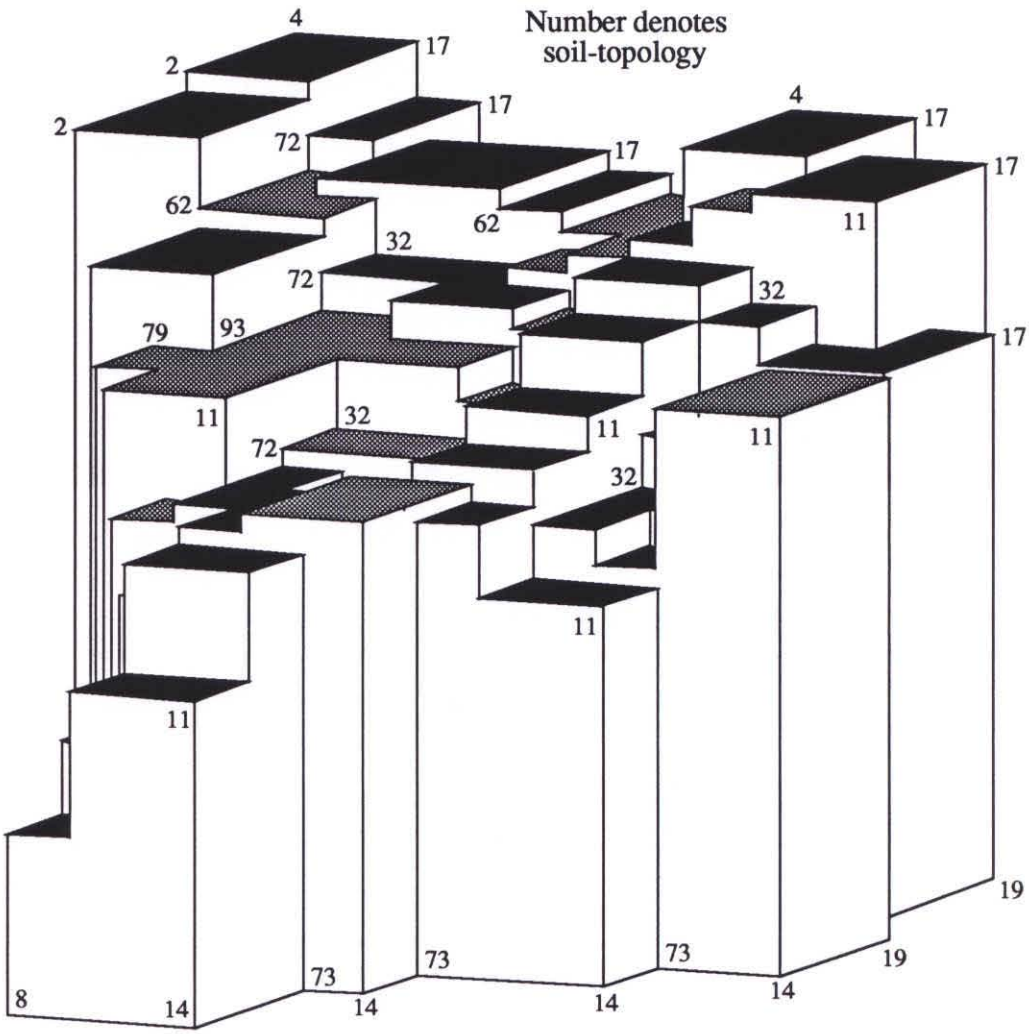

Figure 3.3. Schematic Geometry of the Aquifer after Adjustment to Conform with the Finite-Difference Grid

In any computational direction, the algorithm must recognize the boundary of the domain. For example, the algorithm must recognize that there is a valley between two hills, and computations must be performed on each hill while above the valley, where there is no aquifer-matrix, computations must not be performed. The soil-topology consisting of 118 unique orientations of the aquifer-matrix grid point with respect to the origin of the Cartesian coordinate, is used to define such a geometry. One aquifer-matrix grid point

associates with one unique soil-topology. Therefore, it is possible for several aquifer-matrix grid points to have the same soil-topology.

3.5.2. Split-Direction Approach for Approximating Hydrodynamic Equations

3.5.2.1. Development of the Finite-Difference Equations

This section discusses the finite-difference approximation of Eq. (3.1). To begin with, let us use $\delta_x^2 h$ to denote $\Delta x \frac{\partial}{\partial x}\left(A_x K_x \frac{\partial h}{dx} \right)$. Eq. (3.1) can thus be rewritten in a general finite-difference form as

$$\begin{aligned}&(1-\theta)\,\delta_x^2 h^n + \theta\,\delta_x^2 h^{n+1} + (1-\theta)\,\delta_y^2 h^n + \theta\,\delta_y^2 h^{n+1} + \\ &(1-\theta)\,\delta_z^2 h^n + \theta\,\delta_z^2 h^{n+1} - (1-\theta)\,W^n + \theta\,W^{n+1} = \frac{S_v}{\Delta t}(h^{n+1}-h^n)\end{aligned} \tag{3.11}$$

where θ ($0 \le \theta \le 1$) is an implicitation factor; i.e., $\theta = 1 \Rightarrow$ "fully implicit" and $\theta = 0 \Rightarrow$ "fully explicit." All other symbols have been previously defined.

The exchange term, w (or W), is the term that actually couples the megapore network computation with that of the aquifer-matrix. The aquifer-matrix exchange inflow W^{n+1} can be written as

$$W^{n+1} = W\left(h_m^{n+1}, h_{ijk}^{n+1} \right) \tag{3.12}$$

that is, as some function of the pipe-network nodal head h_m^{n+1} and the aquifer-matrix head h_{ijk}^{n+1} at the aquifer-matrix grid point associated with node m, at future time t_{n+1}.

Now, in general, a Taylor-series expansion of W^{n+1} can be written as

$$W^{n+1} = W(h_m^{n+1}, h_{ijk}^{n+1}) \approx W(h_m, h_{ijk}) + \frac{\partial W}{\partial h_m}\Delta h_m + \frac{\partial W}{\partial h_{ijk}}\Delta h_{ijk} \tag{3.13}$$

where h_m and h_{ijk} represent the latest iterative estimates of h_m^{n+1} and h_{ijk}^{n+1}, and Δh_m and Δh_{ijk} are unknown corrections to those estimates. For convenience, Δh_{ijk} is rewritten as Δh_s so Eq. (3.13) becomes

$$W^{n+1} = W(h_m^{n+1}, h_s^{n+1}) \approx W(h_m, h_s) + \frac{\partial W}{\partial h_m}\Delta h_m + \frac{\partial W}{\partial h_s}\Delta h_s \tag{3.14}$$

Eq. (3.14) must be recast to conform with the split-direction approach. The source term, W^{n+1} or w^{n+1}, must be split into x-, y-, and z-directions. Thus, Eq. (3.14) becomes

$$W^{n+1} = W^n + \frac{\partial W}{\partial h_s}(h^x - h^n) + \frac{\partial W}{\partial h_s}(h^y - h^x) + \frac{\partial W}{\partial h_s}(h^{n+1} - h^y) + \frac{\partial W}{\partial h_m}\Delta h_m$$

or

$$W^{n+1} = W^n + \frac{\partial W}{\partial h_s}(h^x - h^n) + \frac{\partial W}{\partial h_s}(h^y - h^x) + \frac{\partial W}{\partial h_s}(h^{n+1} - h^y) + \frac{\partial W}{\partial h_m}(h_m - h_m^n) \tag{3.15}$$

where n+1 denotes the end of the current time step; h^n is the aquifer piezometric head at the end of the previous time step; h^x is the aquifer piezometric head at the end of the x-direction computational step; h^y is the aquifer piezometric head at the end of the y-direction computational step; h^{n+1} is the aquifer piezometric head at the end of the z-direction computational step, which is the same as the aquifer piezometric head at the end of the current time step; h_m is the latest estimate of the pipe piezometric head; and h_m^n is the pipe piezometric head at the end of the previous time step.

Now $\frac{S}{\Delta t}(h^{n+1} - h^n)$ in Eq. (3.11) can be rewritten as

$$\frac{S}{\Delta t}(h^{n+1} - h^y + h^y - h^x + h^x - h^n) \tag{3.16}$$

Substitution of Eqs. (3.15) and (3.16) into Eq. (3.11) yields

$$\begin{pmatrix} (1-\theta)\,\delta_x^2 h^n + \theta\,\delta_x^2 h^{n+1} - \frac{1}{3} W^n - \theta \frac{\partial W}{\partial h_s}(h^x - h^n) - \frac{\theta}{3}\frac{\partial W}{\partial h_m}(h_m - h_m^n) + \\ (1-\theta)\,\delta_y^2 h^n + \theta\,\delta_y^2 h^{n+1} - \frac{1}{3} W^n - \theta \frac{\partial W}{\partial h_s}(h^y - h^x) - \frac{\theta}{3}\frac{\partial W}{\partial h_m}(h_m - h_m^n) + \\ (1-\theta)\,\delta_z^2 h^n + \theta\,\delta_z^2 h^{n+1} - \frac{1}{3} W^n - \theta \frac{\partial W}{\partial h_s}(h^{n+1} - h^y) - \frac{\theta}{3}\frac{\partial W}{\partial h_m}(h_m - h_m^n) \end{pmatrix} =$$

$$\begin{pmatrix} \frac{S\upsilon}{\Delta t}(h^x - h^n) + \\ \frac{S\upsilon}{\Delta t}(h^y - h^x) + \\ \frac{S\upsilon}{\Delta t}(h^{n+1} - h^y) \end{pmatrix} \tag{3.17}$$

In the fractional-step sense, Eq. (3.17) can be generalized and written as

$$(1-\theta)\,\delta^2 h^n + \theta\,\delta^2 h^{n+1} - \frac{1}{3} W^n - \theta \frac{\partial W}{\partial h_s}(h^{n+1} - h^n) - \frac{\theta}{3}\frac{\partial W}{\partial h_m}(h_m - h_m^n) = \frac{S\upsilon}{\Delta t}(h^{n+1} - h^n) \tag{3.18}$$

Discretization of Eq. (3.18) using the Crank-Nicholson (C-N) scheme yields

$$\begin{aligned} &(1-\theta)\{A\,h_{i-1}^n - (A+B)\,h_i^n + B\,h_{i+1}^n\} + \\ &\theta\{A\,h_{i-1}^{n+1} - (A+B)\,h_i^{n+1} + B\,h_{i+1}^{n+1}\} - \\ &\frac{1}{3} W^p - \theta \frac{\partial W}{\partial h_i}(h_i^{n+1} - h_i^n) - \frac{\theta}{3}\frac{\partial W}{\partial h_m}(h_m - h_m^p) = \frac{S\upsilon}{\Delta t}(h_i^{n+1} - h_i^n) \end{aligned} \tag{3.19}$$

where h_m is the latest estimate of the pipe piezometric head; h_m^p is the pipe piezometric head at the end of the previous time step; A and B are known coefficients as defined in Appendix A. Further manipulation and grouping the terms of Eq. (3.19) yields

$$\begin{aligned} -\theta A\,h_{i-1}^{n+1} + \left\{\theta\left(A + B + \frac{\partial W}{\partial h_i}\right) + \frac{S\upsilon}{\Delta t}\right\} h_i^{n+1} - \theta B\,h_{i+1}^{n+1} = \\ (1-\theta)\{A\,h_{i-1}^n - (A+B)\,h_i^n + B\,h_{i+1}^n\} - \\ \frac{1}{3} W^p + \theta \frac{\partial W}{\partial h_i} h_i^n - \frac{\theta}{3}\frac{\partial W}{\partial h_m}(h_m - h_m^p) + \frac{S\upsilon}{\Delta t} h_i^n \\ \text{for } i = 2, \ldots., N-1 \end{aligned} \tag{3.20}$$

In matrix form, Eq. (3.20) can be written as

$$[\mathbf{M}]\{\mathbf{h}\} = \{\mathbf{F}\} \tag{3.21}$$

where [**M**] is a tri-diagonal matrix whose N–2 elements comprise contributions from the left hand side of Eq. (3.20), and {**F**} is an N–2 element vector of known quantities from the right hand side of Eq. (3.20). In Eq. (3.21), there are N unknowns with (N–2) equations, so two more equations from boundary conditions are needed, as described in the following paragraphs.

3.5.2.2. Boundary Conditions

General boundary conditions (BC) of the problem are of the mixed type:

$$C_1\, h + C_2 \frac{\partial h}{\partial x} = C_t\,(\,x,y,z,t\,) \tag{3.22}$$

where C_1, C_2 are arbitrary constants and C_t is a time dependent constant. By imposing a general BC of the mixed type, it is easy to handle either "Dirichlet" or "Neuman" boundary conditions. The several cases of boundary conditions may be handled as follows:

a. Imposed head — "Dirichlet" type $\Rightarrow$ $(C_2 = 0)$

$$h_i = \frac{C_t}{C_1} \Rightarrow \text{set } A_i = C_i = 0 \text{ and } B_i = 1,\quad D_i = \frac{C_t}{C_1}\ ,\ \text{for}\ \ i = 1,2,\ldots, N \tag{3.23a}$$

b. Imposed discharge — "Neumann" type $\Rightarrow$ $(C_1 = 0)$

$$\frac{\partial h}{\partial x} = \frac{C_t}{C_2} \tag{3.23b}$$

c. Mixed-type boundary:

$$C_1 \neq 0,\ C_2 \neq 0 \tag{3.23c}$$

The discretization of the governing equations on the boundary needs special treatment since the second derivative of piezometric heads must be discretized. For interior nodes, the derivative can always be expressed in terms of the piezometric head of the points which neighbor the node of interest, while on the boundary, there is only one neighboring point. Thus, the discretization used for interior nodes can no longer be used The assumption is

made that, in the neighborhood of boundary points, a Taylor-series expansion is applicable.

Substituting the boundary condition, Eq. (3.22), for the first computational point $-\frac{\partial h}{\partial x} = \frac{C_1}{C_2} h_1 - \frac{C_t}{C_2}$ into the Taylor-series expansion for h_2 around h_1, at any time level, yields

$$K_x \left[\frac{\partial^2 h}{\partial x^2}\right]_1 = \frac{2K_x}{\Delta x^2}\left\{h_2 + \left(\frac{C_1}{C_2}\Delta x - 1\right) h_1 - \frac{C_t}{C_2}\Delta x\right\} \tag{3.24}$$

Rewriting Eq. (3.24) using the C-N scheme and substituting into Eq. (3.18), one obtains the discretized governing equation for the first computational point:

$$\begin{aligned}
&(1-\theta)\frac{2K_x}{\Delta x^2}\{\, h_2^n + (\frac{C_1}{C_2}\Delta x - 1)\, h_1^n - \frac{C_t^n}{C_2}\Delta x\,\} + \\
&\theta\frac{2K_x}{\Delta x^2}\{\, h_2^{n+1} + (\frac{C_1}{C_2}\Delta x - 1)\, h_1^{n+1} - \frac{C_t^{n+1}}{C_2}\Delta x\,\} - \\
&\frac{1}{3} w^p - \theta\frac{\partial w}{\partial h_s}(h_1^{n+1} - h_1^n) - \frac{\theta}{3}\frac{\partial w}{\partial h_m}(h_m - h_m^p) = \frac{S}{\Delta t}(h_1^{n+1} - h_1^n)
\end{aligned} \tag{3.25}$$

Substitution of the boundary condition, Eq. (3.22), for the last computational point into the Taylor-series expansion for h_N around h_{N-1}, at any time level, yields

$$\begin{aligned}
K_x\left[\frac{\partial^2 h}{\partial x^2}\right]_N &= \frac{2K_x}{\Delta x^2}\left\{h_{N-1} - h_N + \left[\frac{\partial h}{\partial x}\right]_N \Delta x\right\} \\
&= \frac{2K_x}{\Delta x^2}\left\{h_{N-1} - h_N + \frac{C_1}{C_2}\Delta x\, h_N - \frac{C_t}{C_2}\Delta x\right\}
\end{aligned} \tag{3.26}$$

Rewriting Eq. (3.26) using the C-N scheme and substituting into Eq. (3.18), one obtains the discretized governing equation for the last computational point:

$$\begin{aligned}
&(1-\theta)\frac{2K_x}{\Delta x^2}\left\{h_{N-1}^n + \left(\frac{C_1}{C_2}\Delta x - 1\right) h_N^n - \frac{C_t^n}{C_2}\Delta x\right\} + \\
&\theta\frac{2K_x}{\Delta x^2}\left\{h_{N-1}^{n+1} + \left(\frac{C_1}{C_2}\Delta x - 1\right) h_N^{n+1} - \frac{C_t^{n+1}}{C_2}\Delta x\right\} - \\
&\frac{1}{3} w^p - \theta\frac{\partial w}{\partial h_s}(h_N^{n+1} - h_N^n) - \frac{\theta}{3}\frac{\partial w}{\partial h_m}(h_m - h_m^p) = \frac{S}{\Delta t}(h_N^{n+1} - h_N^n)
\end{aligned} \tag{3.27}$$

Now all the requirements to solve Eq. (3.21) have been met, except for the first time step, in which an initial condition is needed to start the computation.

3.5.2.3. Initial Condition

The initial condition for the governing equation, Eq. (3.1) or the working equation, Eq. (3.21), consists of given piezometric heads, h, at all computational points in the aquifer-matrix domain.

3.5.3. Split-Direction Approach for Approximating Pollutant Transport Equations

3.5.3.1. Development of the Finite-Difference Equations

The development of the finite-difference approximation uses the technique described in Section 3.5.2. The governing equation is recast to accommodate the split-direction approach and then the C-N scheme is applied to the equation. Equation (3.3) may be written, for the x-direction, as follows:

$$\Delta x \frac{\partial}{\partial x}\left(A_x D_x \frac{\partial C}{\partial x}\right) - \Delta x \frac{\partial}{\partial x}(A_x U_x C) - \frac{C_s W}{3} = \upsilon \frac{\partial C}{\partial t} \tag{3.28}$$

Its discretization using the Crank-Nicholson scheme yields

$$\begin{aligned} &\theta \{A\, C_{i-1}^{n+1} - (A+B)\, C_i^{n+1} + B\, C_{i+1}^{n+1}\} + \\ &(1-\theta) \{A\, C_{i-1}^{n} - (A+B)\, C_i^{n} + B\, C_{i+1}^{n}\} - \\ &\frac{\theta}{2}\left(A_r\, C_{i+1}^{n+1} U_{i+1}^{n+1} + (A_r - A_l)\, C_i^{n+1} U_i^{n+1} - A_l\, C_{i-1}^{n+1} U_{i-1}^{n+1}\right) - \\ &\frac{(1-\theta)}{2}\left(A_r\, C_{i+1}^{n} U_{i+1}^{n} + (A_r - A_l)\, C_i^{n} U_i^{n} - A_l\, C_{i-1}^{n} U_{i-1}^{n}\right) - \\ &\theta \frac{C_s^{n+1} W_i^{n+1}}{3} - (1-\theta) \frac{C_s^{n} W_i^{n}}{3} = \frac{\upsilon\,(C_i^{n+1} - C_i^{n})}{\Delta t} \\ &\text{for } i = 2, \ldots., N-1 \end{aligned} \tag{3.28a}$$

where A_r and A_l indicate the area of the right and left sides of a finite-difference block.

Eq. (3.28a) can be written, in matrix form, as

$$[\mathbf{M}]\{\mathbf{C}\} = \{\mathbf{F}\} \tag{3.29}$$

where [**M**] is a tri-diagonal matrix whose N–2 elements comprise contributions from the left hand side of Eq. (3.28a); {**F**} is an N–2 element vector of known quantities from the right hand side of Eq. (3.28a); and {**C**} is an N–2 element vector of unknown pollutant concentrations.

In Eq. (3.28a), there are N unknowns with (N–2) equations. Two boundary condition equations are required to solve Eq. (3.28a).

3.5.3.2. Boundary Conditions

General boundary conditions (BC) of the problem are of the mixed type:

$$E_1 C + E_2 \frac{\partial C}{\partial x} = E_t (x,y,z,t) \tag{3.30}$$

where E_1, E_2 are arbitrary constants and E_t is a time-dependent constant. As mentioned in Section 3.5.2.2., several cases of boundary conditions may be handled as follows:

a. Imposed concentration — "Dirichlet" type $\Rightarrow$ $(E_2 = 0)$

$$C_i = \frac{E_t}{E_1} \Rightarrow \text{set } P_i = R_i = 0 \text{ and } Q_i = 1,\ S_i = \frac{E_t}{E_1},\ \text{for } i = 1,2, ..., N \tag{3.31a}$$

b. Imposed discharge — "Neumann" type $\Rightarrow$ $(E_1 = 0)$

$$\frac{\partial C}{\partial x} = \frac{E_t}{E_2} \tag{3.31b}$$

c. Mixed-type boundary:

$$E_1 \neq 0,\ E_2 \neq 0 \tag{3.31c}$$

The technique described in Section 3.5.2.2. can be used on the boundary. Using the C-N scheme and changing the appropriate variables, Eq. (3.28) can be rewritten for the first

computational point as

$$\theta \frac{2D_x}{\Delta x^2} \{ C_2^{n+1} + (\frac{E_1}{E_2}\Delta x - 1) C_1^{n+1} - \frac{E_t^{n+1}}{E_2}\Delta x \} +$$
$$(1-\theta) \frac{2D_x}{\Delta x^2} \{ C_2^{n} + (\frac{E_1}{E_2}\Delta x - 1) C_1^{n} - \frac{E_t^{n}}{E_2}\Delta x \} -$$
$$\theta \frac{U_2^{n+1} C_2^{n+1} - U_1^{n+1} C_1^{n+1}}{\Delta x} - (1-\theta) \frac{U_2^{n} C_2^{n} - U_1^{n} C_1^{n}}{\Delta x} -$$
$$\theta \frac{C_s^{n+1} w_1^{n+1}}{3} - (1-\theta) \frac{C_s^{n} w_1^{n}}{3} = \frac{C_1^{n+1} - C_1^{n}}{\Delta t} \qquad (3.32)$$

and for the last computational point as

$$\theta \frac{2D_x}{\Delta x^2} \{ C_{N-1}^{n+1} + (\frac{E_1}{E_2}\Delta x - 1) C_N^{n+1} - \frac{E_t^{n+1}}{E_2}\Delta x \} +$$
$$(1-\theta) \frac{2D_x}{\Delta x^2} \{ C_{N-1}^{n} - (\frac{E_1}{E_2}\Delta x - 1) C_N^{n} - \frac{E_t^{n}}{E_2}\Delta x \} -$$
$$\theta \frac{U_N^{n+1} C_N^{n+1} - U_{N-1}^{n+1} C_{N-1}^{n+1}}{\Delta x} - (1-\theta) \frac{U_N^{n} C_N^{n} - U_{N-1}^{n} C_{N-1}^{n}}{\Delta x} -$$
$$\theta \frac{C_s^{n+1} w_N^{n+1}}{3} - (1-\theta) \frac{C_s^{n} w_N^{n}}{3} = \frac{C_N^{n+1} - C_N^{n}}{\Delta t} \qquad (3.33)$$

In Eqs. (3.28a), (3.32), and (3.33), C_s and w depend on whether w is coming from the aquifer-matrix itself or from megapores. The detailed derivation for both cases is explained in Appendix A.

3.5.3.3. Initial Condition

The initial condition for the governing equation, Eq. (3.3) or the working equation, Eq. (3.29), is given pollutant-concentrations, C, at all computational points in the aquifer-matrix domain.

3.6. Numerical Solution for Megapores

The numerical solution for megapores is achieved by first solving the hydrodynamic equations and then the pollutant transport equation. For hydrodynamic equations, the so-

called Preissmann method is used. For pollutant transport, the split-process approach is used. First, the pure advection equation is solved by a characteristic method using the Holly-Preissmann technique. Second, the pure diffusion equation is solved by the Preissmann method. The advantage of solving the pollutant transport equation using the split-process approach is that one can then compute any complex network in a downstream-marching fashion. That is, the computation starts from the most upstream point in the network and proceeds until it reaches the most downstream node. The split approach saves computer time since it avoids inverting a large matrix as is done in a direct approach.

3.6.1. Approximate Solution of Hydrodynamic Equations

3.6.1.1. Strategy for Approximate Solution

The megapore network, on which all megapore computations are carried out in the study, is manually generated based on data obtained from the study done by Hallberg et al. (1983). The gross megapore layout is presumed to follow gross flow paths from field data. The two-dimensional representation of the network is given in Figure 3.4. All horizontal, almost horizontal, and vertical megapores are represented in Figure 3.4.

The megapore network algorithm is built on the principle of water mass conservation at looped nodes. A looped node is defined herein as a node (i.e., aquifer-matrix grid point through which the pipe network passes) which is either

1. an entrance to or exit from the network, or
2. a junction of multiple (more than two) flow paths.

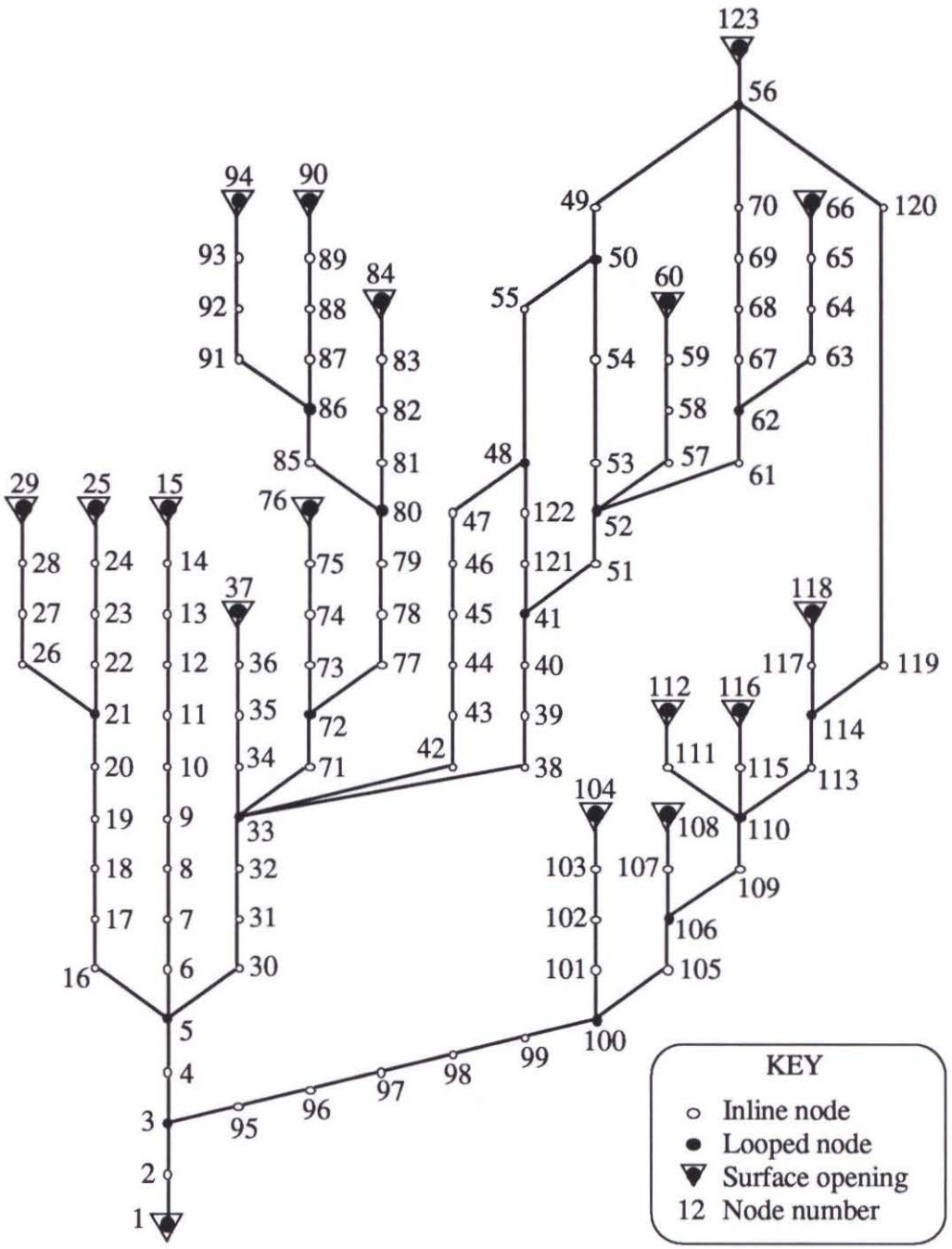

Figure 3.4. Schematic Representation of the Megapore Network

Thus, by this definition, nodes 1, 5, 6, 8, 12, 16, 20, 23, and 33 in Figure 3.2 are all looped nodes. Any unique flow path linking two looped nodes is defined herein as a link. In

connecting two looped nodes, a link may pass through other nodes which are not looped; these are called inline nodes. Any two adjacent nodes, be they inline or looped, are connected by a segment of a link called a pipe. A link may comprise only one pipe. Finally, any pipe can be divided into a series of computational points connected by computational reaches. A pipe always has one computational point contiguous with the node to which it is attached at each end. Figures 3.5 and 3.6 summarize these definitions.

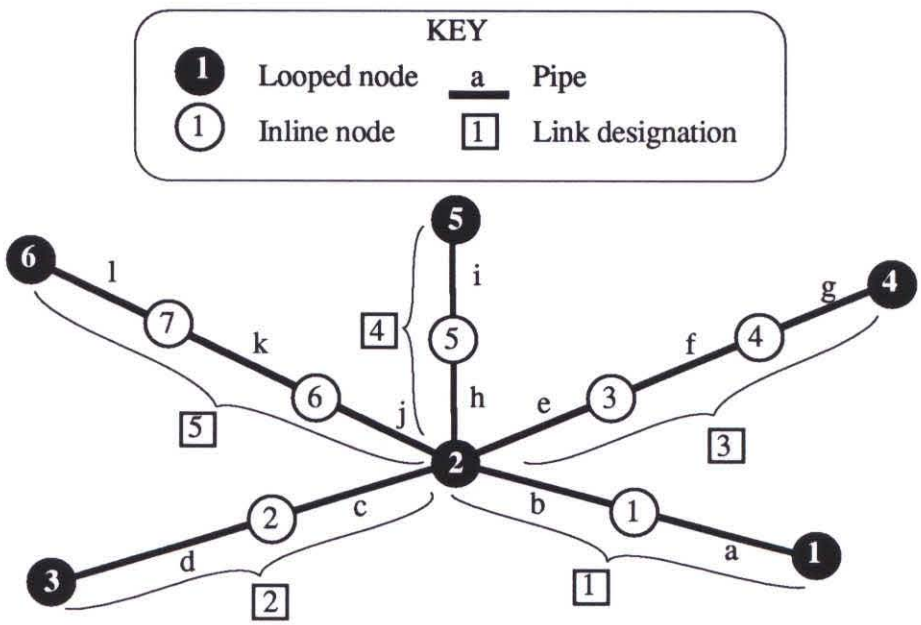

Figure 3.5. Megapore Topological Definitions

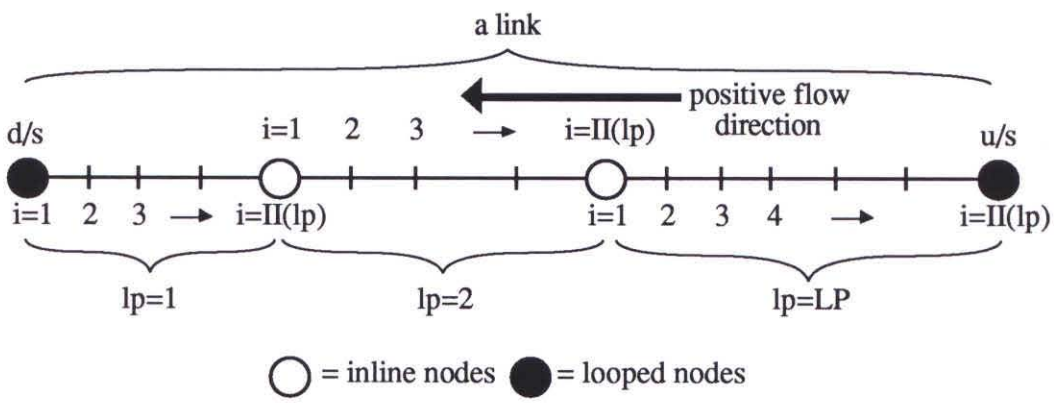

Figure 3.6. Definition Sketch for Link/Pipe Computation

3.6.1.2. Nodal Continuity

At any node m, and in particular at any looped node, the following statement of water continuity (inflow = outflow) must be satisfied at any instant (see Figure 3.7):

$$\sum_{lp} Q_{lp}^{n+1} + Q_m^{n+1} + W_m^{n+1} = 0 \ , \quad m = 1, 2, 3, \ldots \tag{3.34}$$

where n+1 denotes the end of the current time step; Q_{lp}^{n+1} is discharge entering node m from pipe lp; Q_m^{n+1} is external inflow entering node m; W_m^{n+1} is inflow entering node m from the aquifer-matrix; and summation is over all the pipes attached to node m (one at the end of each attached link).

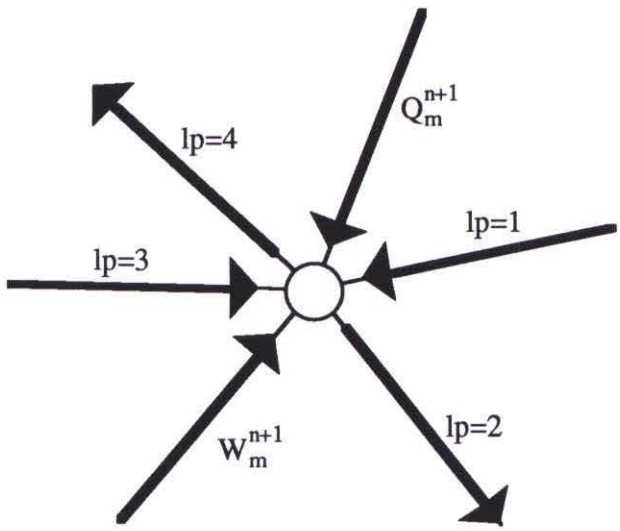

Figure 3.7. Continuity at a Looped Node

Now, the external inflow Q_m^{n+1} is a known quantity; indeed at boundary nodes, it is the sinkhole or other point inflow which drives the system. The pipe inflow can be written as

$$Q_{lp}^{n+1} = Q_{lp} + \Delta Q_{lp} \tag{3.35}$$

where Q_{lp} is the latest iterative estimate of Q_{lp}^{n+1}, and ΔQ_{lp} is an unknown correction to that estimate.

The aquifer-matrix exchange inflow W_m^{n+1} can be written as

$$W_m^{n+1} = W\,(\,h_m^{n+1},\, h_{ijk}^{n+1}\,) \tag{3.36}$$

That is, the aquifer-matrix exchange inflow is represented as a function of the pipe-network nodal head h_m^{n+1} and the aquifer-matrix head h_{ijk}^{n+1} at the aquifer-matrix grid point associated with node m. The Taylor-series expansion of W_m^{n+1} is

$$W_m^{n+1} = W\,(h_m^{\,n+1},\, h_{ijk}^{\,n+1}\,) \approx W\,(h_m\,,\, h_{ijk}\,) + \frac{\partial W}{\partial h_m}\,\Delta h_m + \frac{\partial W}{\partial h_{ijk}}\,\Delta h_{ijk} \tag{3.37}$$

where h_m and h_{ijk} represent the latest iterative estimates of h_m^{n+1} and h_{ijk}^{n+1}, and Δh_m and Δh_{ijk} are unknown corrections to those estimates.

In fractional-step computations, the aquifer-matrix heads h_{ijk}^{n+1} are held fixed during the pipe-network computation. Consequently, in Eq. (3.37), $\Delta h_{ijk} = 0$, and substitution of Eqs. (3.35) and (3.37) into Eq. (3.34) yields

$$\sum_{lp} (Q_{lp} + \Delta Q_{lp}) + Q_m^{n+1} + W_m + \frac{\partial W}{\partial h_m}\,\Delta h_m = 0\,,\quad m = 1, 2, .. \tag{3.38}$$

or

$$\sum_{in} (Q_d + \Delta Q_d\,) - \sum_{out} (Q_u + \Delta Q_u\,) + Q_m^{n+1} + W_m + \frac{\partial W}{\partial h_m}\,\Delta h_m = 0\,,\quad m = 1, 2, .. \tag{3.39}$$

Equation (3.39) is not yet in a form which can be used to compute head corrections, since Δh_m, as well as two or more ΔQ_{lp}, are unknowns. The key to the solution algorithm is the manipulation of the finite-difference approximations for the pipe-flow equations. These can be made to yield linear relations between discharge corrections ΔQ_{lp} and nodal head corrections Δh_{mm} at looped nodes mm at either end of a link. In particular, for a link whose upstream node is denoted u and whose downstream node is denoted d, we can derive the following two relations:

$$\Delta Q_d = \frac{\Delta h_u - FF_u - HH_u \Delta h_d}{EE_u} \tag{3.40}$$

$$\Delta Q_u = \frac{\Delta h_u - F_u - H_u \Delta h_d}{E_u} \tag{3.41}$$

where ΔQ_d and ΔQ_u are the discharge corrections at the pipe computational points contiguous with nodes d and u; Δh_d and Δh_u are the head corrections at nodes d and u; and E_u, F_u, H_u, EE_u, FF_u, and HH_u are known coefficients derived in the link forward sweep as described below.

In Eq. (3.39), the summation over the pipes connected to a node can be thought of as a summation over the connected links, as each connected pipe is simply the end of a link. Moreover, the summation implies consistent recognition of pipe sign conventions, with inflows taken as positive and outflows taken as negative. Substitution of Eqs. (3.40) and (3.41) into Eq. (3.39) yields

$$\sum_{in} Q_d + \sum_{in} \frac{\Delta h_u - FF_u - HH_u \Delta h_m}{EE_u} - \sum_{out} Q_u - \sum_{out} \frac{\Delta h_m - F_u - H_u \Delta h_d}{E_u} + Q_m^{n+1} + W_m + \frac{\partial W}{\partial h_m} \Delta h_m = 0 \tag{3.42}$$

As seen in Figure 3.8, in the "in" summation, Δh_d represents the current node Δh_m, and Δh_u represents the looped node at the other end of the inflow link. Similarly, in the "out" summation, Δh_u represents the current node Δh_m, and Δh_d represents the looped node at the other end of the outflow link. Therefore, Eq. (3.42) can be rewritten as

$$\left(\frac{\partial W}{\partial h_m} - \sum_{in} \frac{HH_u}{EE_u} - \sum_{out} \frac{1}{E_u}\right) \Delta h_m + \sum_{in} \frac{1}{EE_u} \Delta h_u + \sum_{out} \frac{H_u}{E_u} \Delta h_d = - \sum_{in} \left(Q_d - \frac{FF_u}{EE_u}\right) + \sum_{out} \left(Q_u - \frac{F_u}{E_u}\right) - Q_m^{n+1} - W_m \quad \text{for } m = 1, 2, \tag{3.43}$$

Since Eq. (3.43) can be written for each of M looped nodes, the entire system of linear equations is:

$$[\mathbf{A}]\{\Delta \mathbf{h}_m\} = \{\mathbf{B}\} \tag{3.44}$$

where [**A**] is an M x M coefficient matrix whose elements comprise contributions from the left hand side of Eq. (3.43); {**B**} is an M-element vector of known quantities from the right hand side of Eq. (3.43); and $\{\Delta \mathbf{h}_m\}$ is the M-element vector of unknown corrections to heads at looped nodes.

Solving Eq. (3.43) yields the head corrections $\{\Delta \mathbf{h}_m\}$. Thus the looped nodal heads can be corrected immediately; their use in the link return sweep is described below.

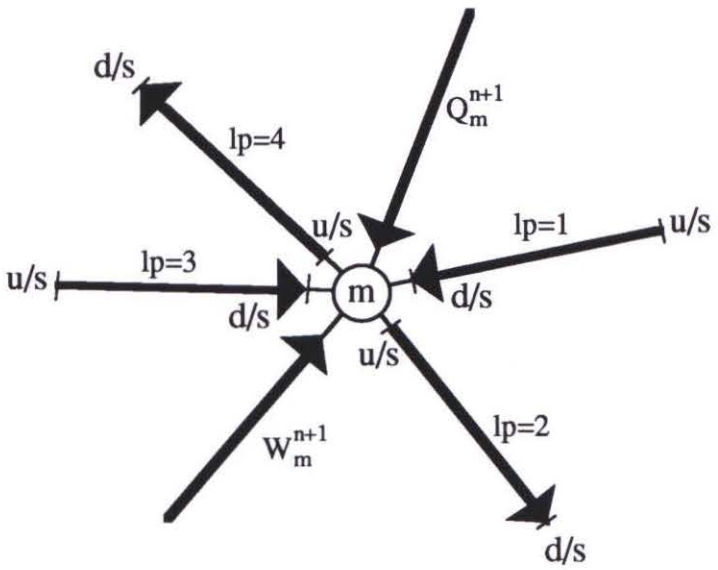

Figure 3.8. Summation Definition at a Node

3.6.1.3. Pipe Flow Dynamics

The coefficients of Eqs. (3.40) and (3.41), result from a so-called *forward sweep* in which the appropriate pipe conservation equations are expressed algebraically through use of finite-difference approximations.

Using Preissmann's four-point scheme (Cunge et al., 1980) to discretize Eq. (3.6) for a reach between two computational points i and i+1 (see Figure 3.6) yields

$$\frac{Q^{n+1}-Q^{n}}{\Delta t}-\left[\varphi\left(\frac{(Q/A)_{i}^{n+1}+(Q/A)_{i+1}^{n+1}}{2}\right)^{2}+(1-\varphi)\left(\frac{(Q/A)_{i}^{n}+(Q/A)_{i+1}^{n}}{2}\right)^{2}\right]\times$$

$$\left[\varphi\frac{A_{i}^{n+1}-A_{i+1}^{n+1}}{\Delta s}+(1-\varphi)\frac{A_{i}^{n}-A_{i+1}^{n}}{\Delta s}\right]+$$

$$g\left(\varphi\frac{A_{i}^{n+1}+A_{i+1}^{n+1}}{2}+(1-\varphi)\frac{A_{i}^{n}+A_{i+1}^{n}}{2}\right)\left\{\varphi\frac{h_{i}^{n+1}-h_{i+1}^{n+1}}{\Delta s}+(1-\varphi)\frac{h_{i}^{n}-h_{i+1}^{n}}{\Delta s}+\right.$$

$$\left.\frac{\varphi}{2}\left(\frac{Q^{n+1}|Q^{n+1}|}{K_{i}^{2}}+\frac{Q^{n+1}|Q^{n+1}|}{K_{i+1}^{2}}\right)+\frac{1-\varphi}{2}\left(\frac{Q^{n}|Q^{n}|}{K_{i}^{2}}+\frac{Q^{n}|Q^{n}|}{K_{i+1}^{2}}\right)\right\}=0 \qquad (3.45)$$

where the n and n+1 superscripts denote times t_n and $t_{n+1} = t_n + \Delta t$; Δs denotes the length of the computational reach; and φ is Preissmann's time weighting parameter, $0.5 \le \varphi \le 1.0$. It should be noted that the full-pipe invariance of Q along the pipe obviates the need for a computational point subscript on Q.

In Eq. (3.45), all quantities with n+1 superscripts are unknown. Since the pipe area and conveyance are known quantities for the full-pipe situation, Eq. (3.45) can be written as

$$F(Q^{n+1}, h_{i}^{n+1}, h_{i+1}^{n+1}) = 0 \qquad (3.46)$$

As long as the function F is continuous in the neighborhood of the solution, Eq. (3.46) can be written as the first term of the Taylor-series expansion

$$F(Q^{n+1}, h_{i}^{n+1}, h_{i+1}^{n+1}) \approx F(Q, h_{i}, h_{i+1}) + \frac{\partial F}{\partial Q}\Delta Q + \frac{\partial F}{\partial h_{i}}\Delta h_{i} + \frac{\partial F}{\partial h_{i+1}}\Delta h_{i+1} \qquad (3.47)$$

in which Q, h_i, and h_{i+1} are the latest available estimate of Q^{n+1}, h_i^{n+1}, and h_{i+1}^{n+1}. It is understood that the partial derivatives $\frac{\partial F}{\partial Q}$, $\frac{\partial F}{\partial h_i}$, and $\frac{\partial F}{\partial h_{i+1}}$ are evaluated at (Q^n, h_i^n, h_{i+1}^n).

Symbolically, Eq. (3.47) can be written as

$$a_i \Delta Q_{lp} + b_i \Delta h_{i,lp} + c_i \Delta h_{i+1,lp} + d_i = 0 \tag{3.48}$$

$$\text{where } a_i = \frac{\partial F}{\partial Q},\ b_i = \frac{\partial F}{\partial h_i},\ c_i = \frac{\partial F}{\partial h_{i+1}},\ \text{and } d_i = F(Q, h_i, h_{i+1}) \tag{3.49}$$

Armed with Eq. (3.48), one can now proceed with the derivations leading to Eqs. (3.40) and (3.41) for each link. The general idea is to conduct a forward sweep from the first (downstream) computational point of the first (downstream) pipe of a link, through successive inline nodes and pipes, to arrive at the last (upstream) pipe of the link. The "u" subscript of Eqs. (3.40) and (3.41) refers to this last point at the end of the forward sweep along a link. For the forward sweep derivations, it is useful to use a double subscript (i,lp) to designate point i on pipe lp; LP denotes the last pipe on the link, and II(lp) denotes the last point on pipe lp. The detailed derivation of Eqs. (3.40) and (3.41) is presented in Appendix A.

After a forward sweep for a link ends at the last point II(LP) of the last pipe LP, one may deduce the following relation:

$$\Delta h_{II(LP),LP} = E_{II(LP),LP}\ \Delta Q_{LP} + F_{II(LP),LP} + H_{II(LP),LP}\ \Delta h_{1,1} \tag{3.50}$$

Eq. (3.50) is essentially equivalent to Eq. (3.41) with "u" denoting the last point of the link (II(LP),LP) and "d" denoting the first point (1,1). From a similar derivation, one may deduce the following relation as well:

$$\Delta h_{II(LP),LP} = EE_{II(LP),LP}\ \Delta Q_1 + FF_{II(LP),LP} + HH_{II(LP),LP}\ \Delta h_{1,1} \tag{3.51}$$

It should be noted that this equation is the same as Eq.(3.40), where "u" denotes the last point of the link and "d" denotes the first one, as in Eq. (3.41).

All the influence coefficients of Eqs. (3.50) and (3.51), that is E, F, H, EE, FF, and HH, are computed during the forward sweep. Thus, head corrections for all looped nodes can be computed using Eq. (3.44). A "backward sweep," in which the discharge correction and the head correction for all computational points in each pipe are computed, can now be performed for each link. At the end of a complete sweep, piezometric head and discharge of all pipes in a network are updated. One can thus proceed to the next time step computation.

The detailed derivation of influence coefficients and their initialization is presented in Appendix A.

3.6.2. Approximate Solution for Pollutant Transport Equations

3.6.2.1. Strategy for Approximate Solution

Sauvaget (1982) points out that Eq. (3.7) represents two physical phenomena; i.e., advection and diffusion. The mathematical nature of the advection equation, Eq. (3.52), and the diffusion equation, Eq. (3.76), in which the diffusion equation poses fewer numerical problems than the advection one, justifies the adoption of different solution methods. Thus, the solution of Eq. (3.7) is split into two processes for each time step; Eqs. (3.52) and (3.76) are solved successively by computational schemes that are appropriate to each of them.

Usseglio-Polatera and Chenin-Mordojovich (1988) show that process-splitting is particularly attractive for 2-D and 3-D simulations in water resources. Within each elementary fractional step, the cost of using stable implicit procedures or specially adapted schemes is small, especially when space-splitting is combined with process-splitting. This combination leads to accurate, powerful and cost-effective schemes with no formal limitations. Furthermore, this splitting framework makes possible a combination of competing numerical techniques (characteristics, finite-differences, finite elements) when these techniques are complementary.

The extension of process-splitting to a megapore network is straightforward; the approach permits calculation of pollutant concentration by proceeding from the most upstream

to the most downstream point in the network. This is done by (1) ordering all computational points from upstream to downstream and, (2) applying the process-splitting technique at each megapore and mass conservation law at each node. Since the approach avoids inverting a large matrix, overall computer time used in the computations decreases.

3.6.2.2. Advection Computation

The advective process is described by the following equation:

$$A\frac{\partial C}{\partial t} + AU\frac{\partial C}{\partial x} = 0 \quad \text{or} \quad \frac{\partial C}{\partial t} + U\frac{\partial C}{\partial x} = 0 \tag{3.52}$$

Since the velocity U is independent of the concentration C, one may write $U = \frac{dx}{dt}$ and rewrite Eq. (3.52) as

$$\frac{\partial C}{\partial t} + \frac{dx}{dt}\frac{\partial C}{\partial x} = 0 \quad \text{or} \quad \frac{dC}{dt} = 0 \tag{3.53}$$

This means that the value of C attached to a fluid volume remains constant during the movement along its characteristic line. Now the integration of Eq. (3.53) along this line as depicted in Figure 3.9 yields

$$C_i^{n+1} = C_\xi^n \tag{3.54}$$

where C_i^{n+1} is the pollutant concentration at node i at the current time step, and C_ξ^n is the pollutant concentration at the foot of the characteristic line at the previous time step. The term C_ξ^n, in the right hand side of Eq. (3.54), is estimated using the Holly-Preissmann third-degree interpolating polynomial as described in the following paragraphs (see Holly et al., 1977). Estimating C_ξ^n using the concentration C and gradient concentration CX from the two

neighboring points of x by constructing the third-order polynomial gives

$$C_{\xi}^{n} \approx y(\alpha) = A\alpha^3 + B\alpha^2 + D\alpha + E \tag{3.55}$$

in which

$$\alpha = \frac{x_{i-k} - x}{\Delta x} = \frac{U\Delta t - k\Delta x}{\Delta x} = Cr - k \tag{3.56a}$$

and

$$Cr = \frac{U\Delta t}{\Delta x} \tag{3.56b}$$

is the Courant number and k is the integer part of Cr.

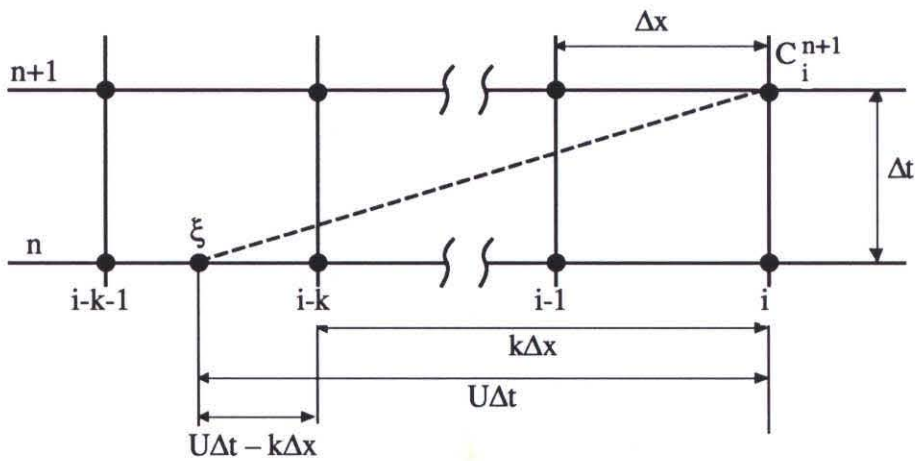

Figure 3.9. Characteristic Curve on Advection Grid System

The four coefficients A, B, D, and E can be evaluated such that the following four conditions are satisfied:

$$y(0) = C_{i-k}^{n};\quad y(1) = C_{i-k-1}^{n};\quad \left.\frac{dy}{dx}\right]_{\alpha=0} = CX_{i-k}^{n}\ ;\ \left.\frac{dy}{dx}\right]_{\alpha=1} = CX_{i-k-1}^{n} \tag{3.57}$$

Through the chain rule of differentiation, $\frac{dy}{dx} = \frac{dy}{d\alpha}\frac{d\alpha}{dx} = \frac{dy}{d\alpha}\frac{-1}{\Delta x}$ which is applied to Eq. (3.55), the four coefficients A, B, D, and E can be computed as

$$\left.\begin{aligned} A &= -2\,C^n_{i-k-1} + 2\,C^n_{i-k} - \Delta x\,CX^n_{i-k-1} - \Delta x\,CX^n_{i-k} \\ B &= 3\,C^n_{i-k-1} - 3\,C^n_{i-k} + \Delta x\,CX^n_{i-k-1} + 2\,\Delta x\,CX^n_{i-k} \\ D &= -\Delta x\,CX^n_{i-k} \\ E &= C^n_{i-k} \end{aligned}\right\} \tag{3.58}$$

Substitution of Eq. (3.58) into Eq. (3.55) yields

$$C^n_\xi = a_1\,C^n_{i-k-1} + a_2\,C^n_{i-k} + a_3\,CX^n_{i-k-1} + a_4\,CX^n_{i-k} \tag{3.59}$$

in which

$$\left.\begin{aligned} a_1 &= \alpha^2\,(3 - 2\,\alpha) \\ a_2 &= 1 - a_1 \\ a_3 &= \alpha^2\,(1 - \alpha)\,\Delta x \\ a_4 &= -\,\alpha\,(1 - \alpha)^2\,\Delta x \end{aligned}\right\} \tag{3.60}$$

where $\Delta x = x_{i-k} - x_{i-k-1}$

One can also evaluate CX^n_ξ from Eq. (3.59) as

$$CX^n_\xi = \frac{\partial C}{\partial x} = b_1\,C^n_{i-k-1} + b_2\,C^n_{i-k} + b_3\,CX^n_{i-k-1} + b_4\,CX^n_{i-k} \tag{3.61}$$

in which

$$\left.\begin{aligned} b_1 &= \frac{6\,\alpha\,(\alpha - 1)}{\Delta x} \\ b_2 &= -\,b_1 \\ b_3 &= \alpha\,(3\,\alpha - 2) \\ b_4 &= (\alpha - 1)(3\,\alpha - 1) \end{aligned}\right\} \tag{3.62}$$

From Eq. (3.59) it is obvious that to solve the problem completely one has to keep track of not only the concentration C^n_i but also CX^n_i for the next time step. This can be done by taking the derivative of Eq. (3.52) with respect to x:

$$\frac{\partial}{\partial x}\left(\frac{\partial C}{\partial t}\right) + U\,\frac{\partial}{\partial x}\left(\frac{\partial C}{\partial x}\right) = -\frac{\partial C}{\partial x}\,\frac{\partial U}{\partial x}$$

or $$\frac{\partial}{\partial t}(CX) + U\frac{\partial}{\partial x}(CX) = -CX\frac{\partial U}{\partial x}$$

or $$\frac{d(CX)}{dt} = -CX\frac{\partial U}{\partial x} \tag{3.63}$$

For the gradient concentration CX, one may write the direct analogy of Eqs. (3.53) and (3.54) using the technique used to compute concentration C:

$$CX_i^{n+1} = CX_\xi^n - \int_{t_n}^{t_{n+1}} CX\frac{\partial U}{\partial x}\,dt \tag{3.64}$$

This is approximated as

$$CX_i^{n+1} = CX_\xi^n - \frac{\Delta t}{2}\left[CX_\xi^n \left[\frac{\partial U}{\partial x}\right]_\xi + CX_i^{n+1}\left[\frac{\partial U}{\partial x}\right]_i^{n+1} \right]$$

Solving for CX_i^{n+1}, one obtains

$$CX_i^{n+1} = CX_\xi^n \left[\frac{1 - \frac{\Delta t}{2}\left[\frac{\partial U}{\partial x}\right]_\xi}{1 + \frac{\Delta t}{2}\left[\frac{\partial U}{\partial x}\right]_i^{n+1}} \right] \tag{3.65}$$

where CX_ξ^n can be evaluated using Eq. (3.61)

3.6.2.2.1. Boundary Conditions

From Eq. (3.54), only one upstream boundary condition is needed to solve the system. A problem appears when the characteristic curve extends to the upstream boundary. From Figure 3.10, Eq. (3.53) can still be used to get

$$C_j^{n+1} = C_\psi^z \tag{3.66}$$

where C_j^{n+1} is the pollutant concentration at node j at the current time step and C_ψ^z is the

pollutant concentration at the foot of a characteristic line at the boundary.

As previously mentioned, to keep track of CX_j^n, one may follow the same procedure as described in Eq. (3.64):

$$CX_j^{n+1} = CX_\psi^z - \int_{t_\psi}^{t_{n+1}} CX \frac{\partial U}{\partial x} dt \tag{3.67}$$

A new parameter is defined as follows:

$$\beta = \frac{t_{n+1} - t_n}{\Delta t} = \frac{z}{\Delta t} \tag{3.68}$$

From Figure 3.10, one may deduce that $\frac{z}{\Delta t} = \frac{(j-1)\Delta x}{U\Delta t} = \frac{(j-1)}{Cr}$ for $j \leq k$. Thus, the parameter in Eq. (3.68) can be rewritten as

$$\beta = \frac{(j-1)}{Cr} \tag{3.69}$$

Eq. (3.55) cannot be used to calculate C_ψ^z. Nevertheless one may estimate C_ψ^z using linear interpolation:

$$C_\psi^z \approx y(\beta) = A\beta + B \tag{3.70}$$

Coefficients A and B are determined by the following conditions:

$$y(1) = C_1^n; \; y(0) = C_1^{n+1} \tag{3.71}$$

Thus one may rewrite Eq. (3.70) as follows:

$$y(\beta) = (C_1^n - C_1^{n+1})\,\beta + C_1^{n+1} \tag{3.72}$$

Rewriting Eq. (3.52) as

$$\frac{\partial C}{\partial x} = -\frac{1}{U}\frac{\partial C}{\partial t} \rightarrow CX_1^{n+1} = -\frac{1}{U\Delta t}(C_1^{n+1} - C_1^n) \tag{3.73}$$

then using the chain rule of differentiation $\frac{dy}{dx} = -\frac{1}{U}\frac{dy}{d\beta}\frac{d\beta}{dt} = \frac{dy}{d\beta}\frac{1}{U\Delta t}$ and substituting both equations into Eq. (3.72) yields the following expression:

$$CX_\psi^z = \frac{dy}{dx} = \frac{C_1^n - C_1^{n+1}}{U\Delta t} \tag{3.74}$$

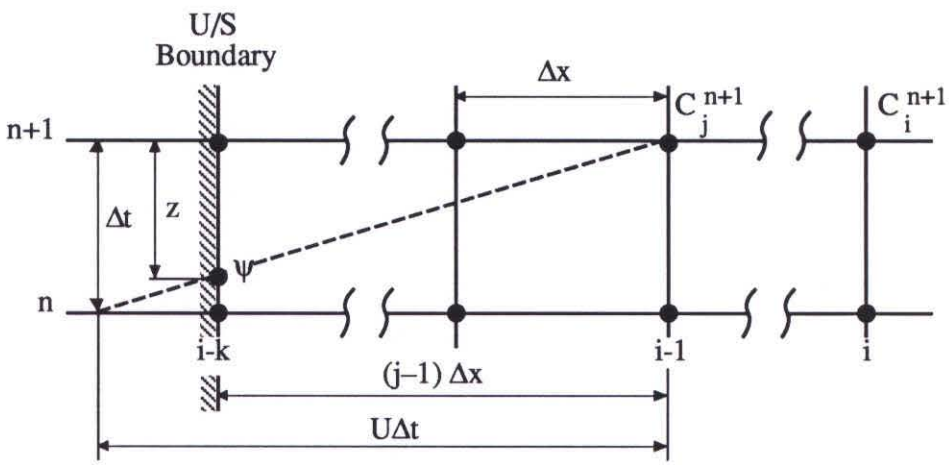

Figure 3.10. Characteristic Curve on the Upstream Boundary

The gradient concentration CX can be evaluated by rewriting Eq. (3.65) as

$$CX_j^{n+1} = CX_\psi^z \left[\frac{1 - \frac{\beta\Delta t}{2}\left[\frac{\partial U}{\partial x}\right]_\psi}{1 + \frac{\beta\Delta t}{2}\left[\frac{\partial U}{\partial x}\right]_j^{n+1}} \right] \tag{3.74a}$$

If the boundary concentration C_1^{n+1} is given, the problem can be solved by first using Eq. (3.73) to calculate CX_1^{n+1} and then by substituting Eqs. (3.72) and (3.74) into

Eq. (3.66) and Eq. (3.74a) to compute C_j^{n+1} and CX_j^{n+1}.

The concentration at the upstream boundary is computed using the same mass conservation law as for any node in the megapore network. In using the mass conservation law, particularly for pollutant conservation, the present study assumes that advection flux is dominant compared to diffusion flux. Therefore at any node m, the following statement of pollutant flux continuity (inflow = outflow) must be satisfied at any instant:

$$\sum_{lp} Q_{lp}^{n+1} C_{lp}^{n+1} + Q_m^{n+1} C_m^{n+1} + W_m^{n+1} C_s = 0 , \quad m = 1, 2, 3, ... \tag{3.75}$$

where n+1 denotes the end of the current time step; Q_{lp}^{n+1} is discharge entering node m from pipe lp; C_{lp}^{n+1} is pollutant concentration entering node m from pipe lp; Q_m^{n+1} is external inflow entering node m; C_m^{n+1} is external pollutant concentration entering node m; W_m^{n+1} is inflow entering node m from the aquifer-matrix; C_s is the latest estimate of pollutant concentration of node m from the aquifer, and summation is over all the pipes attached to node m. All discharges and concentrations in Eq. (3.75) are known or given quantities except for a particular C_{lp}^{n+1}, which is the concentration at the upstream of a pipe whose flow is leaving the corresponding node. Therefore, the upstream boundary condition in the advection computation for each pipe can be obtained from Eq. (3.75).

3.6.2.2.2. Initial Condition

An initial condition is needed to start the computation. The initial conditions for the governing equation Eq. (3.52) or the working equations (3.54), (3.65), and (3.75) are given concentrations C and gradient concentrations CX at all computational points in the domain.

3.6.2.3. Diffusion Computation

The diffusive process is described by the following equation:

$$A\frac{\partial C}{\partial t} = \frac{\partial}{\partial x}(A\,\varepsilon_x\frac{\partial C}{\partial x}) \tag{3.76}$$

Eq. (3.76) is a second-order partial differential equation that can be transformed into an equivalent system of two equations of the first order:

$$\begin{aligned} A\frac{\partial C}{\partial t} &= \frac{\partial}{\partial x}(A\,\varepsilon_x\,CX) \\ \frac{\partial C}{\partial x} &= CX \end{aligned} \tag{3.77}$$

in which concentration C and its gradient CX are the dependent variables. Using the following notation such that

$$\begin{aligned} \Delta x &= x_i - x_{i-1} \\ \Delta C_i &= C_i^{n+1} - C_i^n \\ \Delta CX_i &= CX_i^{n+1} - CX_i^n \end{aligned} \tag{3.78}$$

and a discretization scheme devised by A. Preissmann, which adopts the approximations,

$$\begin{aligned} f(x,t) &= \frac{\theta}{2}(f_i^{n+1} + f_{i-1}^{n+1}) + \frac{1-\theta}{2}(f_i^n + f_{i-1}^n) \\ &= \frac{\theta}{2}(\Delta f_i + \Delta f_{i-1}) + \frac{1}{2}(f_i^n + f_{i-1}^n) \end{aligned}$$

$$\begin{aligned} \frac{\partial f}{\partial x} &= \theta\frac{f_i^{n+1} - f_{i-1}^{n+1}}{\Delta x} + (1-\theta)\frac{f_i^n - f_{i-1}^n}{\Delta x} \\ &= \frac{\theta}{\Delta x}(\Delta f_i - \Delta f_{i-1}) + \frac{1}{\Delta x}(f_i^n - f_{i-1}^n) \end{aligned}$$

$$\frac{\partial f}{\partial t} = \frac{(f_i^{n+1} - f_i^n) + (f_{i-1}^{n+1} - f_{i-1}^n)}{2\Delta t}$$
$$= \frac{1}{2\Delta t}(\Delta f_i + \Delta f_{i-1})$$

Eq. (3.77) becomes the discretized system:

$$\frac{\theta}{\Delta x}(\Delta C_i - \Delta C_{i-1}) + \frac{1}{\Delta x}(C_i^n - C_{i-1}^n) = \frac{\theta}{2}(\Delta CX_i + \Delta CX_{i-1}) + \frac{1}{2}(CX_i^n + CX_{i-1}^n)$$
$$\frac{A}{2\Delta t}(\Delta C_i + \Delta C_{i-1}) = A\,\varepsilon_x\left(\frac{\theta}{\Delta x}(\Delta CX_i - \Delta CX_{i-1}) + \frac{1}{\Delta x}(CX_i^n - CX_{i-1}^n)\right) +$$
$$\frac{\partial A}{\partial x}\varepsilon_x\left(\frac{\theta}{2}(\Delta CX_i + \Delta CX_{i-1}) + \frac{1}{2}(CX_i^n + CX_{i-1}^n)\right)$$

This system can be rewritten as

$$\left.\begin{aligned} a_1\Delta C_i + a_2\Delta CX_i + a_3\Delta C_{i-1} + a_4\Delta CX_{i-1} + a_5 = 0 \\ b_1\Delta C_i + b_2\Delta CX_i + b_3\Delta C_{i-1} + b_4\Delta CX_{i-1} + b_5 = 0 \end{aligned}\right\} \text{ for } \quad i = 2, 3, \ldots\ldots, N \qquad (3.79)$$

where

$$a_1 = \frac{\theta}{\Delta x}$$
$$a_2 = -\frac{\theta}{2}$$
$$a_3 = -a_1$$
$$a_4 = a_2$$
$$a_5 = \frac{C_i^n - C_{i-1}^n}{\Delta x} - \frac{CX_i^n + CX_{i-1}^n}{2}$$
$$b_1 = -\frac{A}{2\Delta t}$$
$$b_2 = \theta\,\varepsilon_x\left(0.5\,\frac{\partial A}{\partial x} + \frac{A}{\Delta x}\right)$$
$$b_3 = b_1$$
$$b_4 = \theta\,\varepsilon_x\left(0.5\,\frac{\partial A}{\partial x} - \frac{A}{\Delta x}\right)$$
$$b_5 = \varepsilon_x\frac{\partial A}{\partial x}\,\frac{CX_i^n + CX_{i-1}^n}{2} + \varepsilon_x A\,\frac{CX_i^n - CX_{i-1}^n}{\Delta x}$$

Eq. (3.79) may be solved efficiently using the classic double-sweep algorithm.

Elimination of ΔCX_{i-1} from Eq. (3.79) yields

$$\Delta C_{i-1} = L_{i-1}\,\Delta C_i + M_{i-1}\,\Delta CX_i + N_{i-1} \tag{3.80}$$

where

$$L_{i-1}=\frac{a_1b_4 - a_4b_1}{a_4b_3 - a_3b_4},\ M_{i-1}=\frac{a_2b_4 - a_4b_2}{a_4b_3 - a_3b_4},\ \text{and}\ N_{i-1}=\frac{a_5b_4 - a_4b_5}{a_4b_3 - a_3b_4} \tag{3.80a}$$

To obtain a relationship that is useful for computing the influence coefficients of the double-sweep method, let $\Delta CX_{i-1} = Q_{i-1}\,\Delta C_{i-1} + R_{i-1}$. Substituting this relationship and Eq. (3.80) into Eq. (3.79), and solving for ΔCX_i, yields

$$\Delta CX_i = Q_i\,\Delta C_i + R_i \tag{3.81}$$

where

$$S_i = a_3 + a_4 Q_{i-1},\ Q_i = -\frac{a_1 + L_{i-1}S_i}{a_2 + M_{i-1}S_i},\ R_i = -\frac{a_5 + N_{i-1}S_i + a_4 R_{i-1}}{a_2 + M_{i-1}S_i} \tag{3.81a}$$

One can solve the system of Eq. (3.79) recursively, using Eqs. (3.80) and (3.81), given the appropriate boundary conditions. The so-called forward sweep starts by initializing Q_1 and R_1 using the imposed upstream boundary condition of the type

$$\Delta CX_1 = Q_1\,\Delta C_1 + R_1 \tag{3.82}$$

The sweep continues for i = 2,3,…,N through computation of the influence coefficients L_{i-1}, M_{i-1}, N_{i-1}, Q_i, and R_i.

After finishing the forward sweep, the algorithm starts the backward sweep by initializing either ΔCX_N or ΔC_N from the imposed downstream boundary condition. The computation continues until it reaches the upstream end by calculating

$$\Delta C_{i-1} = L_{i-1}\,\Delta C_i + M_{i-1}\,\Delta CX_i + N_{i-1}\ \text{and}\ \Delta CX_{i-1} = Q_{i-1}\,\Delta C_{i-1} + R_{i-1}$$

respectively, for each computational point. At each computational point one can update the solution directly by computing

$$C_i^{n+1} = C_i^n + \Delta C_i \quad \text{and} \quad CX_i^{n+1} = CX_i^n + \Delta CX_i \tag{3.83}$$

3.6.2.3.1. Boundary Conditions

The boundary condition for the diffusion computation is of the Neumann type; i.e., an imposed concentration at each of the boundaries. It is possible with this scheme to impose a condition of the following type at each of the boundaries of the model:

$$a\,\Delta C_i = b\,\Delta CX_i + d \;\Rightarrow\; \text{for } i = 1 \text{ and } N \tag{3.84}$$

where a, b, and d are known coefficients. In the present study, at each boundary, the concentrations at the end of the advection computation are used as boundary conditions.

3.6.2.3.2. Initial Condition

In each time step, the initial condition for the diffusive stage is taken from the end condition of the preceding advective stage. Thus at all computational points, the values of the concentrations C and their gradients CX at the end of the advection computation are used as an initial condition for the following diffusion computation.

3.6.2.4. Computation Procedure

For one time step, the advective and diffusive computations can be performed for each pipe over the whole network by marching from the most upstream pipe to the most downstream one. Therefore, before starting the pollutant transport computation, it is essential that all nodes of the megapore network be ordered in an upstream to downstream fashion. The first computation is started by using the initial condition for the advection stage in each pipe. For each pipe, the computation is carried out as described in the following paragraphs.

3.6.2.4.1. Advective Computation

(1) Compute concentration C_i^{n+1} using Eq. (3.59) if the characteristic line does not hit the upstream boundary. If the characteristic hits the upstream boundary, use Eq. (3.72) to compute concentration C_i^{n+1}.

(2) Compute the gradient concentration CX_i^{n+1} using Eq. (3.65) if the characteristic line does not hit the upstream boundary. If the characteristic hits the upstream boundary, use Eq. (3.74a) to compute concentration CX_i^{n+1}.

3.6.2.4.2. Diffusion Computation

(1) Use the concentration at the end of the advection stage as the initial condition of the diffusion stage.

(2) Start the forward sweep by calculating the influence coefficients L_{i-1}, M_{i-1}, N_{i-1}, Q_i, and R_i from the first to the last computational points. Initialization of the influence coefficients Q_1 and R_1 can be performed by using the boundary condition, Eq. (3.84), for the first computational point. Recursion relationships as described in Eqs. (3.81a) and (3.80a) can be used to compute the influence coefficients up to the last computational point.

(3) Start the backward sweep by initializing ΔC_N and using the boundary condition (3.84) for the last computational point. Compute the corrections ΔCX_i and ΔC_i from the last computational point to the first computational point using Eqs. (3.81) and (3.80). The concentration C and its gradient CX can be updated directly using Eq. (3.78).

3.7. Iterative Coupling of Megapore and Aquifer-Matrix Computation

As previously mentioned, a fractional-step method is used to approximate the governing equations. In each time step during the simulation, the computations in the megapore network and those in the aquifer-matrix are coupled through the source or exchange term of the governing equation. For clarity, Eqs. (3.15) and (3.75) are repeated below.

$$W^{n+1} = W^n + \frac{\partial W}{\partial h_s}(h^x - h^n) + \frac{\partial W}{\partial h_s}(h^y - h^x) + \frac{\partial W}{\partial h_s}(h^{n+1} - h^y) + \frac{\partial W}{\partial h_m}(h_m - h_m^n) \qquad (3.15)$$

$$\sum_{lp} Q_{lp}^{n+1} C_{lp}^{n+1} + Q_m^{n+1} C_m^{n+1} + W_m^{n+1} C_s = 0 , \quad m = 1, 2, 3, . \qquad (3.75)$$

where n+1 denotes the end of the current time step; h_m is the latest estimate of the pipe piezometric head; W_m^{n+1} is inflow entering node m from the aquifer-matrix; C_s is the latest estimate of pollutant concentration of node m from the aquifer, and all other symbols are as previously defined.

In each time step, the last terms in Eqs. (3.15) and (3.75) represent the latest estimate of exchange mass between the megapore network and aquifer-matrix. The fractional-step computations have to be carried out until this estimate converges according to some criterion. Thus the fractional step of the hydrodynamic computation will stop when the latest estimate of the megapore piezometric head h_m in Eq. (3.15) satisfies a certain convergence criterion, after which the pollutant computations begin. As with the hydrodynamic computation, the fractional step of the pollutant transport computation will stop after the latest estimates of pollutant fluxes ($W_m^{n+1} C_s$) in Eq. (3.75) satisfy a certain convergence criterion. Thus, in each time step, the fractional-step computations are iterated until the convergence criterion is satisfied.

CHAPTER IV

TEST AND APPLICATION

4.1. Introduction

This chapter presents tests and applications of the computer program Labyrinth. First, the model is compared to analytical solutions on a simple domain to verify the numerical techniques used. Second, the model is applied to the Big Spring Basin. Sensitivity analyses of important system parameters of this basin (megapore diameter, roughness coefficient, hydraulic conductivity of the aquifer, and classes of megapore diameter) are conducted to identify interaction between the parameters and model components. Simulation of dye trace experiments conducted in the basin is performed to demonstrate the capability of the model.

4.2. Schematic Model

4.2.1. Hydrodynamic and Pollutant Transport in a Single Megapore

In saturated cases, the verification of the numerical method for the hydrodynamic equations is straightforward. Since the hydrodynamic equations are based on the mass and momentum conservation laws, in saturated cases where the megapore is flowing full, the input and output hydrographs must be identical, furthermore, at steady-state, piezometric drop along the megapores must satisfy the Darcy–Weisbach equation.

The more important verification deals with the numerical method for the pollutant transport equations. To verify this method, a pollutant having a Gaussian distribution in space is given as an initial condition. From now on such a distribution of pollutant will be referred as a Gaussian cloud. The spreading of the cloud, as well as its position in the megapore, are calculated using the numerical techniques described in Section 3.6. The analytical solution of

the transport of this Gaussian cloud is as follows (Fischer et al., 1979):

$$C(x,t) = \frac{M}{\sqrt{4\pi Dt}} \exp\left(\frac{[x-Ut]^2}{4Dt)}\right) \tag{4.1}$$

where t indicates time; C is pollutant concentration as a function of x and t; M is an initial slug of mass introduced at time zero at the x origin; D is the diffusion coefficient; and U is the advective velocity of flow.

The initial condition of the present test is computed using Eq. (4.1) with the following values: M is 10^5 units, t is 10^4 seconds, D is 10 m^2/s, and U is variable. Using this initial condition, pollutant concentrations along the megapore are computed using the numerical technique described in the previous chapter. The split-process method requires, first, that a natural upstream boundary be imposed for advection, and second, that both upstream and downstream conditions be imposed for diffusion. Thus, zero pollutant flux is imposed at the upstream boundary, while at the downstream end, a boundary condition is not needed since the concentration at the end of the advection step is imposed for diffusion. The values of subreaches, Δx; total number of subreaches, NDX; time increment, Δt; and total number of time steps, NDT, are 100 m, 200, 200 seconds, and 100, respectively. Figure 4.1 presents the results of the numerical and analytical solutions of the pollutant transport within a single megapore for two values of the advection velocity, U. In the figure, the two solutions are plotted at different points to distinguish between them. As depicted in Figure 4.1, the analytical and numerical solutions give graphically indistinguishable results. In Figure 4.1, the analytical solution is computed using Eq. (4.1).

As explained in the previous chapter, the split-process approach is used to compute the pollutant advection and diffusion despite the fact that, physically, these processes occur simultaneously. Since the advection equation, Eq. (3.52), and diffusion equation, Eq. (3.76), are solved successively for each time step, it is necessary to impose conditions at each of the model boundaries for each stage of the process. Nevertheless, the numerical solution still agrees quite well with the analytical one, even though the Gaussian cloud is still at the upstream boundary as depicted in Figure 4.1.b. Thus, the treatment of boundary

conditions in the numerical technique used in the present study is well justified.

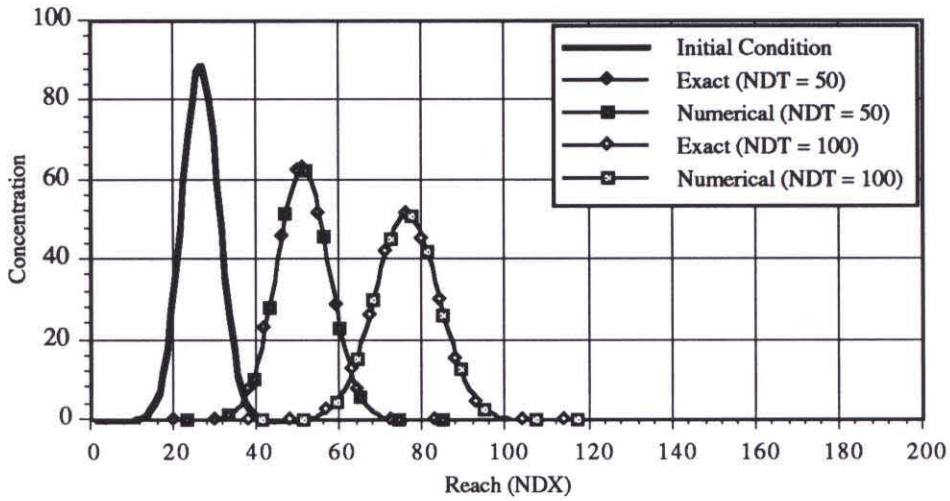

(a) Courant Number = 0.5

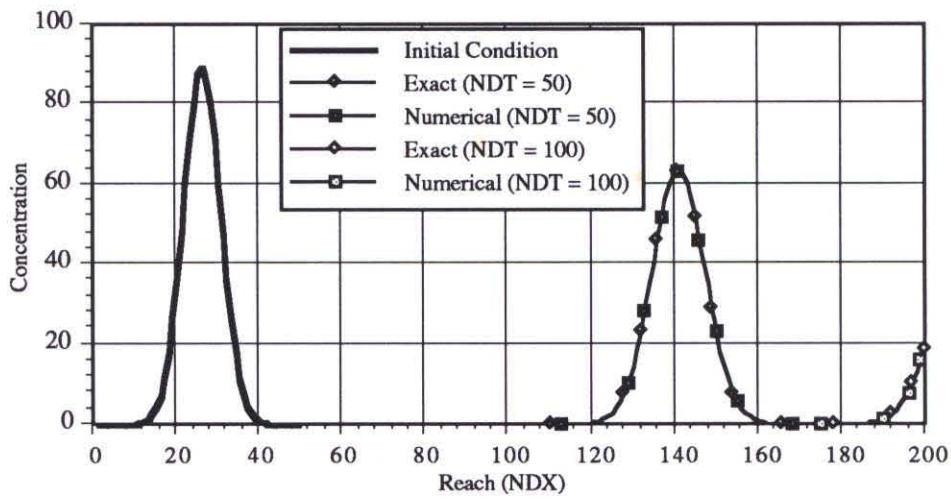

(b) Courant Number = 1.4

Figure 4.1. Analytical and Numerical Solutions of the Pollutant Transport Equation within a Single Megapore for Various Values of Courant Number and NDT

Figure 4.1 shows that the imposed initial conditions in the above two cases are spreading over 13 reaches. Undoubtedly if the initial conditions had spread over a narrower region, the numerical results would have shown some oscillation at the feet of the distribution and some discrepancies at the peak. Nevertheless, the result will still be reasonable, since it is

well known that the characteristic method is the best method to solve advection-dominated problems.

4.2.2. Hydrodynamic and Pollutant Transport in an Aquifer-Matrix

In an aquifer-matrix, as far as the analytical solution is concerned, the hydrodynamic equation, Eq. (3.1), is a specific case of the pollutant transport equation, Eq. (3.3). That is, Eq. (3.3) contains advective terms from pore velocities, while Eq. (3.1) does not. In other words, Eq. (3.1) is, in fact, Eq. (3.3) with pore velocities equal to zero. Source terms are omitted in both equations. In this section, therefore, only Eq. (3.3) is compared to the corresponding analytical solution.

The analytical solution used for comparison is the one that deals with two-dimensional plane dispersion. Consider a homogeneous, isotopic porous medium with a unidirectional steady-state flow with seepage velocity U. A Cartesian coordinate system is chosen with the x axis oriented along the direction of flow (see Figure 4.2). Javandel et al. (1984) state that the governing equation for this problem can be written as

$$D_x \frac{\partial^2 C}{\partial x^2} + D_y \frac{\partial^2 C}{\partial y^2} - U \frac{\partial C}{\partial x} - \lambda RC = R \frac{\partial C}{\partial t} \tag{4.2}$$

where t denotes time; C is pollutant concentration; D_x and D_y are the dispersion coefficients in the x and y directions, respectively; U is a uniform seepage velocity; λ is the radioactive decay constant; and R is the retardation factor.

Assume that initially the medium is free of a particular solute species, and that at a certain time, a strip-type source with length 2a, orthogonal to the direction of groundwater flow, is introduced along the y axis. If the concentration of the solute decays exponentially with time, the initial and boundary conditions of this mathematical model may be written as

$$C(0, y, t) = C_0 e^{-\alpha t} \quad -a \le y \le +a$$

$$C(0, y, t) = 0 \quad \text{other values of } y$$

$$\lim_{y \to \pm\infty} \frac{\partial C}{\partial y} = 0$$

$$\lim_{x \to \infty} \frac{\partial C}{\partial x} = 0$$

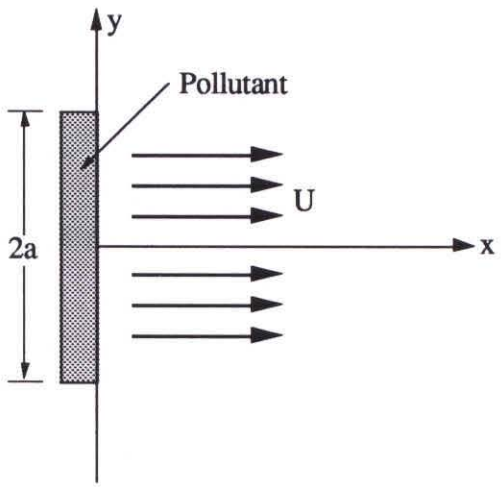

Figure 4.2. Schematic Diagram Showing the Two-Dimensional Plane Dispersion Model.

Cleary and Ungs (1978) present the following analytical solution to the above model:

$$C(x, y, t) = \frac{C_0\, x}{4\sqrt{\pi D_x}} \exp\left(\frac{U\, x}{2D_x} - \alpha t\right) \int_0^{t/R} \exp\left[-\left(\lambda R - \alpha R + \frac{U^2}{4D_x}\right)\tau - \frac{x^2}{4D_x\,\tau}\right] \tau^{-1.5} \left[\operatorname{erf}\left(\frac{a-y}{2\sqrt{D_y\,\tau}}\right) + \operatorname{erf}\left(\frac{a+y}{2\sqrt{D_y\,\tau}}\right)\right] d\tau \qquad (4.3)$$

Javandel et al. (1984) provide a numerical solution of Eq. (4.3) for the following parameter values: $\alpha = \lambda = 0$/day; $R = 1$; $a = 50$ m; $U = 0.1$ m/s; $D_x = 1$ m^2/day; $D_y = 0.1$ m^2/day; and $t = 100$ days. This numerical solution is compared to those obtained by the numerical method used in the Labyrinth code.

In application of the Labyrinth code to this test case, the pollutant source is extended to

three dimensions in which the height of the source is the same as the height of the aquifer, and the dispersion coefficient in the z direction, D_z, is set at zero. The test is done in a three-dimensional aquifer-matrix whose lengths in the x, y, and z directions are 200 m, 300 m, and 150 m, respectively; Δx is 10 m, Δy are 5 m and 10 m, and $\Delta z = 10$ m; the hydraulic conductivities in the x, y, and z directions are 2 m/day, 2 m/day, and 0 m/day, respectively; and the specific storage, S, is 4.37×10^{-6}/m. At $x = 0$ m and $x = 200$ m, piezometric heads of 10 m and 0 m, respectively, are imposed to get a uniform seepage velocity of 0.1 m/s as required in the analytical solution. A plane-type pollutant source of 1000 ppm is imposed along the $x = 0$ m plane where the width is 100 m (in the y direction) and the height is 150 m (in the z direction). All other parameters are the same as those used in the analytical model.

The results of this test and the analytical solutions, presented in Figure 4.3, show that the two solutions agree fairly well. The results also show that smoothing and phase differences occur. The governing equation of pollutant transport for the aquifer-matrix, Eq. (3.3), represents two physical mechanisms: advection and diffusion. It is well known that advection poses more numerical problems than does diffusion because of an artificial diffusion coefficient introduced by the approximate nature of the finite-difference scheme used to approximate the governing equation (Cunge et al. 1980). This artificial coefficient may cause numerical diffusion (smoothing) and an oscillation-like behavior which results in phase shifting. Nevertheless, the result of this test agrees fairly well with the analytical solution. This is understandable because in an aquifer-matrix the seepage velocity is usually small, thus the advection process does not cause severe problems for the numerical results.

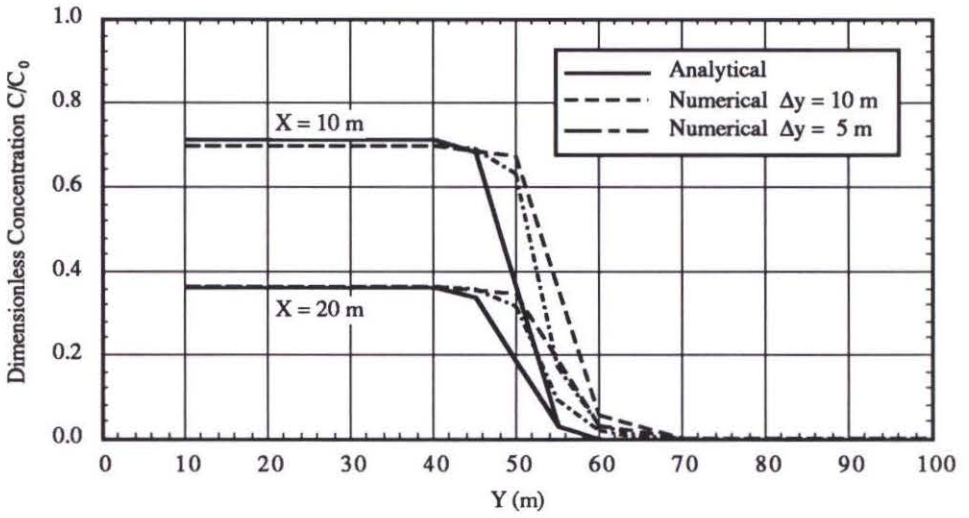

Figure 4.3. Analytical and Numerical Solutions of the Pollutant Transport Equation in an Idealized Aquifer-Matrix after t = 100 days

4.3. The Big Spring Model

This section presents a test of the Labyrinth code for the Big Spring Basin, Clayton County, northeast Iowa. First, sensitivity analyses of important system parameters of this basin (megapore diameter, roughness coefficient, hydraulic conductivity of the aquifer, and classes of megapore diameter) are conducted to identify interaction between these parameters and model components. Second, simulation of dye trace experiments conducted in this basin is performed to demonstrate the capability of the model.

4.3.1. Hydrogeologic Setting of the Big Spring Basin

The Big Spring Basin is located within the Paleozoic Plateau region of northeast Iowa (see Figure 1.2). Through most of the basin, the landscape is moderately rolling but ranges to steeply sloping as the Turkey River valley is approached in the southern portion of the area. Total relief within the basin is approximately 420 ft (130 m) (Hallberg et al., 1989). The basin has a well-integrated surface drainage network. Most of the groundwater basin coincides with the surface-water basin of Roberts Creek. Loess-derived soils, primary

Downs, Fayette, and some Tama soil, occupy over 70% of the land surface (Hallberg et al., 1983).

The bedrock of the basin comprises of the Galena Group carbonate rocks, with the uppermost unit being the overlying Maquoketa Formation. The lower part of the Maquoketa is composed of shaly carbonates, while the upper Maquoketa is shale and claystone. The shaly carbonates of the lower Maquoketa do not significantly retard water movement and generally form open hydrologic connections with the Galena aquifer. The shales and claystones of the upper Maquoketa Formation are the uppermost bedrock in the western portion of the basin. These low permeability strata retard the downward movement of groundwater toward the Galena aquifer, and in the western portion of the basin the aquifer is effectively confined. This area provides a natural background area for the groundwater in the Galena aquifer (Hallberg et al., 1989).

Solutional processes in the Galena aquifer have developed sinkholes. The drainage area to most individual sinkholes is relatively small. However, a number of these sinkholes are associated with surface drainage basins, and following extreme rains or snowmelt, runoff from these basins is captured by the sinkholes and diverted into the Galena aquifer. The surface area draining to sinkholes covers about 11% of Big Spring groundwater basin (Hallberg et al., 1989).

4.3.2. Introductory Remarks to the Model

This section presents a test of the Labyrinth code for the Big Spring Basin, Clayton County, northeast Iowa. The actual geometry of the aquifer is used in this model, but the initial and boundary conditions are fictitious. Aquifer and megapore parameters such as hydraulic conductivity and specific storage of the aquifer, and diameter and roughness of the megapore are not available from field measurements. Therefore, all parameters except megapore diameters are taken from published literature. Sensitivity analyses are performed on several parameters to get a better understanding of their effects on flow and pollutant responses at Big Spring.

4.3.3. Definition of the Model Domain

The model domain is deduced from the topography of the Big Spring Basin. First, the contours of the basin at the surface grid points are extracted from USGS contour maps. Second, bottom and surrounding boundaries of the domain are determined using hydrologic cross-sections and the divides of the Big Spring Basin, respectively (Hallberg et al., 1983). Third, all boundaries are shifted slightly to conform with the requirements of the finite-difference approach. In order to completely solve the working equations, Eqs. (3.21) and (3.29), a minimum of three computational grid points must be maintained in each axis direction. Applying this requirement to the Big Spring Basin yields a three-dimensional domain, shown in Figure 3.3, that is suitable for the finite-difference method and from which, a finite-difference grid is generated. This grid consists of 16 subreaches in the x direction, 13 subreaches in the y direction, and 45 subreaches in the z direction. The values of these subreaches are 5250 ft, 5250 ft, and 10 ft, respectively. The value of the horizontal subreaches, 5250 ft, is based on red grids from the USGS map (indicating U.S. public lands survey: section). The value of vertical subreaches, 10 ft, is chosen in consideration of computer time and memory requirement.

4.3.4. Initial and Boundary Conditions

Hypothetical initial and boundary conditions are used for sensitivity analysis. These conditions correspond to saturated cases, for which all governing equations described in the previous chapter are valid.

All computations in the sensitivity analysis start with a steady-state initial condition. This is achieved by (1) imposing boundary conditions: a piezometric head of 20 ft at Big Spring (Hallberg et al., 1983) and, at certain regions of the aquifer-matrix, piezometric heads that are equal to their surface elevation; and (2) at time zero, setting the discharges in all megapores at zero and all piezometric heads equal to the highest surface elevation in the domain (= 440 ft).

This case is run with a total time step, NDT, of 1500, which corresponds to 3,000 hours prototype time, at which the discharge at Big Spring becomes steady.

The following boundary conditions are imposed: (1) on the aquifer-matrix, piezometric heads equal the surface elevation at I = 2 to 4 and J = 2 to 4, and zero flux at any other aquifer-matrix boundary; (2) at Big Spring, the piezometric head equals 20 ft and; (3) zero discharge at all sinkholes.

Several cases are run to get steady-state initial conditions for one set of megapore diameters and one set of hydraulic conductivities of the aquifer-matrix. As shown Table 4.1, Dilamater et al. (1977) present possible values of the hydraulic conductivity and their corresponding specific storage for three kinds of rock. It is assumed that the values of the hydraulic conductivity and their corresponding specific storage for dense rocks are appropriate for the Big Spring aquifer; therefore in this test the values of 7.6×10^{-6} f/s, 7.6×10^{-5} f/s, and 9.5×10^{-4} f/s are used.

Table 4.1. Typical Values of Hydraulic Conductivity, K, and Specific Storage, S, after Dilamater et al. (1977)

Rock Name	K (f/s)	S (ft^{-1})
Dense Rocks	7.6×10^{-6}	2.06×10^{-7}
	7.6×10^{-5}	1.33×10^{-6}
	9.5×10^{-4}	8.99×10^{-6}
Sands	7.6×10^{-5}	3.11×10^{-4}
	3.8×10^{-4}	1.06×10^{-4}
	3.8×10^{-3}	3.57×10^{-5}
Clays	3.8×10^{-7}	3.05×10^{-3}
	3.8×10^{-6}	1.54×10^{-4}
	1.9×10^{-5}	3.08×10^{-5}

A wide range of megapore diameters (5 to 30 ft) is used. This range is assumed to cover all possibilities of actual megapore diameters. Henceforth, the term "megapore diameter" is

used to indicate the "equivalent megapore diameter"; i.e., the diameter of a circular megapore that has the same wetted area as the real megapore in the field.

Figure 4.4.(a) presents the steady-state discharge calculation for a hydraulic conductivity, K, of 7.6×10^{-5} ft/s, and several megapore diameters. From these results, the steady-state discharge at Big Spring appears to be constant for megapore diameters greater than 5 ft. This is valid because of the way the boundary conditions are imposed. That is, for diameters greater than 5 ft, the megapore network is capable of transporting the maximum discharge due to the piezometric gradient imposed. For megapore diameters less than 5 ft, delivering the same amount of maximum discharge, needs piezometric heads with a greater gradient than the one imposed. Thus, for the given boundary condition, discharge at Big Spring is constrained by the imposed piezometric head only for diameters greater than 5 ft, while for diameters less than 5 ft, the megapore diameter also constrains the system.

Figure 4.4 (b) presents steady-state discharge at Big Spring for megapore diameter, D = 20 ft and several hydraulic conductivities. For a given value of the piezometric gradient, the results show that the discharge is linearly dependent on the hydraulic conductivity; this is in agreement with Darcy's law.

Steady-state discharge serves as baseflows for the Labyrinth code. Field data show that Big Spring baseflows never exceed 80 cfs. During wet conditions, which prevail throughout the entire March–June period, total basin discharge on the average is 60 cfs (Hallberg et al., 1983). Comparison between this data and the results as depicted in Figure 4.4 (b) gives a clear indication that the value of 9.5×10^{-4} ft/s for the hydraulic conductivity of the aquifer-matrix is too high. This value, therefore, is not used for the next tests.

4.3.5. Sensitivity Analysis of Parameters Affecting the Big Spring Basin

Model sensitivity analysis, an important part of the model development process, helps to identify interaction among model components and parameters. By revealing model parameters having insignificant effects on the results, sensitivity analysis permits identification of

parameters important to the model. This identification helps in deciding what data must be collected from the field.

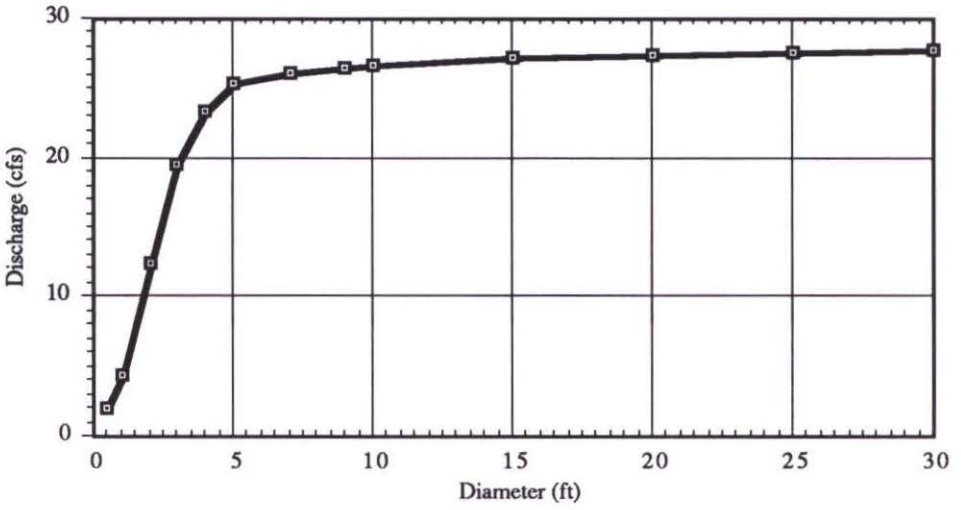

(a) Steady-State Discharge at Big Spring for Various Values of Megapore Diameter and Hydraulic Conductivity of the Aquifer-Matrix, K = 7.6 x 10^{-5} fps

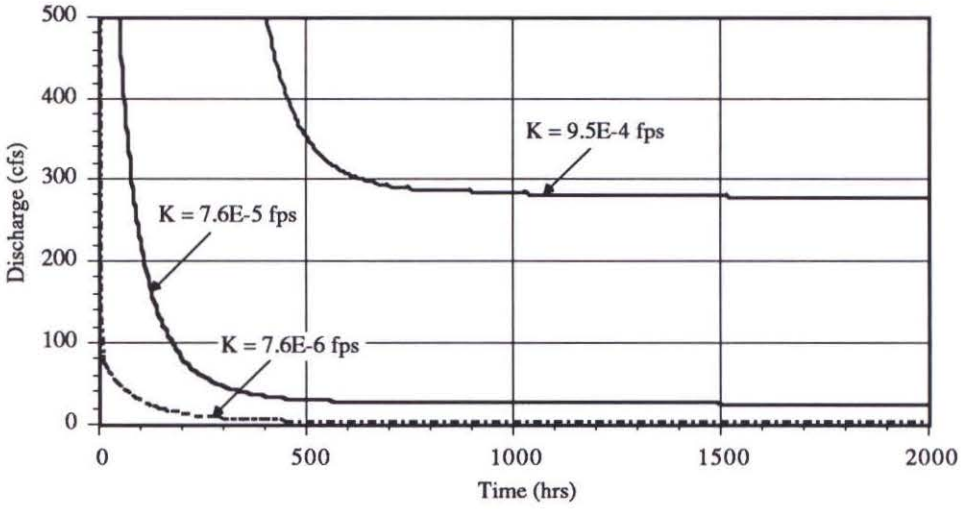

(b) Steady-State Discharge at Big Spring for Various Values of Hydraulic Conductivity of the Aquifer-Matrix and Megapore Diameter, D = 20 ft

Figure 4.4. Steady-State Discharge at Big Spring for Various Values of Megapore Diameter and Hydraulic Conductivity of the Aquifer-Matrix

In this section sensitivity analysis is performed on megapore diameter and several parameters of the megapore and aquifer-matrix — dispersion coefficient, roughness of the megapore, and the hydraulic conductivity of the aquifer-matrix. This analysis is used to identify the important parameters affecting groundwater flow and pollutant transport in the Big Spring Basin.

4.3.5.1. Analysis of Sensitivity to Megapore Diameter

Since there are no field measurements of megapore diameters in the Big Spring Basin, it was decided to make the preliminary analysis on a wide range of megapore diameters (4 ft, 5 ft, 10 ft, 15 ft, 20 ft, and 25 ft). From these preliminary results, the range of diameters could be narrowed and the analysis repeated in more detail.

The analysis is done by varying the megapore diameter while holding the following parameters constant: hydraulic conductivity, $K = 7.6 \times 10^{-5}$ fps; specific storage, $S = 1.33 \times 10^{-6}$/ft; and the megapore Strickler coefficient, $k_s = 30$. The steady-state initial condition and boundary conditions given in Section 4.3.4 are used in this analysis. An inflow hydrograph with constant pollutant concentration enters sinkhole number 60 (see Figure 3.4). Three progressively different time steps, Δt, are used, the total number of time steps, NDT, being 1500. This test simulates 3000 hours of prototype time.

The discharge and pollutant flux hydrographs at Big Spring are presented in Figures 4.5 and 4.6. Figure 4.5 shows that the outflow response varies greatly at Big Spring for megapore diameters less than 15 ft, but is much less sensitive for megapore diameters greater than 15 ft. This means that for the given input hydrograph of 80 cfs peak discharge, megapores with diameter less than 15 ft constrict the system. Megapores with diameter greater than 15 ft are capable of directly conveying the input hydrograph to the outflow. Therefore, the response at Big Spring depends on the input hydrographs rather than on the megapore diameter for megapore diameters greater than 15 ft.

Pollutant flux responses at Big Spring, shown in Figure 4.6, indicate that for megapores with diameters greater than 15 ft, most of the pollutant that enters the system from

sinkhole 60 does not emerge at the spring during the simulation period. This is because the flow velocities inside the megapores are very slow.

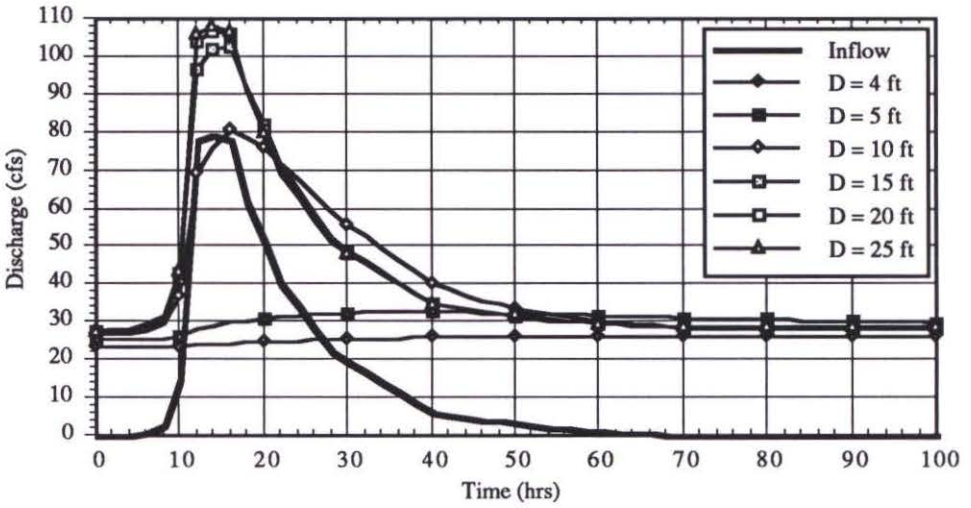

Figure 4.5. Discharge Hydrographs at Big Spring for Megapore Diameter, D, Ranging from 4 ft to 25 ft

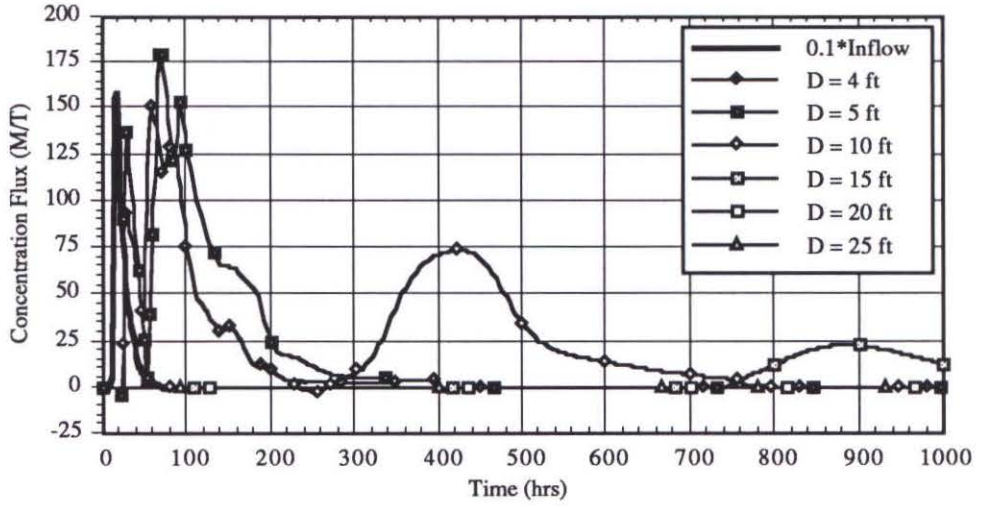

Figure 4.6. Concentration Fluxes at Big Spring for Megapore Diameter, D, Ranging from 4 ft to 25 ft

To get a better understanding of the dynamics of pollutant transport for megapore diameters less than 15 ft, two additional tests were performed with megapore diameters of

7 ft and 9 ft. The discharge and pollutant flux results of these tests are presented in Figures 4.7 and 4.8, respectively.

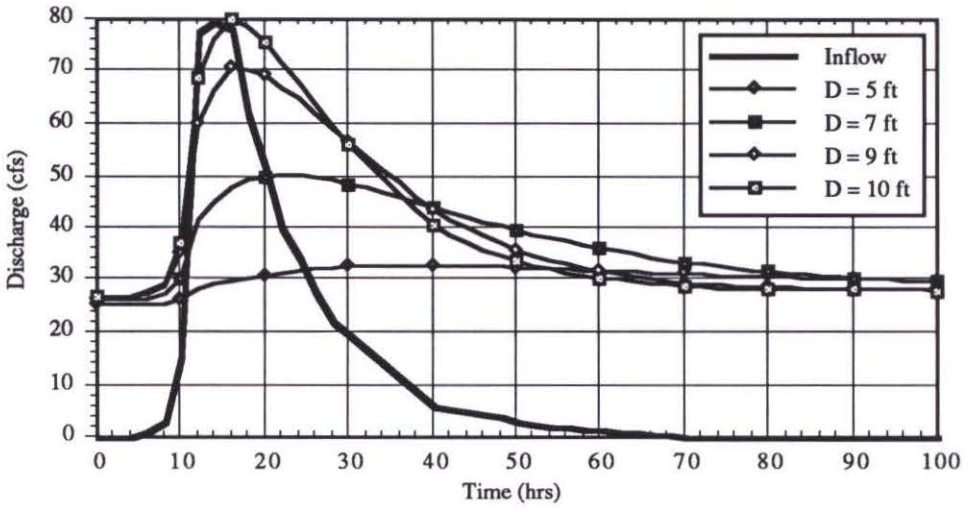

Figure 4.7. Discharge Hydrographs at Big Spring for Megapore Diameter, D, Ranging from 5 ft to 10 ft

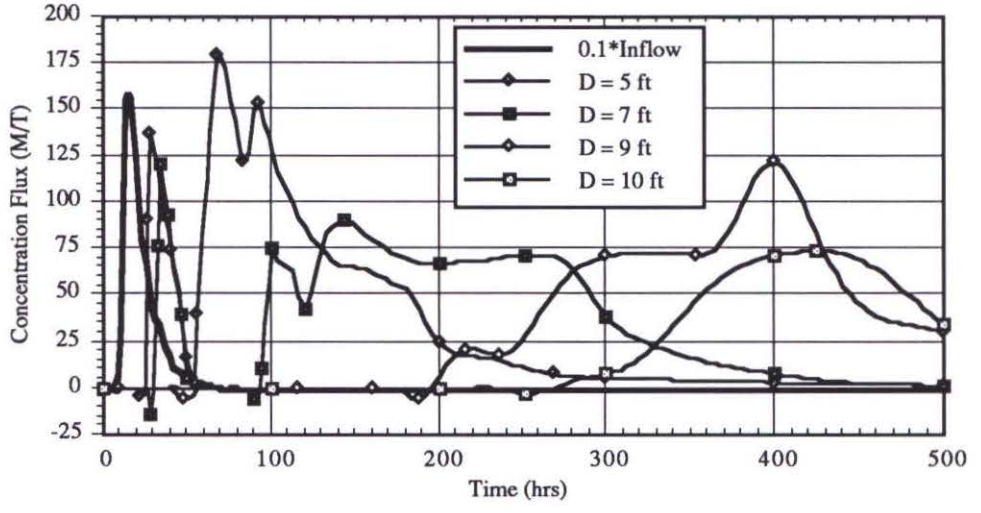

Figure 4.8. Concentration Fluxes at Big Spring for Megapore Diameter, D, Ranging from 5 ft to 10 ft

For discharges, Figure 4.7 basically leads to the same conclusion as that of Figure 4.5, namely, that the discharge responses vary at Big Spring for megapore diameters less than

15 ft. For pollutant fluxes, Figure 4.8 gives more information about the dynamics of pollutant transport than to Figure 4.6. Specifically, for megapore diameters less than 15 ft, Figure 4.8 shows that pollutant flux responses at Big Spring vary greatly with diameter. The larger the diameter, the slower the flow velocities, thus giving more time for pollutants to disperse in the flow. The more dispersed the pollutant, the more the responses look like a Gaussian cloud. At the narrowest diameter tested (5 ft) the particular dynamic of the pollutant flux is due to different paths taken by the flow from sinkhole 60 to Big Spring (see Figure 3.4).

4.3.5.2. Analysis of Sensitivity to Megapore Roughness

In this analysis, the Strickler coefficient, k_s, is chosen to represent megapore roughness. Chow (1959) presents typical values of the Manning coefficient, n (the reciprocal of the Strickler coefficient, k_s), for various types of channels. From this study, the Strickler coefficient, k_s, for a karst region is assumed to be in the range of 20 to 35.

The analysis is done by varying the values of the Strickler coefficient, k_s, while other parameters are held constant. In this analysis, hydraulic conductivity, K, is 7.6×10^{-5} fps and the specific storage, S, is 1.33×10^{-6} /ft. In order to see the effect of k_s on flux responses at Big Spring, two diameters, 5 ft and 10 ft, are chosen based on the previous analysis in which these two diameters gave different responses. The steady-state initial and boundary conditions from Section 4.3.4 are used in this analysis. An inflow hydrograph with constant pollutant concentration is entering sinkhole number 60 (see Figure 3.4).

Figures 4.9 and 4.10 present flow and pollutant transport responses at Big Spring when the megapore diameter, D, is 5 ft. Both figures show that larger values of k_s give larger water discharge and pollutant flux. These results confirm the characteristic of the Strickler coefficient; that is, since larger values of k_s produce less flow resistance, the peak of the flow comes earlier than for smaller values. Despite, the complicated shape of the pollutant fluxes in Figure 4.10, different values of k_s only affect the peaks, not the overall shape of the curve.

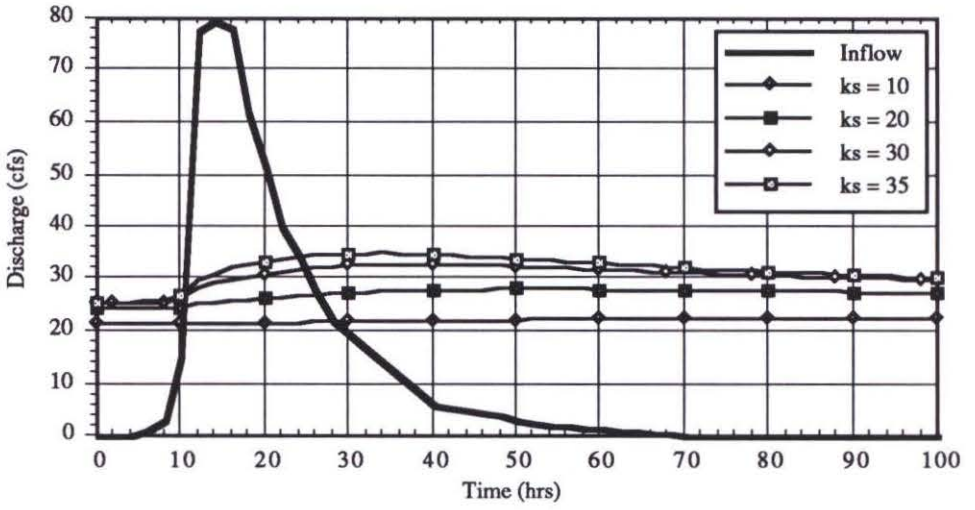

Figure 4.9. Discharge Hydrographs at Big Spring for Various Values of Megapore Strickler Coefficient, k_s, and Diameter, D = 5 ft.

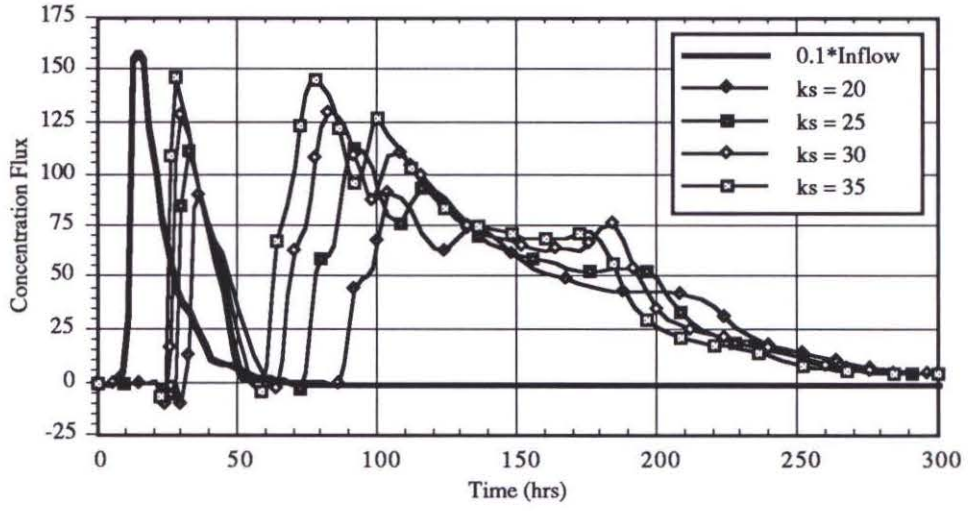

Figure 4.10. Concentration Fluxes at Big Spring for Various Values of Megapore Strickler Coefficient, k_s, and Diameter, D = 5 ft.

The same analysis is also performed with a 10 ft megapore diameter. The results for flow discharges and pollutant transport are given in Figures 4.11 and 4.12, respectively. These results confirm the results obtained with a 5 ft megapore diameter.

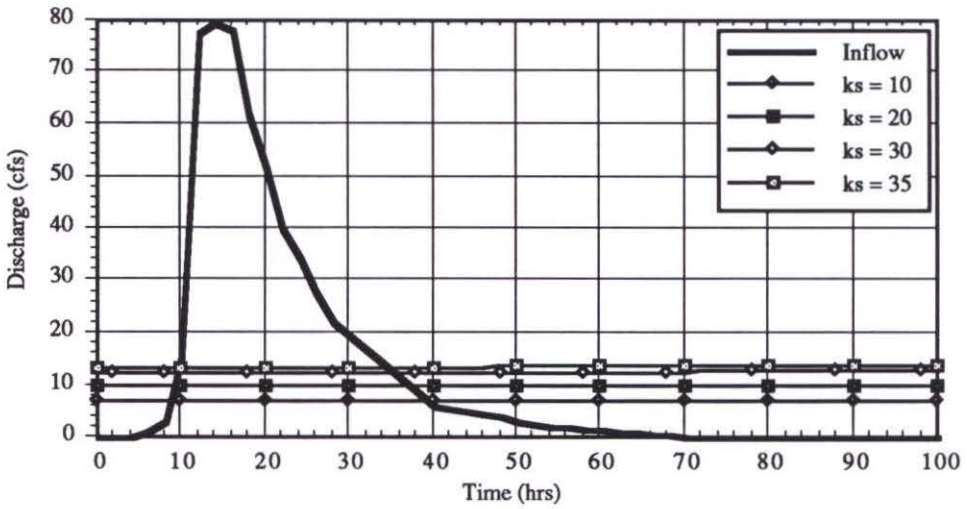

Figure 4.11. Discharge Hydrographs at Big Spring for Various Values of Megapore Strickler Coefficient, k_s, with Diameter, D = 2 ft.

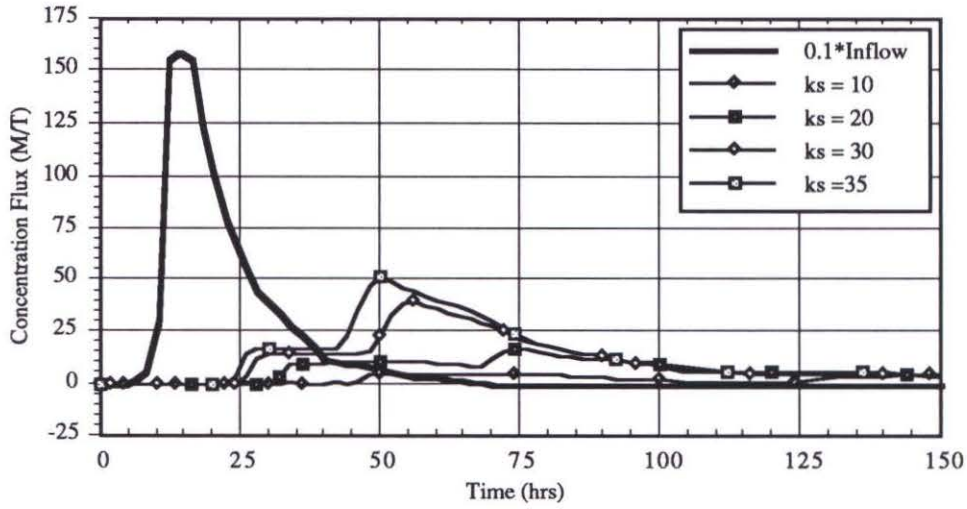

Figure 4.12. Concentration Fluxes at Big Spring for Various Values of Megapore Strickler Coefficient, k_s, with Diameter, D = 2 ft.

4.3.5.3. Analysis of Sensitivity to Aquifer-Matrix Hydraulic Conductivity

The analysis is done by varying the hydraulic conductivity values of the aquifer-matrix while other parameters are held constant. In this analysis, the Strickler coefficient for the megapores, k_s, is 30, and the megapore diameter, D, is 10 ft. The steady-state initial and

boundary conditions given in Section 4.3.4 are used in this analysis. An inflow hydrograph with constant pollutant concentration is entering sinkhole number 60 (see Figure 3.4). Three different time steps, Δt, are used to run the model, the total number of time steps, NDT, being 1500. This test simulates 3000 hours of prototype time.

Figures 4.13 and 4.14 show flow and pollutant flux responses, respectively. Recall from Section 4.3.4 that different values of hydraulic conductivity, K, give different baseflows. Figure 4.13 shows that a lower value of hydraulic conductivity, K, gives a hydrograph with the same shape as the inflow, while a higher K gives a smoother retention curve. For the value of hydraulic conductivity, $K = 7.6 \times 10^{-6}$ fps, the aquifer-matrix can be thought of as "near solid"; that is, only the megapores deliver the flow from the sinkhole to the spring. For larger values of hydraulic conductivity, the aquifer-matrix contributes more to flow delivery, resulting in an outflow hydrograph that is different in shape than the inflow.

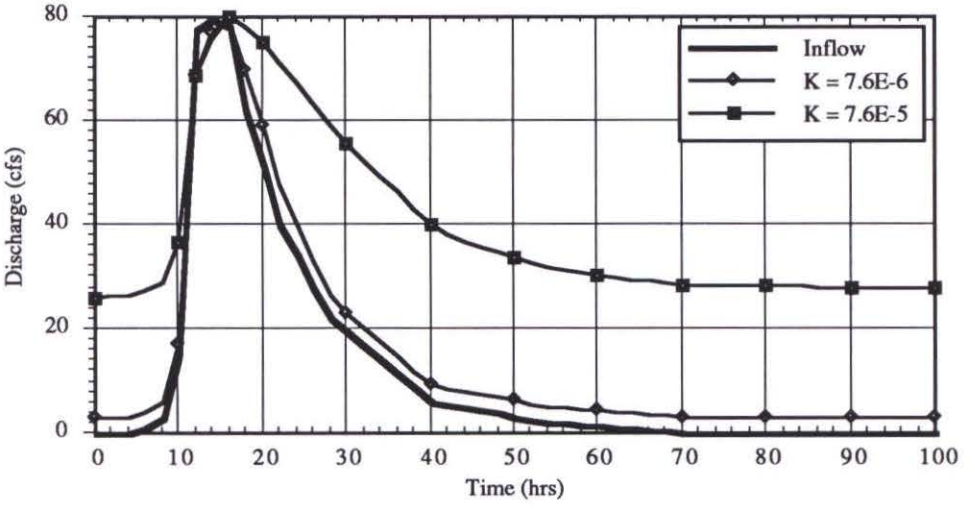

Figure 4.13. Discharge Hydrographs at Big Spring for Various Values of Hydraulic Conductivity of the Aquifer-Matrix and Megapore Diameter, D = 10 ft

For pollutant flux, the two values of hydraulic conductivity of the aquifer-matrix give quite different results. Figure 4.14 shows that for hydraulic conductivity, $K = 7.6 \times 10^{-6}$ fps, the pollutant does not emerge even after 3000 hrs, while for

$K = 7.6 \times 10^{-5}$ fps, the pollutant flux reaches the peak 400 hrs after entering the system. This difference is due to the difference of the baseflow. For hydraulic conductivity, $K = 7.6 \times 10^{-6}$ fps, the baseflow is about 3 cfs, while for $K = 7.6 \times 10^{-5}$ fps, the baseflow is about 25 cfs (see Figure 4.4.b). For the saturated case, most of the water, after entering sinkhole number 60, goes directly to Big Spring. For pollutant which is moving with the advective velocity of the water, the important part of the flow is that which gives that velocity; i.e., the baseflow, which is always available. In this case the inflow hydrograph acts to bring pollutant into the system, while the baseflow acts to transport the pollutant to Big Spring.

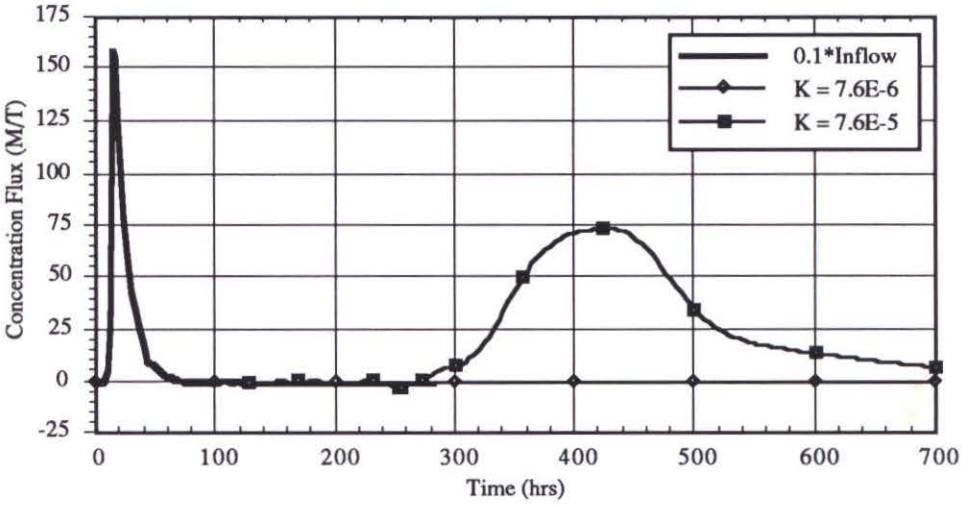

Figure 4.14. Concentration Fluxes at Big Spring for Various Values of Hydraulic Conductivity of the Aquifer-Matrix and Megapore Diameter, D = 10 ft

4.3.5.4. Analysis of Sensitivity to the Megapore Taylor Dispersion Coefficient

The analysis is done by varying the values of the Taylor dispersion constant, ε, of the megapore, while other parameters are held constant. In this analysis, the Strickler coefficient of the megapore, k_s, is 30; the hydraulic conductivity of the aquifer-matrix, K, is 7.6×10^{-5} ft/s; and the megapore diameters, D, are 5 ft and 10 ft. These two values are chosen because they give quite different responses to pollutant flux at Big Spring (see Figure 4.8). The

steady-state initial and boundary conditions mentioned previously are used in this analysis. An inflow hydrograph with constant pollutant concentration is entering sinkhole number 60 (see Figure 3.4). Three different time steps, Δt, are used to run the model, in which the total number of time steps, NDT, is 1500. This test simulates 3000 hours of prototype time.

In this test, the Taylor dispersion coefficient, ε, in Eq. (3.7) is computed by the Taylor formula (Fischer et al., 1979)

$$\varepsilon = C_t \, a \, U^* \tag{4.4}$$

where C_t is the Taylor dispersion constant; a is radius of the megapore; and U^* is the shear velocity which is equal to $\sqrt{\frac{\tau_0}{\rho}}$ or $\sqrt{gRS}$. In the latter expression, τ_0 is the pipe wall shear stress, ρ is the mass density of water, g is the gravitational acceleration, R is the radius hydraulic of the megapore, and S is the energy slope. According to Fischer et al. (1979), the Taylor dispersion constant C_t is 10.1

The analysis is done by using 50% to 200% of the suggested value of the Taylor dispersion constant of the megapore; i.e., C_t ranges from 5.05 to 20.2. The results of all tests show that there are no significant differences in the pollutant transport response at Big Spring for different values of the Taylor dispersion constant, C_t. This is because the flow is dominated by the advective phenomenon rather than the diffusive one. Therefore, the Taylor dispersion constant, C_t, does not significantly contribute to the behavior of pollutant transport.

4.3.5.5. Analysis of Sensitivity to the Classes of Megapore Diameters

From the previous sections, the sensitivity analysis shows that the model is sensitive to megapore diameters. Thus, it is of great interest to see how sensitive the model is to the classes of megapore diameters. The analysis uses different classes of megapore diameters, while other parameters are held constant. Megapore diameters are divided into four classes according to their elevation (see Figure 4.15).

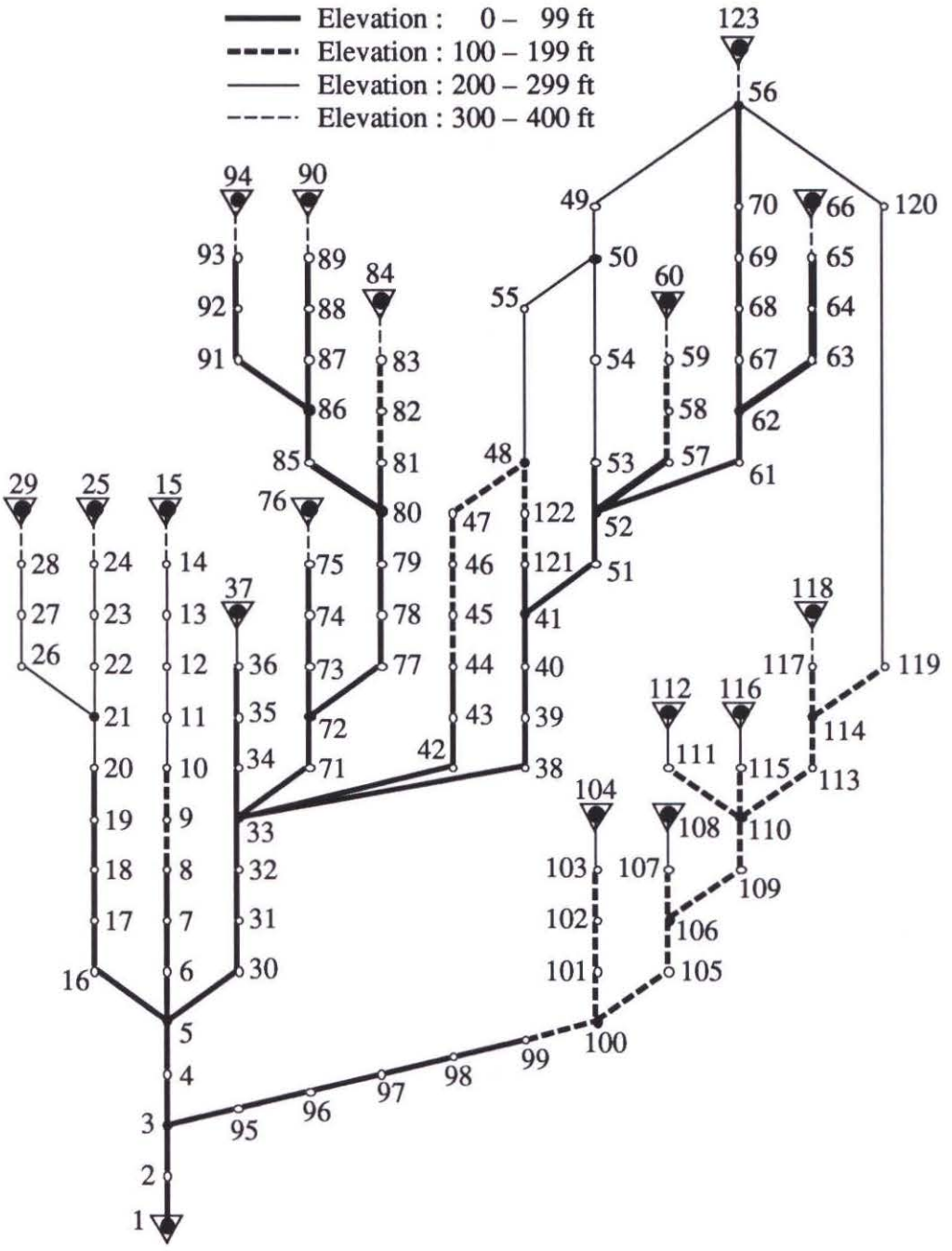

Figure 4.15. Diameter Classes Based on the Elevation of the Megapore Network

Class 1 consists of all megapores which exist between elevation 0 ft to 99 ft. Class 2 consists of all megapores which exist between elevation 100 ft to 199 ft. Class 3 consists of

all megapores which exist between elevation 200 ft to 299 ft. Class 4 consists of all megapores which exist between elevation 300 ft to 400 ft.

Four tests with different sets of the megapore diameter classes are performed, as shown in Table 4.2.

Table 4.2. Four Sets of Classes of Megapore Diameters

Name	Class 1	Class 2	Class 3	Class 4
Set 1	10.0 ft	7.5 ft	5.0 ft	Sinkholes
Set 2	5.0 ft	7.5 ft	10.0 ft	Sinkholes
Set 3	8.0 ft	8.0 ft	8.0 ft	Sinkholes
Set 4	7.0 ft	7.0 ft	7.0 ft	Sinkholes
Elevation (ft)	0–99	100–199	200–299	300–400

Megapore diameters in Set 3 of Table 4.2 are 8 ft, which is the weighted average of the diameters used in Set 1, and megapore diameters in Set 4 are 7 ft, which is the weighted average of the diameters used in Set 2. In this analysis, the Strickler coefficient of the megapore, k_s, is 30 and the hydraulic conductivity of the aquifer-matrix, K, is 7.6×10^{-5} ft/s. The same steady-state initial and boundary conditions used in the previous analyses are used in this analysis. An inflow hydrograph with constant pollutant concentration is entering sinkhole number 60 (see Figure 3.4). Three different time steps, Δt, are used to run the model, in which the total number of time steps, NDT, is 1500. This test simulates 3000 hours of prototype time.

Figures 4.16 and 4.17 present discharge and pollutant flux results, respectively, for Sets 1 and 3. Figure 4.16 shows that there are peak and shape differences in the discharge response at Big Spring depending on the megapore diameters close to Big Spring. For Set 1,

the megapore diameters close to Big Spring are 10 ft, while, for Set 3 the diameters are 8 ft. Comparison of the hydrographs of Set 1 from Figure 4.16 and those of D = 9 ft from Figure 4.7 suggests that Set 1 may be approximated using a uniform diameter of 9 ft instead of 8 ft.

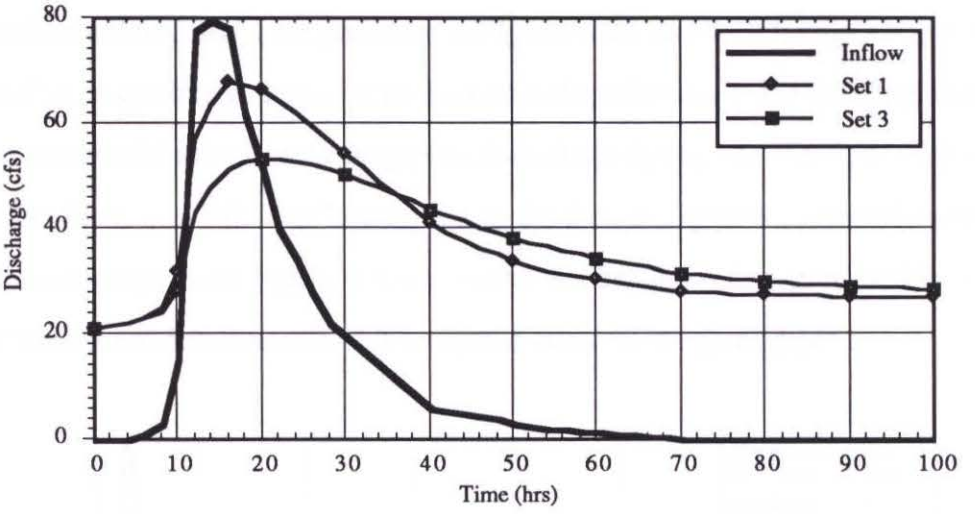

Figure 4.16. Discharge Hydrographs at Big Spring for Megapore Diameter Classes of Set 1 and Set 3.

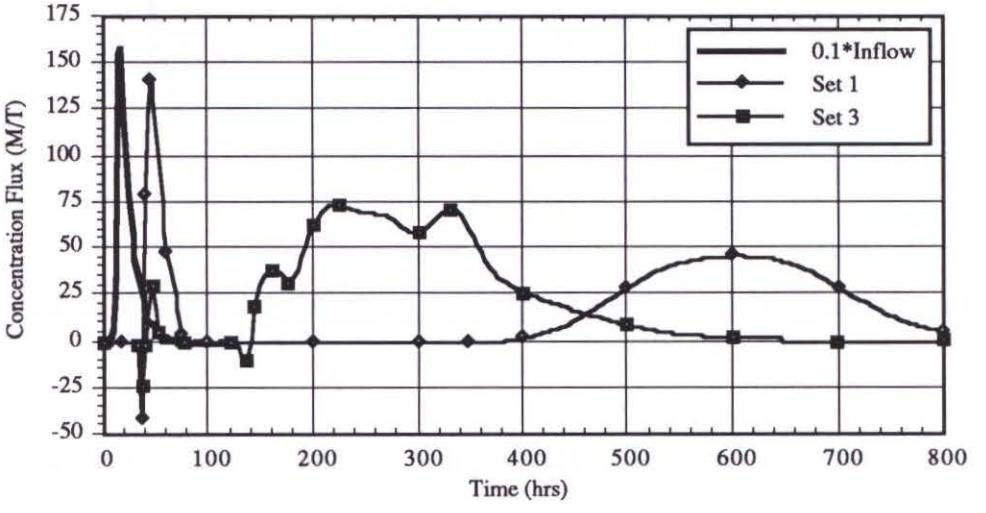

Figure 4.17. Concentration Fluxes at Big Spring for Megapore Diameter Classes of Set 1 and Set 3.

These results also show that the pollutant transport is more velocity-dependent than is discharge. Pollutant transport is, therefore, more strongly influenced by the distribution of megapore diameter classes.

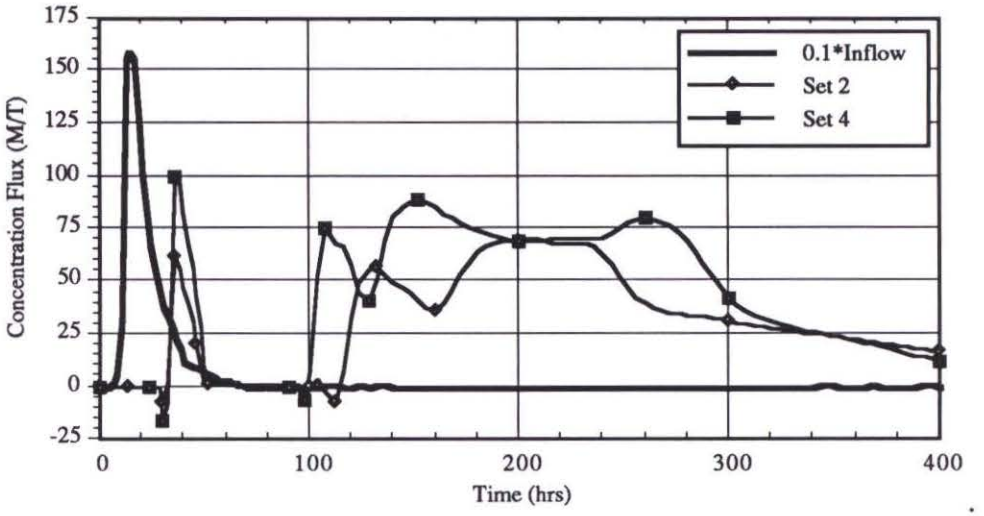

Figure 4.19. Concentration Fluxes at Big Spring for Megapore Diameter Classes of Set 2 and Set 4.

4.3.6. Water Quality Responses of the Big Spring Basin

If the present model is to serve as the basis for a broader range of research, it must be shown to be able to simulate field conditions. To do this, the model was run to simulate two of the dye trace experiments conducted by Hallberg et al. (1983). The purpose of these experiments was to establish direct connections between sinkhole recharge points and discharging springs. In the Big Spring Basin, several dye trace experiments were conducted by the Iowa Conservation Commission (ICC) and Iowa Geological Survey (IGS). Figure 4.20 shows the sinkholes used as dye input points (Hallberg et al. 1983).

4.3.6.1. Simulation of Dye Trace Experiments

In the dye trace experiments, Fluorescein dye was placed at the sinkholes. At least one week prior to both traces, packets of activated coconut charcoal were placed at the collection points. This coconut charcoal was used to capture Fluorescein from the water. These were

replaced with fresh packets the day before each trace and tested for background levels of Fluorescein which, if present, could result in a false trace. Background levels at all collection points tested negative (Hallberg et al., 1983). In the present simulation, Big Spring is the only collection point considered.

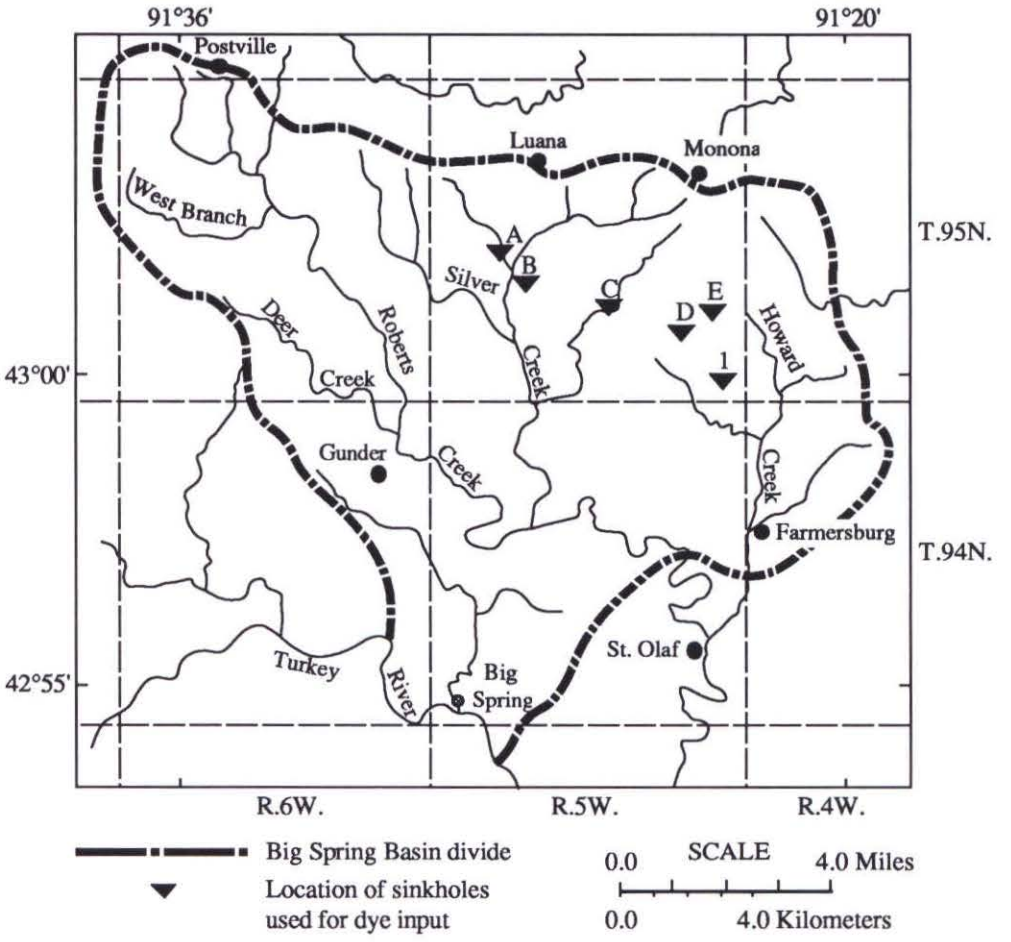

Figure 4.20. Location of Sinkholes Used for Dye Trace Experiments, after Hallberg et al. (1983)

The first dye trace experiment simulated here is the one conducted on the Bugenhagen farm (trace A, see Figure 4.20). The experiment began at 8:30 pm, when 2 pounds of Fluorescein dye were placed in a sinkhole on the farm. At that time, a stream flow of 0.02–0.05 cfs was draining directly into the sinkhole. Charcoal packets were changed

periodically at Big Spring, with the first dye appearing between 39 and 51 hours after the input. Flow at Big Spring during this period varied from 62 to 65 cfs (Hallberg et al. 1983).

To simulate dye trace A, it is first assumed that all sixteen sinkholes have the same inflow of 0.05 cfs, giving a total inflow of 0.8 cfs. This assumption is a very minor one, since total sinkhole inflow only constitutes 1.3% of the total discharge at Big Spring. The rest of the discharge is assumed to originate from the aquifer-matrix. This simulation is done by using the fixed megapore topology previously used in the sensitivity analysis, and by imposing discharge on the aquifer-matrix in the area surrounding the arbitrarily-chosen sinkholes 60, 66, 94, and 118 so that the discharge at Big Spring is within the range of 62 to 65 cfs. The model is run for megapore diameters, D, ranging from 5 to 10 ft; two values of megapore roughness, k_s, 30 and 20; and two values of hydraulic conductivity, K, 7.6×10^{-5} fps and 7.6×10^{-6} fps. At time t = 6 hrs, a pollutant concentration of 2000 units is imposed at sinkhole 60 so that a pollutant flux of 100 units enters the sinkhole. Sinkhole 60 is chosen to represent the sinkhole used in the actual dye trace A experiment since it is the nearest sinkhole in the computational network to the real one.

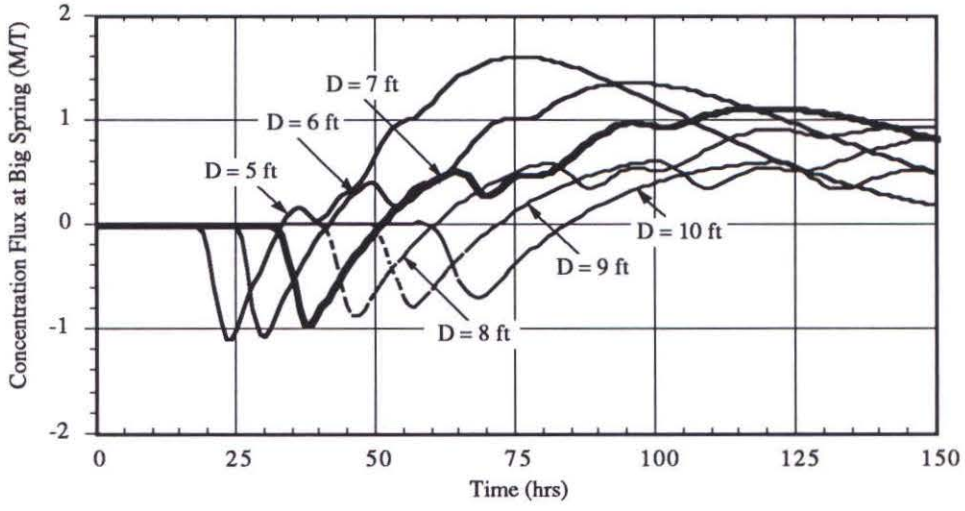

Figure 4.21. Results of Simulation of Dye Trace A for Several Megapore Diameters, D; Megapore Roughness, $k_s = 30$; and Hydraulic Conductivity, $K = 7.6 \times 10^{-5}$ fps

Figure 4.21 presents the results of the simulation for megapore diameter, D, ranging from 5 to 10 ft; megapore roughness, k_s, equal to 30; and hydraulic conductivity, K equal to 7.6×10^{-5} fps. During the simulation, discharge at Big Spring is 63.8 cfs. Complete results are given in Table 4.3.

Table 4.3. Results of Simulation of Dye Trace A

Diameter (ft)	Travel Time (hrs)		
	$K = 7.6 \times 10^{-5}$ fps $k_s = 30$	$K = 7.6 \times 10^{-5}$ fps $k_s = 20$	$K = 7.6 \times 10^{-6}$ fps $k_s = 30$
5	28	28	27
6	36	36	34
7	45	45	43
8	55	55	53
9	67	67	63
10	79	79	75

In Table 4.3, the travel times of the pollutant flux at Big Spring are taken to be the first positive pollutant flux encounters as shown in Figure 4.21. Figure 4.21 shows that due to numerical errors, negative pollutant flux precedes the first positive flux with the same order of magnitude. It should be realized that both the negative and positive pollutant fluxes are almost undetectable compared to the imposed pollutant influx of 100 units entering sinkhole 60.

Figure 4.21 and Table 4.3 show that, for all cases, a megapore diameter of 7 ft produces travel times that lie within the range of the real travel time of dye trace A; i.e., from 39 to 51 hours. Table 4.3 also shows that variation of megapore diameter gives significantly different travel times. Specifically, there is a narrow variation of megapore diameter that

produces the correct travel time of dye trace A; i.e., about 1.25 ft or megapore diameters from 6.25 to 7.5 ft (see Figure 4.22). Table 4.3 shows that variation of megapore roughness, k_s, from 30 to 20 does not affect the travel time, while variation of hydraulic conductivity of the aquifer-matrix gives a difference of travel time ranging from 1 to 4 hours.

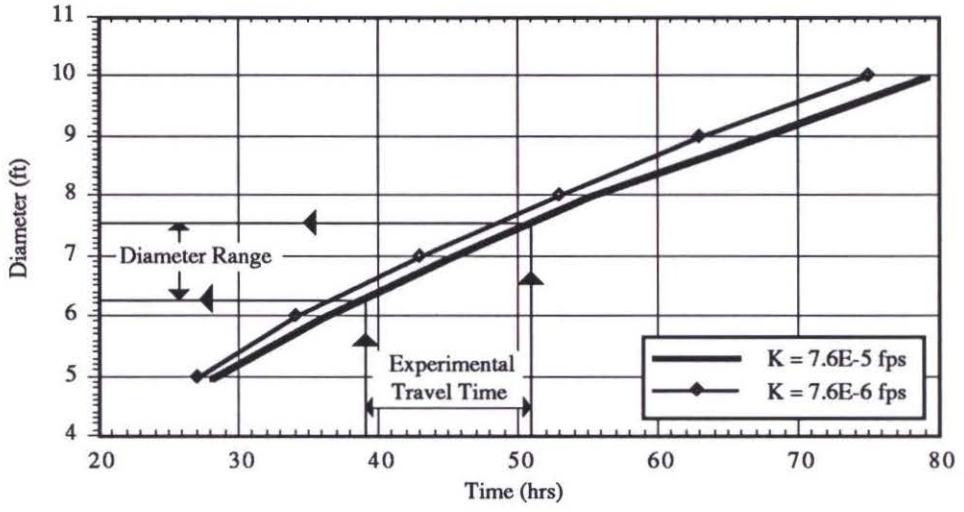

Figure 4.22. Travel Time, in Hours, versus Megapore Diameter, in Feet, in the Simulation of Dye Trace A

The second dye trace experiment simulated here was conducted on the Baade sink (trace 1, see Figure 4.20). The experiment began at 9:00 pm, when 2 pounds of Fluorescein dye were placed in a sinkhole on the Baade sink. At that time, a stream flow of 0.11 cfs was draining directly into the sinkhole, due to a heavy rain in the basin. Charcoal packets were replaced at 1/2 day intervals at Big Spring with the first dye appearing between 44 and 50 hours after input. Flow at Big Spring during this period was approximately 56 cfs (Hallberg et al., 1983).

To simulate dye trace 1, it is first assumed that all sixteen sinkholes have the same inflow of 0.11 cfs, giving a total inflow of 1.67 cfs. This is a minor assumption since the sinkhole inflow only constitutes 3.0% of the total discharge at Big Spring. The rest of the discharge is

assumed to originate from the aquifer-matrix. This simulation is done using the fixed megapore topology as before, and imposing discharge on the aquifer-matrix in the area surrounding sinkholes 25, 60, 66, and 112 so that the discharge at Big Spring is about 56 cfs. As in the previous dye trace experiment, these four sinkholes are chosen arbitrarily. The model is run for megapore diameters, D, ranging from 5 to 10 ft; two values of megapore roughness, k_s, 30 and 10; and two values of hydraulic conductivity, K, 7.6×10^{-5} fps and 7.6×10^{-6} fps. At time t = 6 hrs, a pollutant concentration of 2000 units is imposed at sinkhole 112 giving a pollutant flux of 220 units entering the sinkhole. Sinkhole 112 is chosen to represent the sinkhole used in the actual dye trace 1 experiment since it is the nearest sinkhole in the computational network to the real one.

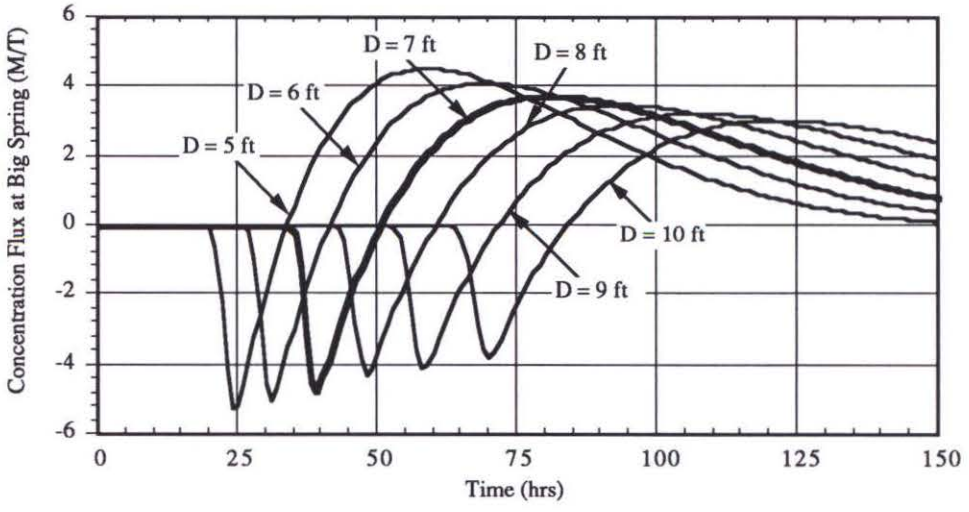

Figure 4.23. Results of Simulation of Dye Trace 1 for Several Megapore Diameters, D; Megapore Roughness, k_s = 30; and Hydraulic Conductivity, K = 7.6×10^{-5} fps

Figure 4.23 presents the results of the simulation for megapore diameter, D, ranging from 5 to 10 ft; megapore roughness, k_s, equal to 30; and hydraulic conductivity, K, equal to 7.6×10^{-5} fps. During the simulation, discharge at Big Spring is 56.0 cfs. Complete results are given in Table 4.4.

Figure 4.23 and Table 4.4 show that, for all cases, a megapore diameter of 7 ft produces travel times that lie within the range of the real travel time of dye trace 1; i.e., from 44 to 50 hours. Table 4.4 also shows that variation of megapore diameter gives significantly different travel times. Specifically, Table 4.4 shows that a narrow variation of megapore diameter produces the actual travel time of dye trace 1; i.e., about 0.6 ft or megapore diameters from 6.8 to 7.4 ft (see Figure 4.24). Table 4.4 shows that variation of megapore roughness, k_s, from 30 to 10 does not affect the travel time, while variation of hydraulic conductivity of the aquifer-matrix gives a difference of travel time ranging from 4 to 7 hours.

Table 4.4. Results of Simulation of Dye Trace 1

Diameter (ft)	Travel Time (hrs)		
	$K = 7.6 \times 10^{-5}$ fps, $k_s = 30$	$K = 7.6 \times 10^{-6}$ fps, $k_s = 30$	$K = 7.6 \times 10^{-6}$ fps, $k_s = 10$
5	28	24	25
6	36	32	32
7	45	40	40
8	55	50	50
9	66	60	60
10	79	72	72

In Table 4.4, the travel times of the pollutant flux at Big Spring are taken to be the first positive pollutant flux encounters as shown in Figure 4.23. Figure 4.23 shows that due to numerical errors, negative pollutant flux precedes the first positive flux with the same order of magnitude. It should be realized that both the negative and positive pollutant fluxes are almost undetectable compared to the imposed pollutant influx of 220 units entering sinkhole 112.

Moreover, the above results are based on following ranges of parameters: megapore diameter, D, from 3 ft to 30 ft; hydraulic conductivity, K, from 7.6×10^{-6} fps to 7.6×10^{-5} fps; megapore roughness, k_s, from 10 to 35; and Taylor dispersion coefficient, C_t, from 5.05 to 20.2, values which are 50% to 200% of the suggested value of C_t (10.1).

The results of sensitivity are summarized in the following paragraphs:

(1) The size of the equivalent megapore dictates whether the overall system is responsive or diffusive. Generally, the smaller the diameter, the less responsive the system to a storm hydrograph entering sinkholes. Moreover, for a given megapore diameter, there is a threshold input hydrograph that the megapore can pass directly.

(2) Megapore diameter classes are particularly important for pollutant transport while this feature does not significantly affect discharge response. The same discharge response at Big Spring may be obtained by replacing several megapore diameter classes by one uniform diameter, but it is difficult to get the same pollutant response using this procedure.

(3) After megapore diameters and their classes, hydraulic conductivity of the aquifer-matrix is the third most important parameter. The importance of hydraulic conductivity is due to its contribution to the baseflow of the system. Generally, in any storm event, if there is pollutant in the water, the storm acts only as a carrier to bring the pollutant from outside into the system (i.e., aquifer-matrix and megapore network). Inside the system itself, the pollutant is usually carried by the baseflow, except for the case of small megapore diameters in which small amounts of the pollutant are also carried by the storm, resulting in a flashy downstream pollutant flux.

(4) Megapore roughness is a mildly important parameter. Generally, this parameter only slightly affects the peak discharge of water and pollutant, as well as the time to peak. The overall behavior of responses at Big Spring is not affected by this parameter.

(5) The dispersion coefficient also does not play an important role in the present study since the advective phenomenon is dominant compared to the diffusive one. Variation of the value of the dispersion coefficient, C_t, from 50% to 200% of the suggested value does not give significant differences in pollutant transport at Big Spring.

Figure 4.25 shows that discharge response at Big Spring for a 20 ft megapore diameter,

The simulation of the dye trace experiments, shows that travel times of the dye traces are very sensitive to megapore diameter, confirming that megapore diameter is the most important parameter affecting the system. The range in magnitude of diameter that produces the actual travel time is within 1.5 ft of the representative diameter. Even though the representative diameters chosen in the previous section are not necessarily the actual ones, the range of deviation from the representative diameter is an important finding. This narrow deviation shows that megapore diameter significantly affects pollutant transport. These results confirm the conclusion of the sensitivity analysis on megapore diameter.

The simulation results show that the maximum outflow at Big Spring usually coincides with a point in the inflow hydrograph. It should be possible, therefore, to predict the flow at Big Spring using a reservoir-type formulation, which avoids the complexity of a detailed mathematical formulation that considers all the water pathways (megapore network). For pollutant transport, however, the pathways are important and the reservoir formulation is not adequate to determine the concentration of pollutants in the Big Spring flow. Thus, the discharge response at Big Spring can be written as:

$$\frac{dO}{dt} = I(t) - O(t) \qquad (4.4)$$

where I(t) is known storm hydrographs entering sinkholes and O(t) is discharge response at Big Spring. When O(t) reaches maximum value, i.e., $\frac{dO}{dt} = 0$, the discharge response at Big Spring is $O(t = t_1) = I(t = t_1)$. As the system becomes a diffusive one, i.e., the megapore diameters decrease, Eq. (4.4) will no longer apply, as shown in Figure 4.9.

CHAPTER V

CONCLUSIONS AND FURTHER RESEARCH

5.1. Conclusions

This section summarizes all results obtained from the present study. First, from sensitivity analysis, important parameters and features of the karst region have been identified. The most important parameter is the equivalent megapore diameter, and its distribution throughout the megapore network is the most important feature of the megapores. Other parameters affecting the Big Spring Basin ranked in order of importance are hydraulic conductivity of the aquifer-matrix, megapore roughness and dispersion coefficient. The megapore dispersion coefficient does not affect the basin, since the pollutant transport is dominated by advection rather than dispersion phenomenon.

Second, the main objective of the present study has been achieved by the computer code Labyrinth. The Labyrinth code is capable of simulating the behavior of saturated groundwater flow and pollutant transport in karst regions. The two modes of the flow; fast-response flow in cave passages and slow-response flow in the aquifer-matrix, have been correctly reproduced by the Labyrinth code.

Third, the results of the dye trace simulation, viewed in a Monte Carlo simulation framework, succeed in producing realizations for dye trace A and 1 experiments. Thus, the Labyrinth code has shown the capability to serve as a "deterministic engine;" suggestions for extension of the code into a complete "deterministic engine" in a Monte Carlo simulation are explained in the following sections.

5.2. Further Research

This section suggests how the present model could be made more reliable and how it could be extended to more general cases. The suggestions range from simple to complex according to the time needed to extend the capability of the Labyrinth code to handle each proposal. These times, however, are only approximate since field data availability and requirements greatly influence the priority of further research.

5.2.1. Field Experiment to Test the Labyrinth code

Field data show that peak discharges at Big Spring typically occur in February or March, sometimes extending to May, during which time the aquifer is still in a near-saturated condition. Thus, the present study, which deals only with saturated cases, may be used to simulate the Big Spring Basin response to a storm in that period.

First, to model the response of the Big Spring Basin due to a storm inflow hydrograph entering sinkholes, the rainfall over the basin, discharge entering sinkholes, and outflow from the basin, all for the same period, are needed.

Second, to model the pollutant transport in the basin, the size and distribution of megapore diameters are needed. From the sensitivity analysis and dye trace simulation, the results show that the pollutant transport is greatly influenced by the megapore diameters and their distribution. Therefore, one may exploit dye trace experiments to predict the megapore diameters and their distribution. For example, variable dye trace tests may be carried out in which variable concentration dye is inputted into a sinkhole over a period of time and the response at Big Spring is recorded. Other dye trace experiments (Hallberg et. al., 1984) might be used to gain more insights into the behavior of pollutant transport at Big Spring because these experiments were conducted when outflow at Big Spring fluctuated.

Since the baseflow also plays an important role in transporting the pollutant, identification of the flow that contributes to the baseflow in the Big Spring Basin is crucial. For example, Hallberg et al. (1983) points out that Roberts Creek (see Figure 4.20) lost 0.3 cfs over a 6 mile reach during winter low-flow periods. Farther downstream, the same

creek lost even more flow into a sinkhole, and standing water in adjacent sinkholes was about 6 ft below the level of the creek. This phenomenon is important to the Labyrinth code since it can serve as a boundary condition of the imposed-head type, giving a major contribution for the baseflow to the model. Other observations suggest that, at other times in the past, nearly the entire flow of Roberts Creek has been swallowed by sinkholes in the losing reach. Although at the present time, all sinkholes along Roberts Creek have been plugged, either by man or natural activity, in the future this phenomenon may occur again. Therefore, field identification of such phenomena is necessary to improve the reliability of the Labyrinth code.

5.2.2. Development of the Labyrinth code to Handle Unsaturated Cases

Extending the Labyrinth code to handle unsaturated cases is challenging because of the complexity of flow in unsaturated karst regions. Complexities arise in the megapore network and aquifer-matrix computation, as discussed in the following paragraphs.

In the megapore network, the difficulties are not due solely to the partially full megapore flow, but from the fact that in karst regions many of the megapores are vertically oriented; i.e., sinkholes or vertical shafts. The present code might be extended without difficulties to handle a partially full flow as long as the megapore is almost horizontal since, in this case, the governing equation (3.5) can still be used (open-channel flow). For vertically oriented megapores, however, the governing equation (3.5) is not applicable, because one of its assumptions, that there is no vertical acceleration in the flow, is violated. Thus, the solution of this problem is needed before extending the Labyrinth code to handle unsaturated cases. Moreover, in order to conform with other megapore solutions, and thus to avoid major revision in the present code, the solution must be cast in the form appropriate for the double-sweep technique explained in Chapter III.

In the aquifer-matrix, complexities arise due to the dependency of soil parameters, such as the hydraulic conductivity, K, the specific storage, S, in Eq. (3.1), and the bulk dispersion coefficient, D, in Eq. (3.3), on the water content of the aquifer. The mathematical formulation of the flow in an unsaturated aquifer-matrix or porous media may be expressed as

the Richards equation. For the case of three-dimensional flow with the Cartesian computational coordinates aligned with the principal direction of anisotropy, the Richards equation becomes

$$\frac{\partial}{\partial x}\left[K_x(\psi)\frac{\partial \psi}{\partial x}\right]+\frac{\partial}{\partial y}\left[K_y(\psi)\frac{\partial \psi}{\partial y}\right]+\frac{\partial}{\partial z}\left[K_z(\psi)\frac{\partial}{\partial z}(\psi+z)\right]=S(\psi)\frac{\partial \psi}{\partial t} \qquad (5.1)$$

where ψ indicates the capillary pressure head, z is the vertical coordinate, and $S(\psi)$ is the specific storage. In this equation, ψ depends on the water content of the aquifer-matrix or porous media.

As with the solution of problems in the saturated zone, the solution of Eq. (5.1) requires the specification of initial and boundary conditions. However, unlike the case of saturated flow, the statement of water content distribution alone is not sufficient because $\psi(\theta_w)$, where θ_w is the water (or moisture) content, is subject to hysteresis. It is also necessary to state whether a drying or a wetting process is taking place along the boundary. Assuming that $\psi(\theta_w)$ is known, if the flow reverses its direction during the period of study, hysteresis must be taken into account.

For pollutant transport in the aquifer-matrix, the governing equation (3.3) can be used as long as the value of the bulk dispersion coefficient of the aquifer-matrix, D, is obtained by taking the water content of the aquifer into consideration. The initial and boundary conditions for unsaturated cases are basically the same as those used in saturated cases.

5.2.3. Development of the Labyrinth Code to Include Stochastic Processes

The output of a numerical model of flow and/or pollutant transport in a groundwater system will normally contain errors of unknown magnitude. These errors arise from several sources:

1. the extent to which actual physical and chemical processes are represented in the model;
2. numerical methods used to solve differential equations;

3. errors in the values of system parameters (aquifer properties; system geometry; initial and boundary conditions).

Thus, there is always a degree of uncertainty involved in modeling a groundwater system, and it would be desirable to be able to estimate this uncertainty. In the following paragraphs, the possible extension of the present study to incorporate uncertainty analysis is outlined.

The governing flow and transport equations used in the present model are partial differential equations (PDEs) relating a variable (e.g., the piezometric head or the concentration) at a point in space and time to the parameters of the aquifer. Classically, both the variables and the parameters are considered deterministically. That is, each parameter is defined by a unique value at each location and time, even though this value may vary with space and/or time. It is possible, however, to consider partial differential equations relating stochastic variables to stochastic parameters; these are simply called stochastic PDEs. Spectral, perturbation, and Monte Carlo methods are used for solving such equations.

The spectral method has been used extensively. This method is well suited to infinite media and analytical models. In this method, both the variable and the parameter are defined as a mean plus a fluctuation around the mean. Introducing this definition into the stochastic PDE, and taking the expected value of the equation, results in two new equations, one for the mean and one for the fluctuation. The first, an ordinary deterministic PDE, which can be solved analytically, provides the mean of the variable as a function of the mean of the parameter. The second equation, relating to the fluctuation, is transformed in the spectral domain by Fourier-Stieljes integrals, and the spectrum of the variable is obtained as a function of the spectrum of the parameter. The spectrum, or spectral density, is the Fourier transform of the covariance function. By an inverse Fourier transform, it is then possible to calculate analytically the covariance function of the variable (Peck et al., 1988).

The perturbation method can be used with analytical and numerical models and in conjunction with spectral methods. In this method, the uncertainty in parameters must be

small. Thus, the fluctuation around the mean can be developed in a Taylor series, neglecting second order terms. As in the spectral method, the variable and the parameter are defined as a mean and a fluctuation, but the fluctuations of both the variable and the parameter are multiplied by a small factor β. This is introduced in the PDE, which is then developed in terms of zero and first order expressions of β, neglecting higher order terms. The zero-order term is a deterministic equation for the mean. By taking the expected value of the first order term, it is possible to obtain an expression for the covariance of the variable as a function of that of the parameter (Peck et al., 1988).

The Monte Carlo simulation method is certainly the most powerful yet the easiest to understand. Unlike the two previous methods, which are better suited to studying uncertainty associated with a single class of parameters, this method can be applied when many classes of parameters are simultaneously uncertain. For this reason, it is proposed that Monte Carlo simulation be used to analyze uncertainty in the present study, or stated more appropriately, that the Labyrinth code be embedded in a Monte Carlo simulation, as depicted in Figure 5.1. A Monte Carlo simulation is described in the following paragraphs.

5.2.3.1. Monte Carlo Simulation

The Monte Carlo simulation works as follows. Given that N parameters in the present model are uncertain, e.g., megapore diameters and their distribution, topology of megapore network, megapore roughness, hydraulic conductivity of the aquifer-matrix, and initial and boundary conditions, one assumes that the probability density functions (PDFs) of their uncertainty are known. Using a random number generator, one then selects a value for each of these N parameters. Depending on the information available, the values taken by these N parameters can be considered as independent or correlated. With these sets of parameters, the Labyrinth code is run and a set of results is obtained. Another random selection of parameters is made and the model is run again, and so on, a very large number of times (e.g., 100, 1000 or 10000 times), thus producing a large number of model results. One then calculates the mean, variance, covariance, or PDF of the model results for each point of interest, or for any desired function of results (see Figure 5.1). The method is expensive in terms of computer

time, but it is easy to implement since any existing numerical model can be used in a Monte Carlo simulation mode. The method requires a subroutine to sample parameter values independently, or jointly in their respective PDF, including, when relevant, their internal correlation.

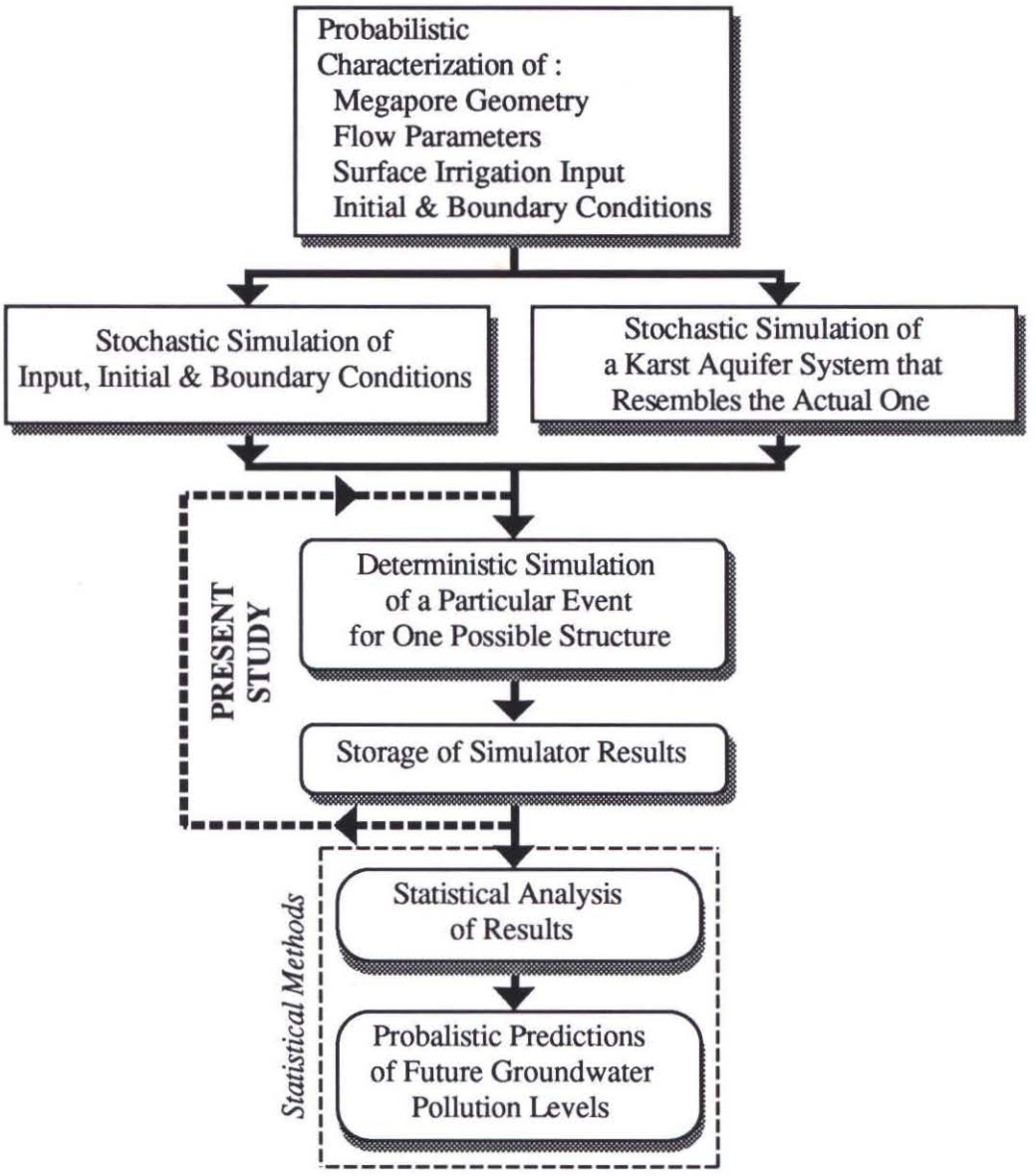

Figure 5.1. Monte Carlo Simulation Diagram for the Big Spring Basin

5.2.3.2. Limitations of Monte Carlo Simulations

Monte Carlo simulations are probably the best available tool for evaluating uncertainty in model predictions. Limitations of this method, however, need to be emphasized.

(1) *Size of sample.* With a limited number of runs (e.g., 100), it may be possible to obtain a reasonable estimation of the first moment of the results (mean). Note that in problems involving nonlinearities, the mean of the model results will not be equal to the results obtained by running the model once with the mean of the parameter. To obtain a reasonable estimate of the second moment of the model results (variance, covariance, etc.), a much larger number of Monte Carlo simulation runs is required (e.g., 1000 or more). The number of runs depends on the variability of the parameters, their number, the sensitivity of the system, etc., so that no general rule can be applied. Finally, to estimate the PDF of the model results, an even larger number of runs must be performed. For instance, the study of uncertainty of model results is aimed at estimating the probability that a given situation is reached (e.g., the pollutant concentration at Big Spring is larger than a specified maximum value). However, the smaller the probability, the larger the number of runs required. Note that it is always possible to estimate an uncertainty band around the estimated PDF of the results, given a finite number of runs.

(2) *Existence of a solution and convergence of the Monte Carlo solution.* To use the Monte Carlo method, it is assumed that the variability or uncertainty of the parameters can be described by stationary random functions, in which case one can define a mean, variance and covariance which must be estimated from the measurements. Generally, in analyzing the results, the implicit assumption is that the Monte Carlo results are stationary and thus the mean, variance and covariance can be computed.

Suppose now that the results are not stationary, but intrinsic. In this case, covariance is replaced by the variogram, and the variance can no longer be defined. For a given number of

runs, it is always possible to calculate a mean, variance and covariance. If, however, these quantities do not exist for the infinite sample, they are only a function of the number of runs performed and cannot tell us anything about the real system. Unfortunately, for a given problem, there is no practical method to determine a priori if the solution will be stationary or not; even analytically this is a problem. Peck et al. (1988) suggests the following steps to deal with these difficulties.

(a) The first step is to make sure that the same type of problem has already been addressed; e.g., by analytical methods, and that a stationary solution has been found. Then one may assume that for another geometry, another value of the parameters, etc., the results are also stationary.

(b) The second step is to calculate the mean, variance and covariance of the results as a function of the number of runs; if these values fluctuate but reach an asymptotic value, one can, with some degree of confidence, assume that they are stationary. If not, then the problem is not stationary, and other assumptions; e.g., intrinsic, can be tested.

(3) *Averaging scale*. When Monte Carlo simulations are used to study the uncertainty of parameters of a numerical model, the statistical properties of the parameters are those of the averaged values of the parameter over each element or block of the model. In the stationary case, the mean is unchanged, but the variance and covariance are changed by spatial averaging.

5.2.3.3. Generation of Megapore Topology

Even though the present study uses a fixed topology for the megapore network, there is no doubt that megapore topology is very important. As shown in Figure 5.1, generation of megapore topology is required to performed a Monte Carlo simulation.

In recent years, reseachers have modeled fractured networks using statistical methods. Specifically the works of Feuga (1988) and Witherspoon et al. (1988) offer insight into generating megapore topology for the present study. Feuga (1988) used the "regionalized

density Poissonian process" to generate fracture fields that are statistically and geostatistically similar to the real fracture field at the Fanay-Augères mine in France. Feuga (1988) and Witherspoon et al. (1988) generated a three-dimensional channel network in fractures. This three-dimensional channel network is particularly fit to the present study with the added requirement that the network must be constrained to pass as many aquifer-matrix grid points as possible, as explained in Chapter III.

5.3. Concluding Remarks

As a part of a larger research objective — to serve as the deterministic engine of a Monte Carlo simulation of water resources in a karst region — the Labyrinth code has a promising future. At present, however, due to limited availability of data and time, the Labyrinth code can only produce the qualitative behavior of saturated groundwater flow and pollutant transport. If more field data and resources become available in the future, more thorough tests can be performed on the Labyrinth code to completely understand its behavior and to calibrate parameters, thus enabling the present code to predict future conditions of the Big Spring Basin during wet seasons. Moreover, the extension of the Labyrinth code to handle unsaturated cases and its inclusion in a Monte Carlo simulation will make the code a powerful tool to analyze water resources in karst regions.

APPENDIX A

DETAILED DERIVATION OF EQUATIONS USED IN CHAPTER III MODEL DEVELOPMENT

This appendix presents detailed derivations of equations mentioned in Chapter III. Equations that start with the number "3" are defined in Chapter III; equations starting with the letter "A" are defined in this appendix.

A.1. Derivation of Eq. (3.18)

To accommodate three fractional steps Eq. (3.17) is split into three fractions as follows:

• First fraction: x-direction

$$(1-\theta)\,\delta_x^2 h^n + \theta\,\delta_x^2 h^{n+1} - \frac{1}{3} W^n - \theta \frac{\partial W}{\partial h_s}(h^x - h^n) - \frac{\theta}{3}\frac{\partial W}{\partial h_m}(h_m - h_m^n) = \frac{S\upsilon}{\Delta t}(h^x - h^n)$$

will be approximated as

$$(1-\theta)\,\delta_x^2 h^n + \theta\,\delta_x^2 \mathbf{h^x} - \frac{1}{3} W^n - \theta \frac{\partial W}{\partial h_s}(h^x - h^n) - \frac{\theta}{3}\frac{\partial W}{\partial h_m}(h_m - h_m^n) = \frac{S\upsilon}{\Delta t}(h^x - h^n) \qquad (A.1)$$

• Second fraction: y-direction

$$(1-\theta)\,\delta_x^2 h^n + \theta\,\delta_x^2 h^{n+1} - \frac{1}{3} W^n - \theta \frac{\partial W}{\partial h_s}(h^x - h^n) - \frac{\theta}{3}\frac{\partial W}{\partial h_m}(h_m - h_m^n) = \frac{S\upsilon}{\Delta t}(h^x - h^n)$$

will be approximated as

$$(1-\theta)\,\delta_y^2 \mathbf{h}^x + \theta\,\delta_y^2 \mathbf{h}^y - \frac{1}{3} W^n - \theta \frac{\partial W}{\partial h_s}(h^y - h^x) - \frac{\theta}{3}\frac{\partial W}{\partial h_m}(h_m - h_m^n) = \frac{S\upsilon}{\Delta t}(h^y - h^x) \tag{A.2}$$

• Third fraction: z-direction

$$(1-\theta)\,\delta_z^2 h^n + \theta\,\delta_z^2 h^{n+1} - \frac{1}{3} W^n - \theta \frac{\partial W}{\partial h_s}(h^{n+1} - h^y) - \frac{\theta}{3}\frac{\partial W}{\partial h_m}(h_m - h_m^n) = \frac{S\upsilon}{\Delta t}(h^{n+1} - h^y)$$

will be approximated as

$$(1-\theta)\,\delta_z^2 \mathbf{h}^y + \theta\,\delta_z^2 h^{n+1} - \frac{1}{3} W^n - \theta \frac{\partial W}{\partial h_s}(h^{n+1} - h^y) - \frac{\theta}{3}\frac{\partial W}{\partial h_m}(h_m - h_m^n) = \frac{S\upsilon}{\Delta t}(h^{n+1} - h^y) \tag{A.3}$$

In the above derivations, the boldfaced variables are the approximations of the original ones. Thus, Eqs. (A.1), (A.2), and (A.3) can be generalized as follows:

$$(1-\theta)\,\delta^2 h^n + \theta\,\delta^2 h^{n+1} - \frac{1}{3} W^n - \theta \frac{\partial W}{\partial h_s}(h^{n+1} - h^n) - \frac{\theta}{3}\frac{\partial W}{\partial h_m}(h_m - h_m^n) = \frac{S\upsilon}{\Delta t}(h^{n+1} - h^n) \tag{3.18}$$

A.2. Derivation of Eq. (3.19)

Eq. (3.18) is discretized using the Crank-Nicholson scheme (C-N scheme). Using the finite-difference grid depicted in Figure A.1, the first derivative is defined as

$$A_x K_x \frac{\partial h}{dx} \approx A_r\, 0.5\,(K_i + K_{i+1})(h_{i+1} - h_i) / \Delta x_2 \tag{A.4}$$

or

$$A_x K_x \frac{\partial h}{dx} \approx A_l\, 0.5\,(K_{i-1} + K_i)(h_i - h_{i-1}) / \Delta x_1 \tag{A.5}$$

The second derivative is defined as

$$\Delta x \frac{\partial}{\partial x}\left(A_x K_x \frac{\partial h}{dx} \right) \approx \Delta x \frac{\text{(IV-12a)} - \text{(IV-12b)}}{0.5\,(\Delta x_1 + \Delta x_2)} \approx A\, h_{i-1} - (A+B)\, h_i + B\, h_{i+1} \tag{A.6}$$

where

$$A = \frac{\Delta x\, A_l (K_{i-1} + K_i)}{\Delta x_1\, (\Delta x_1 + \Delta x_2)} = \frac{0.5\, A_l (K_{i-1} + K_i)}{\Delta x_1} \quad \text{and} \quad B = \frac{\Delta x\, A_r (K_i + K_{i+1})}{\Delta x_2\, (\Delta x_1 + \Delta x_2)} = \frac{0.5\, A_r (K_i + K_{i+1})}{\Delta x_2} \tag{A.7}$$

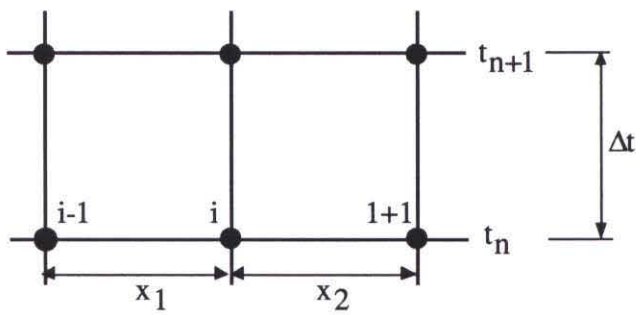

Figure A.1. Finite-Difference Grid

By denoting the right-hand side of Eq. (A.6) as $\delta_x^2 h_i$, the C-N scheme is written as

$$\Delta x \frac{\partial}{\partial x}\left(A_x K_x \frac{\partial h}{dx} \right) \approx \theta\, \delta_x^2 h_i^{n+1} + (1-\theta)\, \delta_x^2 h_i^n, \quad 0 \le \theta \le 1 \tag{A.8}$$

Therefore, using the C-N scheme, and using n, n+1 to denote t, t+1/3, respectively, Eq. (3.18) can be rewritten as

$$\begin{aligned} &(1-\theta)\{A\, h_{i-1}^n - (A+B)\, h_i^n + B\, h_{i+1}^n\} + \\ &\theta\{A\, h_{i-1}^{n+1} - (A+B)\, h_i^{n+1} + B\, h_{i+1}^{n+1}\} - \\ &\frac{1}{3} W^p - \theta \frac{\partial W}{\partial h_i}(h_i^{n+1} - h_i^n) - \frac{\theta}{3}\frac{\partial W}{\partial h_m}(h_m - h_m^p) = \frac{S\upsilon}{\Delta t}(h_i^{n+1} - h_i^n) \end{aligned} \tag{3.19}$$

A.3. The Members of Eq. (3.21)

Eq. (3.20) can be written in matrix form as

$$[\mathbf{M}]\{\mathbf{h}\} = \{\mathbf{F}\} \tag{3.21}$$

where [**M**] is a tridiagonal matrix whose N–2 elements consist of the following contributions from the left hand side of Eq. (3.20):

Subdiagonal elements : $A_i = -\theta A$ (A.9)

Diagonal elements : $B_i = \theta\,(A + B + \frac{\partial W}{\partial h_i}) + \frac{S\upsilon}{\Delta t}$ (A.10)

Superdiagonal elements : $C_i = -\theta B$ (A.11)

{**F**} is an N–2 element vector of known quantities from the right hand side of Eq. (3.20) as described below:

Elements of {**F**} :
$$D_i = (1-\theta)\,\{A\,h_{i-1}^n - (A+B)\,h_i^n + B\,h_{i+1}^n - \frac{1}{3}W^p + \theta\frac{\partial W}{\partial h_i}h_i^n - \frac{\theta}{3}\frac{\partial W}{\partial h_m}(h_m - h_m^p) + \frac{S\upsilon}{\Delta t}h_i^n \tag{A.12}$$

{**h**} is an N–2 element vector of unknown piezometric heads.

A.4. Discretization of the Governing Equation on the Boundaries

The discretization of the governing equation on the boundary needs special treatment, since the discretization used in the middle nodes can no longer be used. To solve this problem, it is assumed that, in the neighborhood of a boundary point, Taylor-series expansion is still applicable.

The Taylor's series expansion for h_2 around h_1 at any time level can be written as follows:

$$h_2 = h_1 + \left[\frac{\partial h}{\partial x}\right]_1 \Delta x + \left[\frac{\partial^2 h}{\partial x^2}\right]_1 \frac{\Delta x^2}{2} +$$

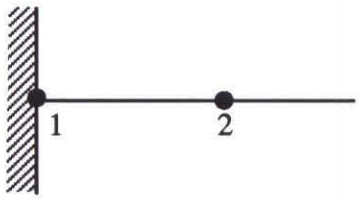

Ignoring the third-order and higher terms and rearranging the above equation,

$$\left[\frac{\partial^2 h}{\partial x^2}\right]_1 = \frac{2}{\Delta x^2}\left\{h_2 - h_1 - \left[\frac{\partial h}{\partial x}\right]_1 \Delta x\right\} \tag{A.13}$$

In order to understand the physical meaning of the above Taylor-series, one may recast Eq. (A.13) in the following form:

$$\left[\frac{\partial^2 h}{\partial x^2}\right]_1 = \frac{\dfrac{h_2 - h_1}{\Delta x} - \left[\dfrac{\partial h}{\partial x}\right]_1}{\dfrac{\Delta x}{2}} \tag{A.14}$$

Substitution of the boundary condition (3.22) $-\dfrac{\partial h}{\partial x} = \dfrac{C_1}{C_2} h_1 - \dfrac{C_t}{C_2}$ into Eq. (A.13) yields

$$K_x\left[\frac{\partial^2 h}{\partial x^2}\right]_1 = \frac{2K_x}{\Delta x^2}\left\{h_2 + \left(\frac{C_1}{C_2}\Delta x - 1\right) h_1 - \frac{C_t}{C_2}\Delta x\right\} \tag{A.15}$$

Using the C-N scheme, one may rewrite Eq. (A.15) as it appears in Eq. (3.25). Then collecting the terms of the first element of Eq. (3.21) gives the following expressions:

Subdiagonal element : $A_1 = 0 \Rightarrow$ not defined for the first point.

Diagonal element : $B_1 = \dfrac{S\upsilon}{\Delta t} + \theta \dfrac{\partial W}{\partial h_s} - \theta \dfrac{2\upsilon K_x}{\Delta x^2}\left(\dfrac{C_1}{C_2}\Delta x - 1\right)$ (A.16)

Superdiagonal element : $C_1 = -\theta \dfrac{2\upsilon K_x}{\Delta x^2}$ (A.17)

Elements of {F} : $$D_1 = (1-\theta)\frac{2\upsilon K_x}{\Delta x^2}\{ h_2^n + (\frac{C_1}{C_2}\Delta x - 1) h_1^n - \frac{C_t^n}{C_2}\Delta x \} - \theta \frac{2\upsilon K_x}{\Delta x}\frac{C_t^{n+1}}{C_2} - \frac{1}{3} W^p - \frac{\theta}{3}\frac{\partial W}{\partial h_m}(h_m - h_m^p) + \theta \frac{\partial W}{\partial h_s} h_1^n + \frac{S\upsilon}{\Delta t} h_1^n \quad (A.18)$$

The Taylor-series expansion for h_N around h_{N-1} at any time level is

$$h_{N-1} = h_N - \left[\frac{\partial h}{\partial x}\right]_N \Delta x + \left[\frac{\partial^2 h}{\partial x^2}\right]_N \frac{\Delta x^2}{2} -$$

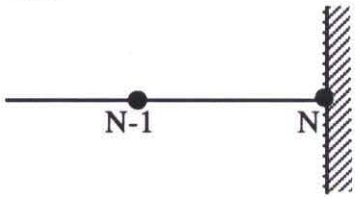

Note that the sign of $\frac{\partial h}{\partial x}$ on the boundary is consistent with the sign convention as depicted in Figure A.2 . On the first node, positive $\frac{\partial h}{\partial x}$ means the flow is leaving the domain, while on the last node, negative $\frac{\partial h}{\partial x}$ means the flow is entering the domain.

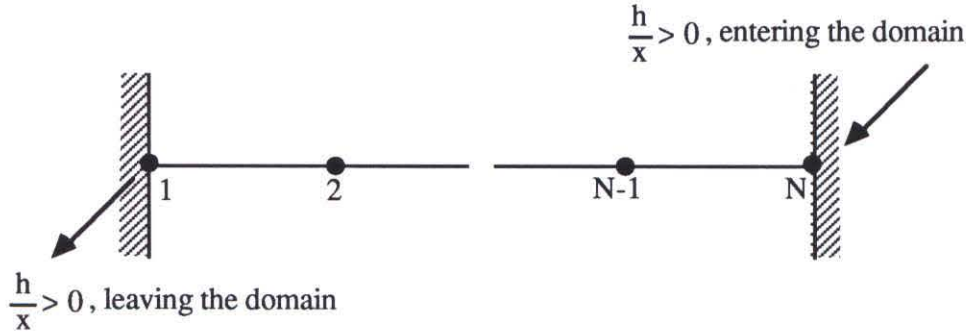

Figure A.2. The Sign of $\frac{\partial h}{\partial x}$ on the Boundaries

The sign convention is used consistently for the entire domain; i.e., a positive sign indicates that flows are leaving the domain and a negative sign indicates otherwise. In order to maintain this convention for the last node, the sign of C_2 in Eq. (3.22) must be changed. For i = N, the boundary condition thus becomes

$$C_1\, h - C_2 \frac{\partial h}{\partial x} = C_t\ (\ x,y,z,t\ )$$

and one may write

$$\begin{aligned} K_x \left[\frac{\partial^2 h}{\partial x^2}\right]_N &= \frac{2K_x}{\Delta x^2}\left\{h_{N-1} - h_N + \left[\frac{\partial h}{\partial x}\right]_N \Delta x\right\} \\ &= \frac{2K_x}{\Delta x^2}\left\{h_{N-1} - h_N + \frac{C_1}{C_2}\Delta x\, h_N - \frac{C_t}{C_2}\Delta x\right\} \end{aligned} \tag{A.19}$$

Using the C-N scheme, Eq. (A.19) may be rewritten as it appears in Eq. (3.27). Then collecting the terms of the last element of Eq. (3.21) gives the following expressions:

Subdiagonal element : $$A_N = -\theta \frac{2\upsilon K_x}{\Delta x^2} \tag{A.20}$$

Diagonal element : $$B_N = \frac{S\upsilon}{\Delta t} + \theta \frac{\partial W}{\partial h_s} - \theta \frac{2\upsilon K_x}{\Delta x^2}\left(\frac{C_1}{C_2}\Delta x - 1\right) \tag{A.21}$$

Superdiagonal element : $C_N = 0 \Rightarrow$ not defined for the last point.

Elements of {F} : $$\begin{aligned} D_N = (1-\theta) \frac{2\upsilon K_x}{\Delta x^2}\{\, h_{N-1}^n + \left(\frac{C_1}{C_2}\Delta x - 1\right) h_N^n - \frac{C_t^n}{C_2}\Delta x\,\} - \\ \theta \frac{2\upsilon K_x}{\Delta x}\frac{C_t^{n+1}}{C_2} - \frac{1}{3} W^p - \frac{\theta}{3}\frac{\partial W}{\partial h_m}(h_m - h_m^p) + \\ \theta \frac{\partial W}{\partial h_s} h_N^n + \frac{S\upsilon}{\Delta t} h_N^n \end{aligned} \tag{A.22}$$

A.5. Derivation of Eq. (3.29) for Middle Nodes

The derivation of Eq. (3.29) starts with the explanation of how the first and second derivatives are discretized. The finite-difference grid used in the derivation is presented in Figure A.1. The first derivative is defined as

$$A_r D_x \frac{\partial C}{\partial x} \approx 0.5\, A_r\, (D_{i+1} + D_i)(C_{i+1} - C_i) / \Delta x_2 \tag{A.23}$$

or

$$A_l D_x \frac{\partial C}{\partial x} \approx 0.5\, A_l\, (D_{i-1} + D_i)(C_i - C_{i-1}) / \Delta x_1 \tag{A.24}$$

The second derivative is defined as

$$\Delta x \frac{\partial}{\partial x}\left(A_x D_x \frac{\partial C}{dx}\right) \approx \frac{\text{(V-4a)} - \text{(V-4b)}}{0.5\,(\Delta x_1 + \Delta x_2)} \Delta x$$
$$\approx A\, C_{i-1} - (A+B)\, C_i + B\, C_{i+1} \tag{A.25}$$

where

$$A = \frac{\Delta x\, A_l\,(D_{i-1} + D_i)}{\Delta x_1\,(\Delta x_1 + \Delta x_2)} = \frac{0.5\, A_l\,(D_{i-1} + D_i)}{\Delta x_1} \quad \text{and} \quad B = \frac{\Delta x\, A_r\,(D_i + D_{i+1})}{\Delta x_2\,(\Delta x_1 + \Delta x_2)} = \frac{0.5\, A_r\,(D_i + D_{i+1})}{\Delta x_2} \tag{A.26}$$

By denoting the right hand side of Eq. (A.25) as $\delta_x^2 C_i$, the Crank-Nicholson scheme of the first term of the left hand side of Eq. (3.28) can be written as

$$\Delta x \frac{\partial}{\partial x}\left(A_x D_x \frac{\partial C}{\partial x}\right) \approx \theta \delta_x^2 C_i^{n+1} + (1-\theta)\delta_x^2 C_i^n, \quad 0 \le \theta \le 1 \tag{A.27}$$

In the same fashion, the second term of the same equation can be written as

$$\Delta x \frac{\partial (A_x U_x C)}{\partial x} \approx \Delta x \frac{0.5\,(C_{i+1}U_{i+1} + C_i U_i)\, A_r - 0.5\,(C_i U_i + C_{i-1}U_{i-1})\, A_l}{0.5\,(\Delta x_1 + \Delta x_2)}$$
$$\approx 0.5\,(A_r\, C_{i+1}U_{i+1} + (A_r - A_l)\, C_i U_i - A_l\, C_{i-1}U_{i-1})$$

Its C-N scheme then becomes

$$\Delta x \frac{\partial (A_x U_x C)}{\partial x} \approx \frac{\theta}{2}\left(A_r\, C_{i+1}^{n+1} U_{i+1}^{n+1} + (A_r - A_l)\, C_i^{n+1} U_i^{n+1} - A_l\, C_{i-1}^{n+1} U_{i-1}^{n+1}\right) + \frac{(1-\theta)}{2}\left(A_r\, C_{i+1}^{n} U_{i+1}^{n} + (A_r - A_l)\, C_i^{n} U_i^{n} - A_l\, C_{i-1}^{n} U_{i-1}^{n}\right) \tag{A.28}$$

and the first term becomes

$$C_s\, W \approx \theta C_s^{n+1} W_i^{n+1} + (1-\theta) C_s^n W_i^n, \quad 0 \le \theta \le 1 \tag{A.29}$$

Substitution of Eqs. (A.27)–(A.29) into Eq. (3.28) yields Eq. (3.29)

$$\theta \{A C_{i-1}^{n+1} - (A+B) C_i^{n+1} + B C_{i+1}^{n+1}\} +$$

$$(1-\theta) \{A C_{i-1}^{n} - (A+B) C_i^{n} + B C_{i+1}^{n}\} -$$

$$\frac{\theta}{2}\left(A_r C_{i+1}^{n+1} U_{i+1}^{n+1} + (A_r - A_l) C_i^{n+1} U_i^{n+1} - A_l C_{i-1}^{n+1} U_{i-1}^{n+1}\right) -$$

$$\frac{(1-\theta)}{2}\left(A_r C_{i+1}^{n} U_{i+1}^{n} + (A_r - A_l) C_i^{n} U_i^{n} - A_l C_{i-1}^{n} U_{i-1}^{n}\right) -$$

$$\theta \frac{C_s^{n+1} W_i^{n+1}}{3} - (1-\theta) \frac{C_s^{n} W_i^{n}}{3} = \frac{\upsilon (C_i^{n+1} - C_i^{n})}{\Delta t}$$

$$\text{for } i = 2, \ldots, N-1 \qquad (3.29)$$

A.6. Elaboration of Source Terms in Eq. (3.29)

In Eq. (3.29), the source terms C_s and w_i depend on their origin, either from the aquifer-matrix itself or from megapores. The following paragraphs elaborate the discretization of all possibilities for the source terms.

A.6.1. Source Term w from the Aquifer-Matrix (Positive w)

For a positive source term, Eq. (3.29) can be written as

$$\theta \{A C_{i-1}^{n+1} - (A+B) C_i^{n+1} + B C_{i+1}^{n+1}\} +$$

$$(1-\theta) \{A C_{i-1}^{n} - (A+B) C_i^{n} + B C_{i+1}^{n}\} -$$

$$\frac{\theta}{2}\left(A_r C_{i+1}^{n+1} U_{i+1}^{n+1} + (A_r - A_l) C_i^{n+1} U_i^{n+1} - A_l C_{i-1}^{n+1} U_{i-1}^{n+1}\right) -$$

$$\frac{(1-\theta)}{2}\left(A_r C_{i+1}^{n} U_{i+1}^{n} + (A_r - A_l) C_i^{n} U_i^{n} - A_l C_{i-1}^{n} U_{i-1}^{n}\right) -$$

$$\theta \frac{C_i^{n+1} W_i^{n+1}}{3e_i} - (1-\theta) \frac{C_i^{n} W_i^{n}}{3e_i} = \frac{\upsilon (C_i^{n+1} - C_i^{n})}{\Delta t}$$

where C_i = aquifer-matrix solute concentration at any grid point.

This is rearranged to get

$$\begin{aligned}
\theta\{A + 0.5\, A_l U_{i-1}^{n+1}\}\, C_{i-1}^{n+1} - \\
\{\theta(A+B) + \theta\frac{W_i^{n+1}}{3e_i} + \frac{\upsilon}{\Delta t} + 0.5\,(A_r - A_l)\, U_i^{n+1}\}\, C_i^{n+1} + \\
\theta\{B - 0.5\, A_r U_{i+1}^{n+1}\}\, C_{i+1}^{n+1} = \\
-(1-\theta)\{A\, C_{i-1}^{n} - (A+B)\, C_i^{n} + B\, C_{i+1}^{n}\} + \\
\frac{(1-\theta)}{2}\left(A_r C_{i+1}^{n} U_{i+1}^{n} + (A_r - A_l) C_i^{n} U_i^{n} - A_l C_{i-1}^{n} U_{i-1}^{n}\right) + \\
(1-\theta)\frac{W_i^{n} C_i^{n}}{3e_i} - \frac{\upsilon C_i^{n}}{\Delta t} \\
\text{for } i = 2, \ldots, N-1
\end{aligned} \tag{A.30}$$

A.6.2. Source Term w from Megapores (Negative w)

For a negative source term, Eq. (3.29) can be written as

$$\begin{aligned}
\theta\{A\, C_{i-1}^{n+1} - (A+B)\, C_i^{n+1} + B\, C_{i+1}^{n+1}\} + \\
(1-\theta)\{A\, C_{i-1}^{n} - (A+B)\, C_i^{n} + B\, C_{i+1}^{n}\} - \\
\frac{\theta}{2}\left(A_r C_{i+1}^{n+1} U_{i+1}^{n+1} + (A_r - A_l) C_i^{n+1} U_i^{n+1} - A_l C_{i-1}^{n+1} U_{i-1}^{n+1}\right) - \\
\frac{(1-\theta)}{2}\left(A_r C_{i+1}^{n} U_{i+1}^{n} + (A_r - A_l) C_i^{n} U_i^{n} - A_l C_{i-1}^{n} U_{i-1}^{n}\right) - \\
\theta\frac{C_m W_i^{n+1}}{3} - (1-\theta)\frac{C_m^{n} W_i^{n}}{3} = \frac{\upsilon\,(C_i^{n+1} - C_i^{n})}{\Delta t}
\end{aligned}$$

where C_m^n is pipe-network solute concentration at a previous time step, and C_m is the latest estimate of pipe-network solute concentration.

This is rearranged to get

$$\begin{aligned}
\theta\{A + 0.5\, A_l U_{i-1}^{n+1}\}\, C_{i-1}^{n+1} - \\
\{\theta(A+B) + \frac{\upsilon}{\Delta t} + 0.5\,(A_r - A_l)\, U_i^{n+1}\}\, C_i^{n+1} + \\
\theta\{B - 0.5\, A_r U_{i+1}^{n+1}\}\, C_{i+1}^{n+1} = \\
-(1-\theta)\{A\, C_{i-1}^{n} - (A+B)\, C_i^{n} + B\, C_{i+1}^{n}\} + \\
\frac{(1-\theta)}{2}\left(A_r C_{i+1}^{n} U_{i+1}^{n} + (A_r - A_l) C_i^{n} U_i^{n} - A_l C_{i-1}^{n} U_{i-1}^{n}\right) + \\
\theta\frac{C_m W_i^{n+1}}{3} + (1-\theta)\frac{C_m^{n} W_i^{n}}{3} - \frac{\upsilon C_i^{n}}{\Delta t} \\
\text{for } i = 2, \ldots, N-1
\end{aligned} \tag{A.31}$$

Eqs. (A.30) and (A.31) can be written in matrix form as

$$[\mathbf{M}]\{\mathbf{C}\} = \{\mathbf{F}\} \tag{3.29}$$

where [**M**] is a tridiagonal matrix whose N–2 elements comprise contributions from the left hand side of Eqs. (A.30) and (A.31) as described below:

Subdiagonal elements : $P_i = \theta\{A + 0.5\ A_l\ U_{i-1}^{n+1}\}$ (A.32)

Diagonal elements : $Q_i = -\{\theta(A+B) + \frac{\upsilon}{\Delta t} + 0.5\ (A_r - A_l)\ U_i^{n+1}\}$ (A.33)

or (for positive W) $Q_i = -\{\theta(A+B) + \theta\frac{W_i^{n+1}}{3e_i} + \frac{\upsilon}{\Delta t} + 0.5\ (A_r - A_l)\ U_i^{n+1}\}$ (A.34)

Superdiagonal elements: $R_i = \theta\{B - 0.5\ A_r\ U_{i+1}^{n+1}\}$ (A.35)

{**F**} is an N–2 element vector of known quantities from the right hand side of Eqs. (A.30) and (A.31) as described below:

Elements of {F} : $S_i = -(1-\theta)\{A\ C_{i-1}^n - (A+B)\ C_i^n + B\ C_{i+1}^n\} +$
$\frac{(1-\theta)}{2}\left(A_r\ C_{i+1}^n U_{i+1}^n + (A_r - A_l)\ C_i^n U_i^n - A_l\ C_{i-1}^n U_{i-1}^n\right) +$
$\theta\frac{W_i^{n+1}\ C_m}{3} + (1-\theta)\frac{W_i^n\ C_m^n}{3} - \frac{\upsilon C_i^n}{\Delta t}$ (A.36)

or (for positive W) $S_i = -(1-\theta)\{A\ C_{i-1}^n - (A+B)\ C_i^n + B\ C_{i+1}^n\} +$
$\frac{(1-\theta)}{2}\left(A_r\ C_{i+1}^n U_{i+1}^n + (A_r - A_l)\ C_i^n U_i^n - A_l\ C_{i-1}^n U_{i-1}^n\right) +$
$(1-\theta)\frac{W_i^n\ C_i^n}{3e_i} - \frac{\upsilon C_i^n}{\Delta t}$ (A.37)

{**C**} is an N–2 element vector of unknown solute concentrations.

A.7. Elaboration of Source Terms in Eq. (3.32)

This section elaborates source terms, C_s and w_i, in the boundaries as described in Eq. (3.32). For clarity, the equation is repeated here.

$$\theta \frac{2D_x}{\Delta x^2} \{ C_2^{n+1} + (\frac{E_1}{E_2}\Delta x - 1) C_1^{n+1} - \frac{E_t^{n+1}}{E_2}\Delta x \} +$$
$$(1-\theta) \frac{2D_x}{\Delta x^2} \{ C_2^{n} + (\frac{E_1}{E_2}\Delta x - 1) C_1^{n} - \frac{E_t^{n}}{E_2}\Delta x \} -$$
$$\theta \frac{U_2^{n+1} C_2^{n+1} - U_1^{n+1} C_1^{n+1}}{\Delta x} - (1-\theta) \frac{U_2^n C_2^n - U_1^n C_1^n}{\Delta x} -$$
$$\theta \frac{C_s^{n+1} w_1^{n+1}}{3} - (1-\theta) \frac{C_s^n w_1^n}{3} = \frac{C_1^{n+1} - C_1^n}{\Delta t} \qquad (3.32)$$

In Eq. (3.32), the source terms, C_s and w_i, depend on their origin, either from the aquifer-matrix itself or from megapores. The following paragraphs elaborate the discretization of all possibilities for the source terms on the boundaries.

A.7.1. Source Term w from the Aquifer-Matrix (Positive w) at the Beginning of a Reach

For a positive source term, Eq. (3.32) can be written as

$$\theta \frac{2D_x}{\Delta x^2} \{ C_2^{n+1} + (\frac{E_1}{E_2}\Delta x - 1) C_1^{n+1} - \frac{E_t^{n+1}}{E_2}\Delta x \} +$$
$$(1-\theta) \frac{2D_x}{\Delta x^2} \{ C_2^{n} + (\frac{E_1}{E_2}\Delta x - 1) C_1^{n} - \frac{E_t^{n}}{E_2}\Delta x \} -$$
$$\theta \frac{U_2^{n+1} C_2^{n+1} - U_1^{n+1} C_1^{n+1}}{\Delta x} - (1-\theta) \frac{U_2^n C_2^n - U_1^n C_1^n}{\Delta x} -$$
$$\theta \frac{C_1^{n+1} w_1^{n+1}}{3e_1} - (1-\theta) \frac{C_1^n W_1^n}{3e_1} = \frac{C_1^{n+1} - C_1^n}{\Delta t}$$

and rearranged to get

$$\left\{\theta \frac{2D_x}{\Delta x^2}(\frac{E_1}{E_2}\Delta x - 1) + \theta \frac{U_1^{n+1}}{\Delta x} - \theta \frac{w_1^{n+1}}{3e_1} - \frac{1}{\Delta t}\right\} C_1^{n+1} +$$
$$\theta \left(\frac{2D_x}{\Delta x^2} - \frac{U_2^{n+1}}{\Delta x}\right) C_2^{n+1} =$$
$$-(1-\theta) \frac{2D_x}{\Delta x^2} \{ C_2^{n} + (\frac{E_1}{E_2}\Delta x - 1) C_1^{n} - \frac{E_t^{n}}{E_2}\Delta x \} +$$
$$(1-\theta) \frac{U_2^n C_2^n - U_1^n C_1^n}{\Delta x} + \theta \frac{2D_x}{\Delta x} \frac{E_t^{n+1}}{E_2} + (1-\theta) \frac{C_1^n W_1^n}{3e_1} - \frac{C_1^n}{\Delta t} \qquad (A.38)$$

A.7.2. Source Term w from Megapores (Negative w) at the Beginning of a Reach

For a negative source term, Eq. (3.32) can be written as

$$\theta \frac{2D_x}{\Delta x^2} \{ C_2^{n+1} + (\frac{E_1}{E_2}\Delta x - 1) C_1^{n+1} - \frac{E_t^{n+1}}{E_2}\Delta x \} +$$
$$(1-\theta) \frac{2D_x}{\Delta x^2} \{ C_2^{n} + (\frac{E_1}{E_2}\Delta x - 1) C_1^{n} - \frac{E_t^{n}}{E_2}\Delta x \} -$$
$$\theta \frac{U_2^{n+1} C_2^{n+1} - U_1^{n+1} C_1^{n+1}}{\Delta x} - (1-\theta) \frac{U_2^{n} C_2^{n} - U_1^{n} C_1^{n}}{\Delta x} -$$
$$\theta \frac{C_m w_1^{n+1}}{3} - (1-\theta) \frac{C_m w_1^{n}}{3} = \frac{C_1^{n+1} - C_1^{n}}{\Delta t}$$

and rearranged to get

$$\left\{\theta \frac{2D_x}{\Delta x^2}(\frac{E_1}{E_2}\Delta x - 1) + \theta \frac{U_1^{n+1}}{\Delta x} - \frac{1}{\Delta t}\right\} C_1^{n+1} +$$
$$\theta \left(\frac{2D_x}{\Delta x^2} - \frac{U_2^{n+1}}{\Delta x}\right) C_2^{n+1} =$$
$$-(1-\theta) \frac{2D_x}{\Delta x^2} \{ C_2^{n} + (\frac{E_1}{E_2}\Delta x - 1) C_2^{n} - \frac{E_t^{n}}{E_2}\Delta x \} +$$
$$(1-\theta) \frac{U_2^{n} C_2^{n} - U_1^{n} C_1^{n}}{\Delta x} + \qquad (A.39)$$
$$\theta \frac{2D_x}{\Delta x} \frac{E_t^{n+1}}{E_2} + \theta \frac{C_m w_1^{n+1}}{3} + (1-\theta) \frac{C_m^n w_1^n}{3} - \frac{C_1^n}{\Delta t}$$

Collecting terms from Eqs. (A.38) and (A.39) for the first element of (3.29) yields:

Subdiagonal element : $P_1 = 0 \Rightarrow$ not defined for the first point (A.40)

Diagonal element : $Q_1 = \upsilon\left\{\theta \frac{2D_x}{\Delta x^2}(\frac{E_1}{E_2}\Delta x - 1) + \theta \frac{U_1^{n+1}}{\Delta x} - \frac{1}{\Delta t}\right\}$ (A.41)

or (for positive W) $Q_1 = \upsilon\left\{\theta \frac{2D_x}{\Delta x^2}(\frac{E_1}{E_2}\Delta x - 1) + \theta \frac{U_1^{n+1}}{\Delta x} - \frac{1}{\Delta t}\right\} - \theta \frac{W_1^{n+1}}{3e_1}$ (A.42)

Superdiagonal element : $R_1 = \theta\upsilon \left(\frac{2D_x}{\Delta x^2} - \frac{U_2^{n+1}}{\Delta x}\right)$ (A.43)

Elements of {F} : $S_1 = -(1-\theta) \frac{2\upsilon D_x}{\Delta x^2} \{ C_2^{n} + (\frac{E_1}{E_2}\Delta x - 1) C_1^{n} - \frac{E_t^{n}}{E_2}\Delta x \} +$
$$(1-\theta)\upsilon \frac{U_2^n C_2^n - U_1^n C_1^n}{\Delta x} + \theta\upsilon \frac{2D_x}{\Delta x} \frac{E_t^{n+1}}{E_2} +$$

$$\theta \frac{C_m W_1^{n+1}}{3} + (1-\theta) \frac{C_m^n W_1^n}{3} - \frac{\upsilon C_1^n}{\Delta t} \tag{A.44}$$

or (for positive W) : $S_1 = -(1-\theta) \frac{2\upsilon D_x}{\Delta x^2} \{ C_2^n + (\frac{E_1}{E_2} \Delta x - 1) C_1^n - \frac{E_t^n}{E_2} \Delta x \} +$

$$(1-\theta)\upsilon \frac{U_2^n C_2^n - U_1^n C_1^n}{\Delta x} + \theta\upsilon \frac{2D_x}{\Delta x} \frac{E_t^{n+1}}{E_2} +$$

$$(1-\theta) \frac{C_1^n W_1^n}{3e_1} - \frac{\upsilon C_1^n}{\Delta t} \tag{A.45}$$

The same technique can also be applied to elaborate the discretized equations at the last computational point, as explained in the following paragraphs. Eq. (3.33) from Chapter III is repeated below for clarity.

$$\begin{aligned} &\theta \frac{2D_x}{\Delta x^2} \{ C_{N-1}^{n+1} + (\frac{E_1}{E_2} \Delta x - 1) C_N^{n+1} - \frac{E_t^{n+1}}{E_2} \Delta x \} + \\ &(1-\theta) \frac{2D_x}{\Delta x^2} \{ C_{N-1}^n - (\frac{E_1}{E_2} \Delta x - 1) C_N^n - \frac{E_t^n}{E_2} \Delta x \} - \\ &\theta \frac{U_N^{n+1} C_N^{n+1} - U_{N-1}^{n+1} C_{N-1}^{n+1}}{\Delta x} - (1-\theta) \frac{U_N^n C_N^n - U_{N-1}^n C_{N-1}^n}{\Delta x} - \\ &\theta \frac{C_s^{n+1} w_N^{n+1}}{3} - (1-\theta) \frac{C_s^n w_N^n}{3} = \frac{C_N^{n+1} - C_N^n}{\Delta t} \end{aligned} \tag{3.33}$$

In Eq. (3.33), the source terms, C_s and w_N, depend on their origin, either from the aquifer-matrix itself or from megapores. The following paragraphs elaborate the discretization of all possibilities for the source terms on the boundaries.

A.7.3. Source Term w from the Aquifer-Matrix (Positive w) at the End of a Reach

For a positive source term, Eq. (3.33) can be written as

$$\begin{aligned} &\theta \frac{2D_x}{\Delta x^2} \{ C_{N-1}^{n+1} + (\frac{E_1}{E_2} \Delta x - 1) C_N^{n+1} - \frac{E_t^{n+1}}{E_2} \Delta x \} + \\ &(1-\theta) \frac{2D_x}{\Delta x^2} \{ C_{N-1}^n + (\frac{E_1}{E_2} \Delta x - 1) C_N^n - \frac{E_t^n}{E_2} \Delta x \} - \\ &\theta \frac{U_N^{n+1} C_N^{n+1} - U_{N-1}^{n+1} C_{N-1}^{n+1}}{\Delta x} - (1-\theta) \frac{U_N^n C_N^n - U_{N-1}^n C_{N-1}^n}{\Delta x} - \end{aligned}$$

$$\theta \frac{C_N^{n+1} w_N^{n+1}}{3e_N} - (1-\theta) \frac{C_N^n w_N^n}{3e_N} = \frac{C_N^{n+1} - C_N^n}{\Delta t}$$

and rearranged to get

$$\theta \left(\frac{2D_x}{\Delta x^2} + \frac{U_{N-1}^{n+1}}{\Delta x} \right) C_{N-1}^{n+1} +$$

$$\left\{ \theta \frac{2D_x}{\Delta x^2} \left(\frac{E_1}{E_2} \Delta x - 1 \right) - \theta \frac{U_N^{n+1}}{\Delta x} - \theta \frac{w_N^{n+1}}{3e_N} - \frac{1}{\Delta t} \right\} C_N^{n+1} =$$

$$- (1-\theta) \frac{2D_x}{\Delta x^2} \left\{ C_{N-1}^n + \left(\frac{E_1}{E_2} \Delta x - 1 \right) C_N^n - \frac{E_t^n}{E_2} \Delta x \right\} + \qquad \text{(A.46)}$$

$$(1-\theta) \frac{U_N^n C_N^n - U_{N-1}^n C_{N-1}^n}{\Delta x} + \theta \frac{2D_x}{\Delta x} \frac{E_t^{n+1}}{E_2} +$$

$$(1-\theta) \frac{C_N^n w_N^n}{3e_N} - \frac{C_N^n}{\Delta t}$$

A.7.4. Source Term w from Megapores (Negative w) at the End of a Reach

For a negative source term, Eq. (3.33) can be written as

$$\theta \frac{2D_x}{\Delta x^2} \left\{ C_{N-1}^{n+1} + \left(\frac{E_1}{E_2} \Delta x - 1 \right) C_N^{n+1} - \frac{E_t^{n+1}}{E_2} \Delta x \right\} +$$

$$(1-\theta) \frac{2D_x}{\Delta x^2} \left\{ C_{N-1}^n + \left(\frac{E_1}{E_2} \Delta x - \right) 1 \, C_N^n - \frac{E_t^n}{E_2} \Delta x \right\} -$$

$$\theta \frac{U_N^{n+1} C_N^{n+1} - U_{N-1}^{n+1} C_{N-1}^{n+1}}{\Delta x} - (1-\theta) \frac{U_N^n C_N^n - U_{N-1}^n C_{N-1}^n}{\Delta x} -$$

$$\theta \frac{C_m w_N^{n+1}}{3} - (1-\theta) \frac{C_m^n w_N^n}{3} = \frac{C_N^{n+1} - C_N^n}{\Delta t}$$

and rearranged to get

$$\theta \left(\frac{2D_x}{\Delta x^2} + \frac{U_{N-1}^{n+1}}{\Delta x} \right) C_{N-1}^{n+1} +$$

$$\left\{ \theta \frac{2D_x}{\Delta x^2} \left(\frac{E_1}{E_2} \Delta x - 1 \right) - \theta \frac{U_N^{n+1}}{\Delta x} - \frac{1}{\Delta t} \right\} C_N^{n+1} =$$

$$- (1-\theta) \frac{2D_x}{\Delta x^2} \left\{ C_{N-1}^n + \left(\frac{E_1}{E_2} \Delta x - 1 \right) C_N^n - \frac{E_t^n}{E_2} \Delta x \right\} +$$

$$(1-\theta) \frac{U_N^n C_N^n - U_{N-1}^n C_{N-1}^n}{\Delta x} + \theta \frac{2D_x}{\Delta x} \frac{E_t^{n+1}}{E_2} +$$

$$\theta \frac{C_m w_N^{n+1}}{3} + (1-\theta) \frac{C_m^n w_N^n}{3} - \frac{C_N^n}{\Delta t} \qquad \text{(A.47)}$$

Collecting terms from Eqs. (A.46) and (A.47) for the last element of Eq. (3.29) yields:

$$\text{Subdiagonal element} \quad : P_N = \theta\upsilon\left(\frac{2D_x}{\Delta x^2} + \frac{U_{N-1}^{n+1}}{\Delta x}\right) \tag{A.48}$$

$$\text{Diagonal element} \quad : Q_N = \upsilon\left\{\theta\frac{2D_x}{\Delta x^2}\left(\frac{E_1}{E_2}\Delta x - 1\right) - \theta\frac{U_N^{n+1}}{\Delta x} - \frac{1}{\Delta t}\right\} \tag{A.49}$$

$$\text{or (for positive W)} \quad Q_N = \upsilon\left\{\theta\frac{2D_x}{\Delta x^2}\left(\frac{E_1}{E_2}\Delta x - 1\right) - \theta\frac{U_N^{n+1}}{\Delta x} - \frac{1}{\Delta t}\right\} - \theta\frac{W_N^{n+1}}{3e_N} \tag{A.50}$$

$$\text{Superdiagonal element} \quad : R_N = 0 \Rightarrow \text{not defined for the last point} \tag{A.51}$$

$$\begin{aligned}\text{Elements of } \{\mathbf{F}\} \quad : S_N = &-(1-\theta)\upsilon\frac{2D_x}{\Delta x^2}\left\{C_{N-1}^n + \left(\frac{E_1}{E_2}\Delta x - 1\right)C_N^n - \frac{E_t^n}{E_2}\Delta x\right\} + \\ &(1-\theta)\upsilon\frac{U_N^nC_N^n - U_{N-1}^nC_{N-1}^n}{\Delta x} + \theta\upsilon\frac{2D_x}{\Delta x}\frac{E_t^{n+1}}{E_2} + \\ &\theta\frac{C_mW_N^{n+1}}{3e_N} + (1-\theta)\frac{C_m^nW_N^n}{3e_N} - \frac{\upsilon C_N^n}{\Delta t}\end{aligned} \tag{A.52}$$

$$\begin{aligned}\text{or (for positive W)} \quad : S_N = &-(1-\theta)\upsilon\frac{2D_x}{\Delta x^2}\left\{C_{N-1}^n + \left(\frac{E_1}{E_2}\Delta x - 1\right)C_N^n - \frac{E_t^n}{E_2}\Delta x\right\} + \\ &(1-\theta)\upsilon\frac{U_N^nC_N^n - U_{N-1}^nC_{N-1}^n}{\Delta x} + \theta\upsilon\frac{2D_x}{\Delta x}\frac{E_t^{n+1}}{E_2} + \\ &(1-\theta)\frac{C_N^nW_N^n}{3e_N} - \frac{\upsilon C_N^n}{\Delta t}\end{aligned} \tag{A.53}$$

A.8. Double-Sweep Method in the Megapore-Network

In Chapter III, the double-sweep method is used to solve hydrodynamic equations in the megapore-network. The heart of the method is finding the relationships between the head corrections at both ends of a link and the discharge corrections of the first or the last pipe in the corresponding link. The relationships are derived from the mass conservation law (3.34) and the discretized hydrodynamic equation (3.45) at each junction of a pipe. From the aforementioned relationships, one may deduce the influence coefficients of the double-sweep method, as well as how to initialize them. In the following paragraphs, how to obtain the coefficients is explained in detail.

A.8.1. Derivation of Eq. (3.41)

Suppose there exists a relation

$$\Delta h_{i,lp} = E_{i,lp}\,\Delta Q_{lp} + F_{i,lp} + H_{i,lp}\,\Delta h_{1,1} \tag{A.54}$$

in which influence coefficients E, F, and H are considered unknown for the moment. Substitution of Eq. (A.54) into Eq. (3.48) yields a linear relationship among ΔQ_{lp}, Δh_{lp+1}, and $\Delta h_{1,1}$ that can be recognized as:

$$\Delta h_{i+1,lp} = E_{i+1,lp}\,\Delta Q_{lp} + F_{i+1,lp} + H_{i+1,lp}\,\Delta h_{1,1} \tag{A.55}$$

in which

$$E_{i+1,\,lp} = -\frac{a_i + b_i\,E_{i,lp}}{c_i} \tag{A.56}$$

$$F_{i+1,\,lp} = -\frac{d_i + b_i\,F_{i,lp}}{c_i} \tag{A.57}$$

$$H_{i+1,\,lp} = -\frac{b_i\,h_{i,lp}}{c_i} \tag{A.58}$$

(Note that it is not necessary to doubly subscript a, b, c, and d). Therefore, since a, b, c, and d are always known values, E, F, and H can be recursively calculated from one point to the next along the forward sweep once E, F, and H have been initialized.

Initialization of E, F, and H is based on Eq. (3.48) written for the first computational reach of the first pipe:

$$\Delta h_{2,1} = -\frac{a_1}{c_1}\,\Delta Q_1 - \frac{d_1}{c_1} - \frac{b_1}{c_1}\,\Delta h_{1,1} \tag{A.59}$$

Comparison with Eq. (A.54), written for i = 2, reveals:

$$E_{2,1} = -\frac{a_1}{c_1} \tag{A.60}$$

$$F_{2,1} = -\frac{d_1}{c_1} \tag{A.61}$$

$$H_{2,1} = -\frac{b_1}{c_1} \tag{A.62}$$

(Note that, in fact, E, F, and H are not needed at point 1 of pipe 1; see discussion below.)

Once E, F, and H are initialized through Eqs. (A.60) to (A.62), they can be recursively calculated using Eqs. (A.56)–(A.58) up to the last point on the first pipe on the link; these values are designated as $E_{II(1),1}$, $F_{II(1),1}$, and $H_{II(1),1}$. Now, in general, this last point is contiguous with an inline node. Special recursive relations are needed to carry E, F, and H "through" the node; these are developed using the principles of nodal continuity.

The nodal continuity Eq. (3.38) can be written as follows for the special case of an inline node m:

$$(Q_{lp+1}+\Delta Q_{lp+1})-(Q_{lp}+\Delta Q_{lp})+Q_m^{n+1}+W_m+\frac{\partial W}{\partial h_m}\Delta h_m=0 \tag{A.63}$$

However, ΔQ_{lp} can be replaced by its value derived from Eq. (A.54) for i = II(lp). Thus, if one again requires that the node m and its contiguous computational points, (II(lp), lp) and (1, lp+1), share the same piezometric head (and thus head correction, i.e., $\Delta h_{II(lp),lp} = \Delta h_{1,lp+1} = \Delta h_m$), one can write Eq. (A.54) as:

$$\Delta h_{1,lp+1}=E_{II(lp),lp}\,\Delta Q_{lp}+F_{II(lp),lp}+H_{II(lp),lp}-\Delta h_{1,1} \tag{A.64}$$

or

$$-\Delta Q_{lp}=\frac{F_{II(lp),lp}}{E_{II(lp),lp}}+\frac{H_{II(lp),lp}}{E_{II(lp),lp}}\Delta h_{1,1}-\frac{1}{E_{II(lp),lp}}\Delta h_{1,lp+1} \tag{A.65}$$

Substitution into Eq. (A.63) yields

$$\left(\frac{\partial W}{\partial h_m}-\frac{1}{E_{II(lp),lp}}\right)\Delta h_{1,lp+1}=-\Delta Q_{lp+1}+Q_{lp}-Q_{lp+1}-Q_m^{n+1}-W_m-\frac{F_{II(lp),lp}}{E_{II(lp),lp}}-\frac{H_{II(lp),lp}}{E_{II(lp),lp}}\Delta h_{1,1} \tag{A.66}$$

Eq. (A.66) can then be solved for $\Delta h_{1,lp+1}$ as follows:

$$\Delta h_{1,lp+1}=E_{1,lp+1}\,\Delta Q_{lp+1}+F_{1,lp+1}+H_{1,lp+1}\Delta h_{1,1} \tag{A.67}$$

One can recognize that this is a particular realization of Eq. (A.54) in which

$$E_{1,lp+1}=\frac{-1}{Denom} \tag{A.68}$$

$$F_{1,lp+1}=\frac{Q_{lp}-Q_{lp+1}-Q_m^{n+1}-W_m-\frac{F_{II(lp),lp}}{E_{II(lp),lp}}}{Denom} \tag{A.69}$$

$$H_{1,lp+1}=\frac{-H_{II(lp),lp}/E_{II(lp),lp}}{Denom} \tag{A.70}$$

where $$Denom=\frac{\partial W}{\partial h_m}-\frac{1}{E_{II(lp),lp}} \tag{A.71}$$

The forward sweep for a link ends when the recursion process reaches the last computational point II(LP) of the last pipe LP. At this point, Eq. (A.54) becomes:

$$\Delta h_{II(LP),LP}=E_{II(LP),LP}\ \Delta Q_{LP}+F_{II(LP),LP}+H_{II(LP),LP}\ \Delta h_{1,1} \tag{3.50}$$

This is equivalent to Eq. (3.41), with "u" denoting the last point of the link (II(LP),LP) and "d" denoting the first point (1,1).

A.8.2. Derivation of Eq. (3.40)

Equation (3.40) results from a derivation similar to the one shown above for Eq. (3.41). Suppose that there exists a relation

$$\Delta h_{i,lp}=EE_{i,lp}\Delta Q_1+FF_{i,lp}+HH_{i,lp}\Delta h_{1,1} \tag{A.72}$$

From Eq. (A.55), one finds that

$$\Delta Q_{lp}=\frac{1}{E_{i+1,lp}}\Delta h_{i+1,lp}-\frac{F_{i+1,lp}}{E_{i+1,lp}}-\frac{H_{i+1,lp}}{E_{i+1,lp}}\ \Delta h_{1,1} \tag{A.73}$$

Substitution of Eqs. (A.72) and (A.73) into Eq. (A.54) produces:

$$\left(\frac{a_i}{E_{i+1,lp}} + c_i\right) \Delta h_{i+1,lp} = -b_i\, EE_{i,lp} \Delta Q_1 - b_i\, FF_{i,lp} - d_i + \frac{a_i\, F_{i+1,lp}}{E_{i+1,lp}} + \left(\frac{a_i\, H_{i+1,lp}}{E_{i+1,lp}} - b_i\, HH_{i,lp}\right) \Delta h_{1,1} \tag{A.74}$$

or $$\Delta h_{i+1,lp} = EE_{i+1,lp} \Delta Q_1 + FF_{i+1,lp} + HH_{i+1,lp} \Delta h_{1,1} \tag{A.75}$$

Eq. (A.75) is another linear relation among $\Delta h_{i+1,lp}$, $\Delta h_{1,1}$, and ΔQ_1. Thus it is equivalent to Eq. (A.72) written for point (i+1, lp), and one can identify:

$$EE_{i+1,lp} = \frac{-b_i\, EE_{i,lp}}{Denom} \tag{A.76}$$

$$FF_{i+1,lp} = \frac{a_i\, F_{i+1,lp} / E_{i+1,lp} - b_i\, FF_{i,lp} - d_i}{Denom} \tag{A.77}$$

$$HH_{i+1,lp} = \frac{a_i\, H_{i+1,lp} / E_{i+1,lp} - b_i\, HH_{i,lp}}{Denom} \tag{A.78}$$

where $$Denom = \frac{a_i}{E_{i+1,lp}} + c_i \tag{A.79}$$

Therefore, once a_1, b_1, c_1, and d_1 have been calculated for a computational reach (i, i+1), and E, F, and H have been calculated for point i+1, then EE, FF, and HH can be recursively carried through to point i+1 using their values at point i.

Initialization of EE, FF, and HH for point (2, 1) is obtained directly from Eq. (A.59); in fact, this initialization is identical to that used for E, F, and H in Eqs. (A.60)–(A.62). Thus

$$EE_{2,1} = -\frac{a_1}{c_1} \tag{A.80}$$

$$FF_{2,1} = -\frac{d_1}{c_1} \tag{A.81}$$

$$HH_{2,1} = -\frac{b_1}{c_1} \tag{A.82}$$

Just as for the E, F, and H recursion, one must also be able to carry EE, FF, and HH

"through" an inline node separating two pipes. At the last point II(lp) of pipe lp,

$$\Delta h_{II(lp),lp} = EE_{II(lp),lp}\Delta Q_1 + FF_{II(lp),lp} + HH_{II(lp),lp}\Delta h_{1,1} \tag{A.83}$$

The requirement of a common head at both points contiguous with an inline node is expressed as

$$h_{II(lp),lp} + \Delta h_{II(lp),lp} = h_{1,lp+1} + \Delta h_{1,lp+1} \tag{A.84}$$

Solution of Eq.(A.84) for $\Delta h_{II(lp),lp}$ and substitution into Eq. (A.83) then yields

$$h_{1,lp+1} + \Delta h_{1,lp+1} - h_{II(lp),lp} = EE_{II(lp),lp}\Delta Q_1 + FF_{II(lp),lp} + HH_{II(lp),lp}\Delta h_{1,1}$$

or
$$\Delta h_{1,lp+1} = EE_{II(lp),lp}\Delta Q_1 + FF_{II(lp),lp} + h_{II(lp),lp} - h_{1,lp+1} + HH_{II(lp),lp}\Delta h_{1,1} \tag{A.85}$$

which is the same as Eq. (A.72) written for point (1, lp+1) with

$$EE_{1,lp+1} = EE_{II(lp),lp} \tag{A.86}$$

$$FF_{1,lp+1} = FF_{II(lp),lp} + h_{II(lp),lp} - h_{1,lp+1} \tag{A.87}$$

$$HH_{1,lp+1} = HH_{II(lp),lp} \tag{A.88}$$

Thus during the link forward sweep not only E, F, H, but also EE, FF, HH, can be initialized and recursively calculated along pipes and through inline nodes. At the end of the last pipe of the link, Eq. (A.72) is written as

$$\Delta h_{II(LP),LP} = EE_{II(LP),LP}\ \Delta Q_1 + FF_{II(LP),LP} + HH_{II(LP),LP}\ \Delta h_{1,1} \tag{3.51}$$

This equation is the same as Eq. (3.40) with "u" denoting the last point of the link and "d" denoting the first one, as was the case for Eq. (3.41).

A.8.3. Link Return Sweep

The preceding derivations have shown that Eqs. (3.40) and (3.41), combined with the nodal continuity Eq. (3.38) for all looped nodes, lead to a solution for all looped nodal head corrections, Eq. (3.44). The only remaining task in an iteration is to recover the pipe discharges and head corrections.

In the so-called link return sweep, each link is considered individually. The return sweep proceeds back down the link in the reverse order of the forward sweep. The discharge correction in the last pipe, ΔQ_{LP}, is first computed from Eq. (3.50). Thus

$$\Delta Q_{LP} = \frac{\Delta h_{II(LP),LP} - F_{II(LP),LP} - H_{II(LP),LP}\,\Delta h_{1,1}}{E_{II(LP),LP}} \tag{A.89}$$

(Recall that $\Delta h_{1,1}$ and $\Delta h_{II(LP),LP}$ are both known from the looped-nodal solution Eq. (3.44), these two points being contiguous with, and sharing the same head as, their associated looped nodes). Once ΔQ_{LP} is thus known, Eq. (A.54) can be successively applied to each point of the pipe LP to recover the head corrections. Thus;

$$\Delta h_{i,LP} = E_{i,LP}\,\Delta Q_{LP} + F_{i,LP} + H_{i,LP}\,\Delta h_{1,1} \tag{A.90}$$

When the return sweep proceeds down to the first point of the last pipe LP, the head correction for the associated inline node m is recovered simply as

$$\Delta h_m = \Delta h_{1,LP} \tag{A.91}$$

and also

$$\Delta h_{II(LP-1),LP-1} = \Delta h_m \tag{A.92}$$

Then ΔQ_{LP-1} is computed using Eq. (A.92) and Eq. (A.89), with LP–1 replacing LP. Using Eq. (A.90), the return sweep continues in this fashion down to the second point of the first

pipe. (Recall that E, F, H, and EE, FF, HH were initialized for this point). The head correction for the first point of the first pipe is obtained quite simply from that of its associated looped node.

At the end of one iteration of this entire procedure, all pipe heads and discharges are corrected so as to better satisfy water continuity at nodes and energy conservation in pipes. The chief advantage of the procedure is that it deals only with a matrix involving only the number of looped nodes, not all nodes, thereby minimizing computational time required to solve the matrix.

APPENDIX B

DESCRIPTION OF THE COMPUTER CODE LABYRINTH

B.1. Introduction

This appendix presents an overview of the Labyrinth code. First, the general skeleton of the code is explained briefly. Then preparatory operations to run the code are presented. Next, the major parts of the code are explained. Required input data and memory and time requirements to run the present model are given.

Currently the computer code Labyrinth can model three-dimensional groundwater flow and pollutant transport in karst regions; that is, where a megapore- or pipe-network exists inside an aquifer or porous media. The topology of both the megapore- or pipe-network and porous media or aquifer are needed as geometric input data. Despite the importance of this information, detailed explanations of topology data are not given in this appendix due to the limited space, but may be found in the Labyrinth manual.

The Labyrinth code was written in FORTRAN 77 for implementation in Apollo workstations. The code was written to adhere as much as possible to standard FORTRAN 77. Porting the code to any other computer needs only minor modification, in particular in subroutines that calculate CPU time of the simulation. Since calculation of CPU time usually depends on the specific machine used in the simulation, the aforementioned subroutines calculate CPU time by calling the Apollo-specific routines, PROC1_$GET_CPUT, CAL_$FLOAT_CLOCK, CAL_$DECODE_LOCAL_TIME, and CAL_$WEEKDAY.

An overview of the Labyrinth code is presented in the general flow chart, Figure B.1. The code is divided into 52 files, consisting of 86 subroutines. Since the code is modularly

developed, it is easy to modify for specific needs or additional capabilities. All linear algebra computations are carried out using LINPACK, a linear package solver developed by Argonne National Laboratory, Chicago, Illinois, U.S.A. The Labyrinth code uses the following subroutines from LINPACK: IDAMAX, DAXPY, DSCAL, DGEFA, DGESL, and DGTSL.

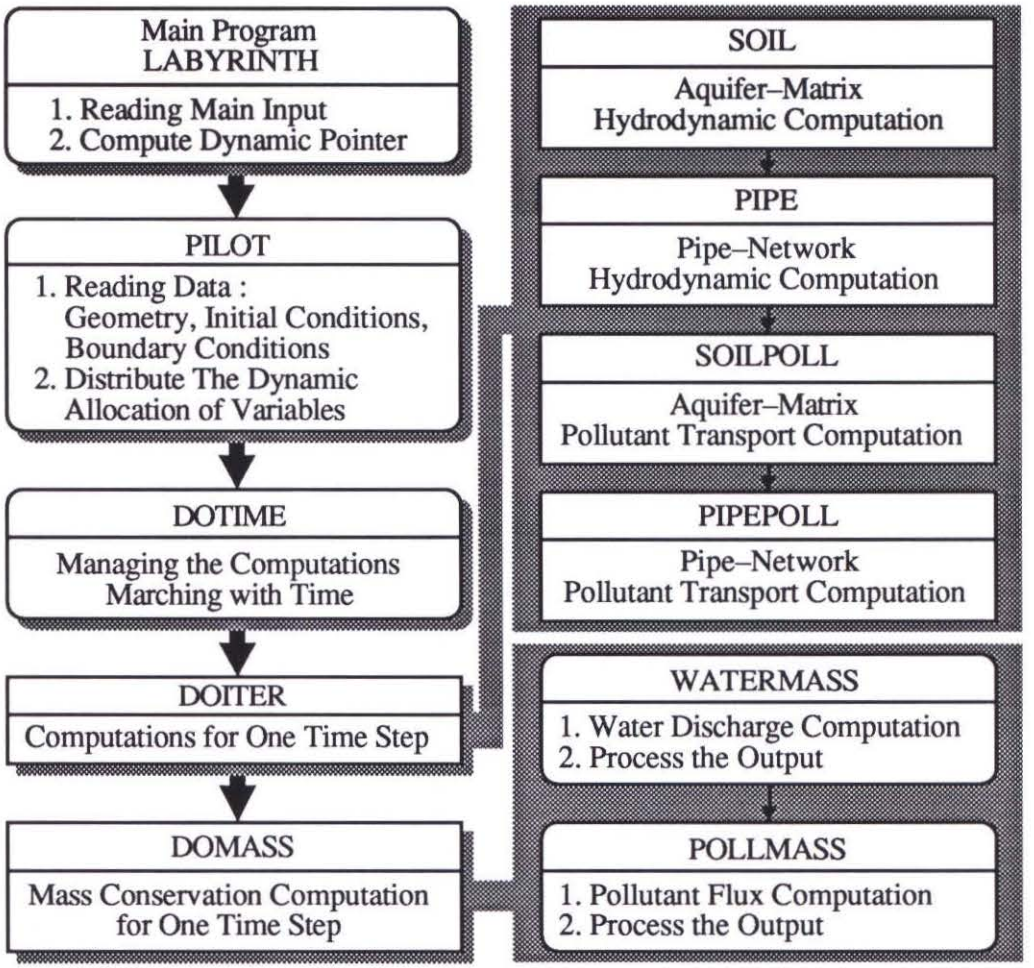

Figure B.1. General Flowchart of the Labyrinth Code

B.2. Preparatory Operations

The first important step in preparing the input data is visualization of the porous media or aquifer-matrix in a three-dimensional grid. The geometry of the aquifer must, then, be made to conform to the finite-difference grid used in the simulation. All the corner points of the

aquifer geometry are numbered according to the convention of the so-called "soil-topology." The second important step is numbering all the nodes and pipes in the megapore- or pipe-network. The first step takes approximately 50% of the overall preparation time while the second step takes 25%. The Labyrinth code has the capability of checking the input data for errors, but this capability is not 100% reliable. After these two steps are finished, one can proceed to write the data into a FORTRAN input file.

Input data is divided into 26 records, some of fixed and others of variable length. Section 4 below explains input data needs in general, and each record is explained in detail in the Labyrinth manual. Since the second record performs a unique function for the code, it must be explained before other records. This record consists of fourteen inputs that define the "words" needed to run the simulation. If the available "words" are less than the needed "words," then the code will stop even before starting the simulation. In such a case, one should change the DIMENSION of the variable T in the main program to a higher number and recompile the code. A "word" is defined as total bytes of random access memory occupied by one REAL FORTRAN variable.

B.3. Hydrodynamic and Pollutant Computations

In each time step during the simulation, before actual computations are done in other subroutines, the DOTIME subroutine manages necessary preparations for the next time step. Transfer of variables; i.e., keeping records of value of the variables for the previous time step, and loading input of time dependent boundary conditions are carried out in this subroutine. The DOTIME subroutine also handles necessary operations before and after time-step marching operations, such as initializing variables in the beginning of the marching, and at the end of the marching, generating binary output if needed. (Binary output is usually needed if users want to continue a previous simulation. By reading this binary output, the new simulation may continue from the end of the previous simulation, without having to repeat the previous simulation.) After these preparations, for one time step, the computation of

hydrodynamic and pollutant transport is passed to the DOITER subroutine, and the computation of mass conservation is passed to the DOMASS subroutine.

B.3.1. Piezometric Head and Discharge Computations

Piezometric head and discharge computations are divided into two parts. The first part is the computation in the aquifer-matrix or porous media in the SOIL subroutine. The second part is the computation in the megapore- or pipe-network using the subroutine PIPE.

For each time step, the aquifer-matrix computation is carried out in the SOIL subroutine. In this subroutine, the piezometric head in the aquifer-matrix is computed and stored in HSOIL. The same computation for the megapore- or pipe-network is done in the PIPE subroutine. In the PIPE subroutine, both piezometric heads and discharges for all pipes are computed and stored in HPIPE and QP, respectively.

In the WATERMASS subroutine, the discharges at points of interest are computed, as well as those coming into and leaving the pipe-network or aquifer-matrix. This subroutine uses the results from both the PIPE and SOIL subroutines. Users may sense whether the mass conservation law is satisfied by checking the overall discharge continuity produced by the WATERMASS subroutine.

All output from the WATERMASS subroutine can be controlled by putting appropriate values into control variables provided in the code. The control variables themselves are explained in great detail in the Labyrinth manual. Users may also request a hard copy of the piezometric head of the aquifer-matrix, HSOIL, at several elevations. This output is specially prepared to be inputted into any graphic or charting program to produce contour graphs. A tabular form of the discharge history at sinks and springs can also be produced so users may make hydrographs. All hard copies from the WATERMASS subroutine that are intended to be used in a charting program are tab-delimited ASCII files.

B.3.2. Concentration and Concentration-Flux Computations

The structure of concentration and concentration-flux computations is analogous to those

of piezometric head and discharge computations mentioned in the previous section. For each time step, the computation in the aquifer-matrix is carried out in the SOILPOLL subroutine and in the PIPEPOLL subroutine for the megapore- or pipe-network. In SOILPOLL, pollutant concentration in the aquifer-matrix is computed and stored in CSOIL variables. In PIPEPOLL, pollutant concentration for all pipes is computed and stored in CPIPE.

In the POLLMASS subroutine, the pollutant-fluxes at points of interest are computed, as well as those coming into and leaving the pipe-network or aquifer-matrix. This subroutine uses the results from both the PIPEPOLL and SOILPOLL subroutines.

B.4. Input Data Needs

This section explains in general the input requirements of the Labyrinth code. More detailed explanations may be found in the code manual. The input data is divided into 26 records.

The first 4 records are needed in the main program. Record 1 defines the title of a run. Record 2, consisting of 14 integer dimensional inputs, defines the maximum size of the corresponding input. Record 3, consisting of 20 inputs, defines logical and integer-type control parameters. This record controls which computation is to be carried out and also defines the printing control variables. Record 4 consists of 10 inputs controlling iterations and frequency of output to files. This record also turns a binary restart file off or on.

The following records are needed in several subroutines. Record 5 consists of 5 real variables defining the time variables, such as beginning and ending simulation times, time increment, etc. Record 6 consists of 5 real variables defining the implicitation factor of the finite-difference method, acceleration of gravity, and default values for megapore equivalent diameter and Strickler coefficients. Record 7, which is of variable length, consists of three groups of inputs defining the aquifer-matrix grid. Record 8 consists of 5 integer-type inputs. This record has to. be inputted for each megapore or pipe node. Record 9 is an 80-character alphanumeric identifier for a link. Record 10 consists of 5 integer variables defining the topology of the megapore- or pipe-network. Since one Record 9 for each link must be

followed by a Record 10 for each pipe on the corresponding link, Records 9 and 10 must be inputted in pairs for all links in the network. Record 11–13 lists all the node numbers, link numbers, and elevation numbers, respectively, whose data needs to be printed. Record 14, which is of variable length, consists of three groups of inputs defining the type of boundary conditions in the aquifer-matrix. Record 15 consists of one integer variable and several sets of real variables defining the time dependent boundary conditions for each boundary point. Record 16 defines the boundary of a cubical aquifer-matrix. If the geometry of the aquifer-matrix is not cubical, then users must set the CUBE variable to F (= logical variable .FALSE.).

The most challenging record of all is Record 17, which defines the arbitrary geometry of an aquifer-matrix. By inputting data into this record, the user assigns one of 118 distinct soil nomenclatures or soil topologies to each boundary point in the aquifer-matrix. For one aquifer-matrix shape there will be several ways to input data into Record 17. This record has variable length depending on the complexity of the aquifer-geometry. This is a complex task since it defines a three-dimensional geometry, and most of the input preparation time is spent on it.

Record 18 consists three groups of inputs in which the last input is of variable length. This record defines aquifer-matrix properties such as hydraulic conductivity, specific storage, and coefficient of mass-exchange. Record 19 consists of five groups of inputs in which the fourth input is of variable length. This record essentially defines initial conditions of both the pipe-network and aquifer-matrix. The last input of this record is intended to be used as a continuation run of a simulation. That is, users can end any simulation at any time and then store all results in a binary file, for use as an initial condition input file for the next simulation. Record 20 defines the distribution factor used in fractional step computations. Record 21, which is of variable length, defines the surface boundary condition for the aquifer-matrix.

The rest of the inputs define all variables for pollutant transport computations. If pollutant transport is not needed; i.e., if DOPOLL in Record 3 is set to FALSE, these inputs are ignored by the program. Record 22, which is of variable length and has the same

structure as Record 14, consists of three groups of inputs defining the type of pollutant boundary conditions in the aquifer-matrix. Record 23, which has the same structure as Record 15, consists of one integer variable and several sets of real variables defining the time dependent boundary conditions for pollutants at each boundary point. Record 24, consisting of four groups of inputs, in which the last is of variable length, defines aquifer-matrix properties such as effective void ratio and bulk dispersion coefficients. Record 25, consisting of four groups of inputs in which the third input is of variable length, essentially defines pollutant initial conditions for both the pipe-network and aquifer-matrix. The last input of this record is intended to be used as a continuation run of a simulation, as explained for Record 19. The last record, Record 26, which is of variable length, defines the pollutant boundary condition at the surface of the aquifer-matrix. Record 26 has the same structure as Record 21.

B.5. Memory and Time Requirements

Memory and time requirements depend on the complexity of the simulation performed. For the present study, memory reserved by the code was about 700,000 words of which only 85% was needed to run simulations performed during this study. The memory requirement is greatly influenced by the grid size used in the finite-difference computation, in particular, the grid size for the aquifer-matrix. The memory requirement is computed by the code based on the input in Record 2.

At the end of each simulation, the time needed to run the simulation is recorded. For the present study, time needed to finish one simulation typically ranged from one to five hours using an Apollo 400t computer. On an Apollo DN10000 the execution time decreased by 25%. Hydrodynamic computations used 81% of the time as compared with 17% of time for pollutant transport computations; the remaining 2% of the time was used for managing input and output of the code.

REFERENCES

Andersson, Johan and Dverstorp, Björn, (1987), Conditional Simulations of Fluid Flow in Three-Dimensional Networks of Discrete Fractures, Water Resources Research, Vol. 23, No. 10, pages 1876–1886.

Avdagic, Izet, (1976), Determination of Flow Through Flooded Karst Poljes by Use of Poljes and Piezometric Boreholes Water Level, Karst Hydrology and Water Resources, Vol.1, pages (16–1) to (16–14), Water Resources Publications, Fort Collins, Colorado 80522, USA.

Baecher, G. B. and Lanney, N. A., (1978), Trace Length Biases in Joint Surveys, Proceeding 19th U.S. Rock Mechanics Symposium, pages 56–65

Bear, Jacob, (1972), Dynamics of Fluids in Porous Media, American Elsevier, New York, USA.

Bear, Jacob, (1979), Hydraulics of Groundwater, McGraw-Hill Book Company, USA.

Bear, Jacob and Berkowitz, Brian, (1983), Groundwater Flow and Pollution in Fractured Rock Aquifers, Developments in Hydraulic Engineering – 4, Chapter 4, Elsevier Applied Science, London and New York.

Cacas, M. C., Ledoux, E., de Marsily, G., Tillie, B., Barbreau, A., Durand, E., Feuga, B., and Peaudecerf, P., (1990a), Modeling Fracture Flow With a Stochastic Discrete Fracture Network and Validation 1. The Flow Model, Water Resources Research, Vol. 26, No. 3, pages 479–489.

Cacas, M. C., Ledoux, E., de Marsily, G., Barbreau, A., Calmels, P., Gaillard, B., and Margritta, R., (1990b), Modeling Fracture Flow With a Stochastic Discrete Fracture Network and Validation 2. The Transport Model, Water Resources Research, Vol. 26, No. 3, pages 491–500.

Chow, Ven Te, Ph.D., (1959), Open-Channel Hydraulics, International Student Edition, McGraw-Hill International Book Company

Cleary, R. W., and Ungs, M. J., (1978), Groundwater Pollution and Hydrology, Mathematical Models and Computer Programs, Report 78–WR–15, Water Resources Program, Princeton Univ., Princeton, N. J.

Cunge, J. A., Holly Jr., F. M., and Verwey, A., (1980), Practical Aspects of Computational River Hydraulics, Pitman Advanced Publishing Program, Boston • London • Melbourne.

Dilamater, Ronald R. and Csallany, Sandor C., (1977), Hydrologic Problems in Karst Regions, Western Kentucky University, Bowling Green, Kentucky.

Endo, H. K., Long, J. C. S., Wilson, C. R., and Witherspoon, P. A., (1984), A Model for Investigating Mechanical Transport in Fracture Networks, Water Resources Research, Vol. 20, No.10, pages 1390–1400.

Feuga, Bernard, (1988), Modelling of Flow Through Fractured Rocks: Geostatistical Generation of Fracture Networks, Stress–Flow relationship in Fractures, Groundwater Flow and Quality Modeling, Editor: E. Custodio, A. Gurgui and J. P. Lobo Ferreira, NATO ASI Series, Series C: Mathematical and Physical Sciences Vol. 224, pages 269–297

Fischer, Hugo B., List, E. John, Koh, Robert C. Y., Imberger, Jörg, and Brooks, Norman H., (1979), Mixing in Inland and Coastal Waters, Academic Press, Inc., Orlando, Florida 32887.

Fujikawa, Yoko and Fukui, Masami, (1990), Adsorptive Solute Transport in Fractured Rock: Analytical Solutions for Delta-Type Source Conditions, Journal of Contaminant Hydrology, Vol. 6, pages 85–102.

Haldeman, W. R., Chuang, Y., Rasmussen, T. C., and Evans, D. D., (1991), Laboratory Analysis of Fluid Flow and Solute Transport Through a Fracture Embedded in Porous Tuff, Water Resources Research, Vol. 27, No. 1, pages 53–65.

Hallberg, G. R., Libra, R. D., Quade, D. J., Littke, B. and Nations, B., (1989), Groundwater Monitoring in the Big Spring Basin 1984–1987: A Summary Review, Energy and Geological Resources Division, Geological Survey Bureau, Technical Information Series 16, Iowa Department of Natural Resources.

Hallberg, George R., Hoyer, Bernard E., Bettis III, E. Arthur, and Libra, Robert D., (1983), Hydrogeology, Water Quality, and Land Management in The Big Spring Basin, Clayton County, Iowa, Iowa Geological Survey, Open-File Report 83–3, Iowa City, Iowa 52242.

Hallberg, George R., Libra, Robert D., Bettis III, E. Arthur, and Hoyer, Bernard E., (1984), Hydrogeologic and Water Quality Investigations in The Big Spring Basin, Clayton County, Iowa; 1983 Water-Year, Open-File Report 84–4, Iowa Geological Survey, Iowa City, Iowa 52242.

Holly Jr., Forrest M. and Preissmann, Alexandre, (1977), Accurate Calculation of Transport in Two Dimensions, Journal of the Hydraulics Division, Vol. 103, No. HY11, pages 1259–1276.

Iwai, K., (1976), Fundamental Studies of Fluid Flow Through a Single Fracture, Ph.D. Dissertation, University of California, Berkeley.

Javandel, I., Doughty, C., and Tsang, C. F., (1984), Groundwater Transport: Handbook of Mathematical Models, Water Resources Monograph Series 10, American Geophysical Union, Washington, D.C.

Kilbury, R. K., Rassmussen, T. C., Evans, D. D., and Warrick, A. W, (1986), Water and Air Intake of Surface-Exposed Rock Fractures in Situ, Water Resources Research, Vol. 22, No. 10, pages 1431–1443.

Liggett, James A and Medina, Daniel, (1988), Flow in Three-Dimensional Fracture Networks Using a Discrete Approach, Groundwater Flow and Quality Modeling, Editor: E. Custodio, A. Gurgui and J. P. Lobo Ferreira, NATO ASI Series, Series C: Mathematical and Physical Sciences Vol. 224, pages 363–374

Long, Jane C. S. and Billaux, Daniel M., (1987), From Field Data to Fracture Network Modeling: An Example Incorporating Spatial Structure, Water Resources Research, Vol. 23, No. 7, pages 1201–1216.

Marcus, H., (1962), The Permeability of a Sample of an Anisotropic Porous Medium, Journal of Geophysic. Resources., 67, pages 5215–5225.

Marcus, H. and Evanson, D. E., (1961), Directional Permeability in Anisotropic Porous Media, Contribution 31 Water Resources Center, University of California, Berkeley, page 105.

Milanovic, Petar, (1976), Water Regime in Deep Karst. Case Study of the Ombla Spring Drainage Area, Karst Hydrology and Water Resources, Vol.1, pages (7–1) to (7–27), Water Resources Publications, Fort Collins, Colorado 80522, USA.

Moreno, L., Neretnieks, I., and Eriksen, T., (1985), Analysis of Some Laboratory Tracer Runs in Natural Fissures, Water Resources Research, Vol. 21, No. 7, pages 951–958.

Peck, Adrian, Gorelick, Steven, de Marsily, Ghislain, Foster, Stephen, and Kovalevsky, Vladimir, (1988), Consequences of Spatial Variability in Aquifer Properties and Data Limitations for Groundwater Modelling Practice, the International Association of Hydrological Sciences Publication No. 175, IAHS Press, Institute of Hydrology, Wallingford, Oxfordshire OX10 8BB, UK.

Pollard, D. D., (1976), On the Form and Stability of Open Hydraulic Fractures in the earth's Crust, Geophysics Res. Letters, 3, no. 9, pages 513–516

Robertson, A., (1970), The Interpretation of Geological Factors for Use in Slope Stability, Proc. Symposium on the Theoretical Background to the Planning of Open Pit Mines with Special References to Slope Stability, South African Institute of Mining and Metallurgy, Johannesburg, South Africa, pages 55–71

Sauvaget, Patrick, (1982), Dispersion in Rivers and Coastal Waters — 2. Numerical Computation of Dispersion, Developments in Hydraulic Engineering – 3, Chapter 2, Elsevier Applied Science, London and New York.

Schrauf, T. W. and Evans, D. D., (1986), Laboratory Studies of Gas Flow Through a Single Natural Fracture, Water Resources Research, Vol. 22, No. 7, pages 1038–1050.

Sharp, J. C., (1986), Fluid Flow Through Fissured Media, Ph.D. Dissertation, Imperial College, London, 1986.

Tsang, Y. W. and Tsang, C. F., (1987), Channel Model of Flow Through Fractured Media, Water Resources Research, Vol. 23, No. 3, pages 467–479.

Tsang, Y. W., (1984), The Effect of Tortuosity on Fluid Flow Through a Single Fracture, Water Resources Research, Vol. 20, No. 9, pages 1209–1215.

Usseglio-Polatera, J.M. and Chenin-Mordojovich, M.I., (1988), Fractional Steps and Process Splitting Methods for Industrial Codes, Developments in Water Science 36, Computational Methods in Water Resources, Vol. 2 Numerical Methods for Transport and Hydrologic Processes, Editors: Celia, M.A., et. al., pages 167–172

Witherspoon, P. A., Long, J. C. S., Majer, E. L., and Myer, L. R., (1988), Combined Seismic and Hydraulic Method of Modeling Flow in Fractured Low Permeability Rocks, Groundwater Flow and Quality Modeling, Editor: E. Custodio, A. Gurgui and J. P. Lobo Ferreira, NATO ASI Series, Series C: Mathematical and Physical Sciences Vol. 224, pages 299–329